Measurement and Modelling of Gas Permeability and Solubility in Polymers for Offshore Pipelines

Melo de Almeida, Susana Raquel

Publication date:
2018

Document Version
Peer reviewed version

Technical University of Denmark

Measurement and Modelling of Gas Permeability and Solubility in Polymers for Offshore Pipelines

Ph.D.-Thesis

Susana Raquel Melo de Almeida

Center for Energy Resources Engineering
Department of Chemical and Biochemical Engineering
Technical University of Denmark
Kongens Lyngby, Denmark

CERE
Center for Energy Resources Engineering

NATIONAL OILWELL VARCO

"Life is not easy for any of us. But what of that? We must have perseverance and above all confidence in ourselves. We must believe that we are gifted for something and that this thing must be attained."

Marie Curie

Preface

This thesis constitutes the partial fulfilment of the requirements for obtaining the Ph.D. degree at the Technical University of Denmark (DTU). The work has been carried out at the Department of Chemical and Biochemical Engineering, Center for Energy Resources and Engineering (CERE) at Technical University of Denmark (DTU) from December 2013 to June 2017 under the supervision of Nicolas von Solms and Georgios Kontogeorgis, from DTU, and Adam Rubin, Christian Wang and Jacob Sonne, from National Oilwell Varco (NOV), formerly NKT Flexibles. The project was funded by NOV and the Department of Chemical and Biochemical Engineering, Technical University of Denmark.

I express a sincere feeling of gratitude to my supervisors. First, I would like to thanks to Nicolas, for trusting me during my master and later my Ph.D., even with one-year break in the middle. To Christian and Jacob for all the fruitful discussions and for bringing the real world to academia. To Georgios and Adam for the valuable time supporting the project.

I thank my colleagues at CERE, who walked with me for the last 3 years; you all made me grow in several aspects. For the talk, work related or not, and all the shared cakes I thank you. A special thanks to Louise and Patricia for all the Ph.D. "non-scientific questions" or just questions about life. I thank to Hanne for had the time to translate my *Resumé*; it would be impossible without you! To Ebba, from Civil Engineering Department, for sharing her knowledge and experience with SEM analysis.

To my parents and brother, for all the support through the years, who made it possible to come to this day, for always standing by me, for the encouragement, inspiration and love, *um muito, muitíssimo obrigada!*

A special thanks goes to Hugo, the love of my life, I cannot express how much your presence means to me. You are my everything in this distant land. We close one chapter in our life, but I hope to have you at my side to open many more to come.

Kongens Lyngby, February 2018

Susana Raquel Melo de Almeida

Abstract

Several techniques of Enhanced Oil Recovery (EOR) emerged during the last decades to increase oil extraction levels in existent reservoirs[1]. Among these techniques, CO_2 injection is one of the most promising. CO_2 is also produced as a by-product in many industries, especially in the energy sector. This greenhouse gas raises concerns regarding its concentration in the atmosphere. Thus, it should ideally be stored or recycled. Therefore, it is an intrinsic advantage to use CO_2 as an EOR gas, since the storage location of the CO_2 can be the reservoir itself. Oil reservoirs are increasing in depth, pressure and temperature, beyond 3000 m, where the pressure can exceed 1000 bar and the temperature can be higher than 423 K. Since the injected gas needs to match the oil reservoir conditions of pressure and temperature, the fluid must be transported at such extreme conditions. Fluid transportation is an often-overlooked step in the process between capture and storage of CO_2.

Flexible pipelines represent an economical solution compared with rigid pipelines, because they adapt better to the field layout, they have faster and safer installation and have better chemical and mechanical resistance[2]. Because of these advantages, they are a key component in the oil and gas industry, especially for offshore applications. A flexible pipeline consists of different layers of materials, including both polymer and metal. There are two polymeric layers: the first is located at the outer-shell and the second (the major barrier liner) is in permanent contact with the fluid being transported. Both of the polymers have the function of protecting the inner metallic layer from corrosion, by seawater and the fluid, respectively. The layer under study is the inner polymeric layer, which needs to have chemical and mechanical compatibility with the fluid being transported, in order to safely transport it. There are three main polymers that are currently used for the inner layer: poly(vinylidene fluoride) (PVDF, crosslinked polyethylene (XLPE) and polyamide 11 (PA11). The choice of the polymer is determined by cost and by the operational conditions, such as temperature, pressure and fluid type. CO_2 is likely to be in the supercritical state upon transport, because of the required temperature and pressure for storage and use. Despite being non-toxic and non-flammable, the interaction of supercritical CO_2 with the inner polymeric layer is a phenomenon of great importance for the pipeline stability. Under this stage, there are two main integrity challenges regarding the contact of supercritical CO_2 with polymers: the swelling of the polymer, which can lead to rupture of the pipeline, and the gradual degradation of the polymer, that can lead to a loss of some key barrier properties of the polymer. The removal of plasticizer from the polymer by supercritical CO_2 may also be an unwanted effect in the case of PA-11 (which is the only polymer of the three mentioned above, and considered in this work, which contains plasticizer). In the design of flexible pipelines, the thermodynamic and transport properties, in particular the solubility, diffusion and

permeability of the gas in the polymer, need to be carefully understood, since they determine how much gas escapes from the pipeline through the polymer barrier. These properties vary with temperature, pressure, fluid composition and polymer type. The experimental study of these properties proved to be quite challenging, since the polymer physical properties, such as density, free-volume, volume, are dynamic, and so they change during operation at extreme conditions. Furthermore high pressure/high temperature measurements – especially with CO_2 – are never straightforward. Measurements were made at pressures up to 650 bar The permeability represents the overall mass transport across the membrane and accounts for the diffusion and solubility of the gas in the membrane (e.g. quantifies the amount of gas escaping to the metal confinement).

In this work, the solubility of pure CO_2 is measured using a Magnetic Suspension Balance (MSB) for XLPE and for PVDF, for temperatures up to 403 K and pressures up to 300 bar. It is observed that the solubility temperature dependence followed the Arrhenius equation, decaying with temperature increase. The solubility also increased with pressure. The experimental results for the solubility were modelled with the sPC-SAFT equation of state, which was able to correlate the experimental data; although a temperature dependent, binary interaction parameter was required. The polymer swelling is estimated based on an experimental method and using sPC-SAFT. Modelling the swelling allows for different choices of the binary interaction parameters: It can be obtained from solubility in order to predict swelling or directly fitted to the experimental data. The polymer swelling increases with temperature for PVDF and decreases for XLPE, this effect might be due to the very high degree of crosslinking present in XLPE and not in PVDF.

A 2D-permeation cell is used to measure the permeability of pure CO_2 and gas mixtures with high concentration of CO_2 in PVDF, XLPE and PA11. The permeability of gas through PVDF was measured at pressures up to 345 bar and temperatures up to 403 K. In the case of XLPE and PA-11 the permeability is measured up to 650 bar, and at temperatures up to 363 K. It is shown that the permeability always increases with increasing temperature, although the permeability increases with pressure for PVDF and PA-11 and decreases with pressure for XLPE. This trend is explained by the contrary effects that the pressure has on the free-volume, which may decrease because of the increase in the polymer density, or increase due to the penetrant increase that can lead to the plasticization of the polymeric chains. The only plasticized polymer in the studied set of polymers (PA11), shows a loss in weight, from the pre to post-test, on average by 2.58% loss by weight. This effect is not observed in the other polymers, so it is assumed that the plasticizer is being removed from the polymer. Besides pure CO_2, gas mixtures were also studied: several measurements were made for the mixture 90 mol% CO_2 + 10 mol% CH_4, although other concentrations of this mixture were also considered. The presence of CH_4 tends to decrease the

total gas permeability, as expected, since CH_4 is less permeable than CO_2. In the other gas concentrations studied, it was difficult to draw clear conclusions regarding the effect of CO_2 gas concentration, since only two pressures were studied and both show different behaviour. The selectivity of the permeation through the membrane was analysed by gas chromatography. For XLPE the initial concentration was maintained (i.e. there was no clear selectivity for CO_2), whereas PVDF was more permeable to CO_2 than CH_4, meaning that at the end of the experiments the concentration of CO_2 increase compared to the initial concentration.

With the measured solubility and permeability, the diffusion was calculated. It shows the diffusion has a more pronounced effect in the permeability than the solubility, with respect both to temperature and pressure dependence; with increasing pressure, diffusion increases in PDVF and decreases in XLPE, while solubility increases in both polymers, the permeability shows the same pressure behaviour as diffusion, opposite to the solubility.

Resumé

I de seneste årtier er der kommet adskillige nye teknikker til forbedret olieudvinding (’Enhanced Oil Recovery’ (EOR)) i eksisterende reservoirer. Blandt disse teknikker er CO_2-injektion en af de mest lovende. CO_2 produceres også som et biprodukt i mange industrier, især i energisektoren, hvilket er bekymrende i forhold til koncentrationen i atmosfæren, og man bør enten forsøge at genanvende eller opbevare CO_2en. CO_2 kan med fordel bruges som EOR-gas, da CO_2en kan opbevares i selve reservoiret. Oliereservoirernes dybde, tryk og temperatur øges til stadighed, og kan nu være over 3000 m, med tryk over 1000 bar, og temperatur over 423 K. Da den indsprøjtede gas skal være i overensstemmelse med oliereservoirets betingelser for tryk og temperatur, forventes det, at væsken også transporteres under ekstreme temperatur- og trykforhold. Et ofte overset trin i denne proces er transporten af denne væske.

Fleksible rørledninger er en mere økonomisk løsning i forhold til stive rørledninger, fordi de tilpasser sig bedre til feltet, de er hurtigere og sikrere at installere og har højere kemisk og mekanisk modstandsdygtighed[1]. På grund af disse fordele er de en nøglekomponent i olie- og gasindustrien, især til offshore-applikationer. En fleksibel rørledning består af forskellige lag af materialer, herunder polymer og metal. Der er to polymere lag: Et som er placeret ved den ydre skal, og et som permanent er i kontakt med væsken, der transporteres. Begge polymerer skal beskytte det indre lag af metal mod korrosion fra henholdsvis havvand og den transporterede væske. Det lag, vi har undersøgt, er det indre polymere lag, som skal have kemisk og mekanisk kompatibilitet med væsken, for at kunne transportere den sikkert. Der er tre hovedtyper af polymerer, som kan anvendes i det indre lag: poly (vinylidenfluorid) (PVDF), tværbundet polyethylen (XLPE) og polyamid 11 (PA11). Valg af polymer afhænger af driftsmæssige betingelser, såsom temperatur, tryk og væsketype. CO_2 er sandsynligvis i superkritisk tilstand ved transport på grund af den nødvendige temperatur og tryk. Selvom den er giftfri og ikke-brandfarlig, er superkritisk CO_2-interaktion med det indre polymerlag rørledningens af stor vigtighed for rørledningsstabiliteten. I denne fase er der to store udfordringer i forbindelse med kontakten mellem superkritisk CO_2 og polymerer: polymeren kan enten svulme op, hvilket kan føre til brud på rørledningen, eller den kan nedbrydes gradvis med tab af nogle af de vigtige barriereegenskaber til følge. Fjernelsen af blødgøringsmidlet fra polymererne er et eksempel på førstnævnte. Ved udformningen af fleksible rørledninger er det vigtigt med en grundig forståelse af transportegenskaber, såsom opløselighed og permeabilitet, da de er en funktion af temperatur, tryk, væskesammensætning og polymer. Eksperimentelle undersøgelser af disse egenskaber er meget udfordrende, da de polymere psykokemiske egenskaber, såsom tæthed, fri-volumen, volumen, er dynamiske og således ændrer sig i drift under ekstreme forhold. Permeabiliteten repræsenterer den samlede massetransport over membranen og

redegør for diffusionen og opløseligheden af gassen i membranen (for eksempel kvantificerer den mængden af gas, der trænger ind til metalsammenslutningen).

I dette projekt har vi målt opløseligheden af ren CO_2 ved hjælp af Magnetic Supension Balance (MSB) for XLPE og PVDF, for temperaturer på op til 403 K, og tryk på op til 300 bar. Det kunne observeres, at afhængigheden mellem opløselighed og temperatur fulgte Arrhenius-ligningen, eftersom den faldt som følge af temperaturforøgelse og steg som følge af trykforøgelse. Temperaturafhængigheden kan forklares af, at CO_2 har sværere ved at kondensere ved højere temperaturer. De eksperimentelle resultater af opløseligheden blev matchet med sPC-SAFT, og vi observerede en god korrelation med vores eksperimentelle data, og kunne konstatere, at der findes en binær interaktionsparameter. Opsvulmen blev først estimeret på basis af en eksperimentel metode og senere estimeret med sPC-SAFT, hvor der anvendtes to binære interaktionsparametre: det første fra opløseligheden og den anden til at matche den eksperimentelle estimering. De to sæt parametre for binær interaktion blev sammenlignet, og vi konkluderede, at den binære parameter fra opløseligheden er lavere end den, der passer til den eksperimentelle estimering. Opsvulmen viste sig at øges med stigende temperatur for PVDF og reduceres for XLPE. Denne effekt kan skyldes tværbindingen, som findes i XLPE men ikke i PVDF.

En 2D-permeationscelle anvendtes til at beregne permeabiliteten af rene CO_2- og gasblandinger med høj koncentration af CO_2 i PVDF, XLPE og PA11. Permeabiliteten af gassen for PVDF var begrænset til tryk på op til 345 bar og temperaturer op til 403 K. Ved XLPE og PA11 måltes permeabiliteten op til 650 bar, men dog kun til temperaturer op til 363 K. Det blev påvist, at permeabiliteten steg som følge af stigende temperatur, selv om permeabiliteten steg som følge af tryk for PVDF og PA11 og faldt som følge af tryk for XLPE. Denne tendens forklares af de modsatte virkninger, som trykket har i frivolumen, som kan falde på grund af stigningen i polymertætheden eller forøges på grund af den øgede permeabilitet, der kan føre til plastificering af de polymere kæder. Den eneste plastificerede polymer i det undersøgte sæt af polymerer (PA11) viste et vægttab, fra præ til post-test, på i gennemsnit 2,58%. Denne virkning observeredes ikke i de andre polymerer, så det antages, at blødgøreren fjernedes fra polymeren. Ud over rent CO_2 blev også gasblandinger undersøgt. Der var særligt fokus på 90 mol% CO_2 + 10 mol% CH_4, grundet den hyppige anvendelse på fleksible rørledninger. På trods af at undersøgelsen var begrænset til PVDF og XLPE, havde tilstedeværelsen af metan tendens til at reducere den totale gaspermeabilitet. Andre gaskoncentrationer blev undersøgt, men der blev ikke draget yderligere konklusioner angående CO_2-koncentration, eftersom der kun blev undersøgt to tryk, og begge viste forskellig adfærd. Selektiviteten af gennemtrængningen gennem membranen blev analyseret ved gaskromatografi, og konklusionen var, at XLPE bebeholdt den oprindelige sammensætningsmæssige balance, men det samme blev ikke observeret for PVDF, der viste sig at være mere permeabelt for CO_2

end CH_4, hvilket betød at koncentrationen af CO_2 steg i forhold til den oprindelige koncentration i slutningen af eksperimentet.

På baggrund af den målte opløselighed og permeabilitet blev diffusionen beregnet. Det viste sig, at diffusionen har en mere udtalt virkning på permeabiliteten end opløseligheden, både hvad angår temperatur og trykafhængighed; ved stigende tryk stiger diffusion i PDVF, men falder i XLPE, mens opløseligheden stiger i begge polymerer, viser permeabiliteten det samme trykadfærd som diffusion i modsætning til opløselighed.

Contents

Figure Captions

Table Captions

Chapter 1

Chapter 1. Introduction

The 2016 outlook provided by the International Energy Agency continues to predict a major challenge in the energy sector, defined by the steep growth of energy demand[3]. Total world energy consumption is project to increase from 549 quadrillion British Thermal Units (Btu) in 2012 to 629 quadrillion Btu in 2020 and to 815 quadrillion Btu in 2040, representing a 48% increase from 2012 to 2040 (Figure 1.1).

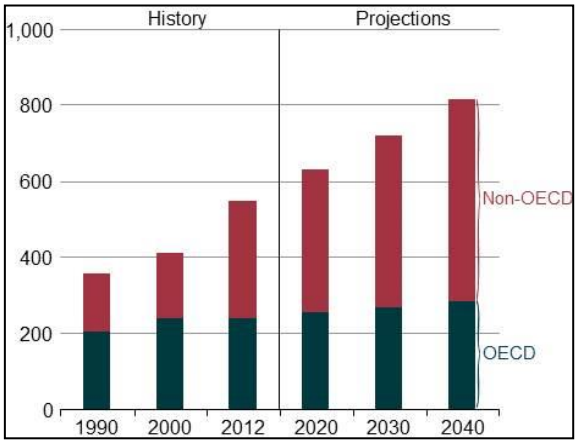

Figure 1.1 – World energy consumption from 1990 to 2040 in quadrillion Btu[3].

The projections are based on strong economic growth and population expansion of nations outside the Organization for Economic Cooperation and Development (OECD). Despite the strong debate surrounding the use of fossil fuels and its impact on climate change, fossil fuels will continue to meet 78% of the world energy demands by 2040. The consumption of oil, and other liquid fuels, is estimated to increase from 90 million barrels per day in 2012 to 100 in 2020 and 121 million barrels per day in 2040[3]. However, oil is a limited resource and some of the less optimistic predictions indicate a 20 years and 80 years production time left for sandstone[4] and carbonate fields[5], respectively. To keep pace with energy demand levels, the oil and gas industry is forced to sustain production, while searching for new oil fields that are uncertain and often are located in less accessible areas (e.g. offshore, deep offshore), or to optimize the production with more efficient recovery methods. In fact, efficiency is a keyword in the industry, considers the ratio between oil produced versus total amount in the reservoirs. For instance, in 1993, from the 536 billion barrels of oil discovered in United States, only 162 billion barrels were produced economically through conventional methods, which means that up to 66% of the discovered oil remains in place[4]. This introduces the importance of Enhanced Oil Recovery (EOR) methods and

technology-driven supplies of oil, as a strategy to further exploit the existent reserves and answer to the increasing demand of oil in the upcoming future [6].

1.1. Enhanced Oil Recovery

During the production life of an oil reservoir, its recovery is usually divided into three stages[7], where in the so-called primary stage, oil recovery is naturally driven and does not require the use of external sources of energy, reaching 20-30% of recovery levels[8]. However, on a secondary stage, recovery is conducted through injection of external fluids, usually water and/or gas, with the purpose of increasing the reservoir pressure and promoting artificial lift.

This may increases recovery up to 40%. The final stage is the tertiary recovery, which involves the injection of special fluids, such as chemicals[9,10], miscible gases[11], microbial[12] and/or injection of thermal energy[13,14]. The concept of Enhanced Oil Recovery (EOR), does not depend on the production life of the reservoir, but is by definition, characterized by injection of gases, chemicals (eg. surfactant, miscible solvent), and/or thermal energy into the reservoir, to extract oil to a further extent[4]. When using such advanced techniques, recovery can reach up to 60-65%. The mechanism of the enhanced oil recovery relates to the control of properties at the pore and reservoir scales, such as interfacial effects, wettability, mobility ratio, fluid properties and reservoir pressure.

1.1.1. Classification of EOR methods

A common approach is to divide EOR methods according to the following classification:

- Thermal methods where steam and heat are applied to the reservoir, having the effect of decreasing the viscosity of oil to promote an easier flow, and also providing an increase of pressure.
- Chemical methods, involving the injection of interfacial-active components, such as polymers, surfactants, alkalis, and chemical blends.
- Miscible or solvent injection methods, usually related to gas injection of hydrocarbons, carbon dioxide and nitrogen. Supercritical phases, such as high-pressure carbon dioxide, have high solubility for oil recovery.

Despite the broad choice of techniques within each branch of methods, the economical advantages of CO_2 enhanced oil recovery make this technique attractive, especially when comparing with chemical methods[15]. The use of CO_2 enhances oil production, due to high efficiency of CO_2 in the extraction of heavy hydrocarbons, and increase oil mobility through a decrease of viscosity and oil swelling effect. In fact, CO_2 EOR process is recognized as the second most applied EOR process, just behind thermal recovery processes[15]. An important additional advantage of the process is the possibility of decreasing the environmental impact of CO_2[16–20], while using reservoirs as a capture point and avoiding its release to the atmosphere.

1.1.2. CO_2 enhanced oil recovery and Flexible pipelines.

A key component of CO_2 enhanced oil recovery methods is the use of flexible pipelines[21]. Since the mid-1980s flexible pipelines have found increasing application, not only in newly discovered fields, but also replacing rigid pipeline systems. The reasons for this profound impact are the combined advantages of flexible pipelines compared to rigid systems:

- easier storage and transportation of the pipelines;
- lower operating costs;
- simpler maintenance;
- higher chemical and mechanical resistance;
- safer operation.

National Oilwell Varco (NOV) is the largest U.S. oilfield equipment maker and is currently expanding their capabilities in flexible pipelines supplies for offshore transport of fluids in deep water conditions. The company provides solutions for floating production storage and offloading (FPSO) units and static production facilities. FPSO units are floating vessels designed for production and processing of hydrocarbons and storage of oil, which have the advantage of being simpler to install. The process, as seen in Figure 1.2, is largely dependent on flexible pipeline usage.

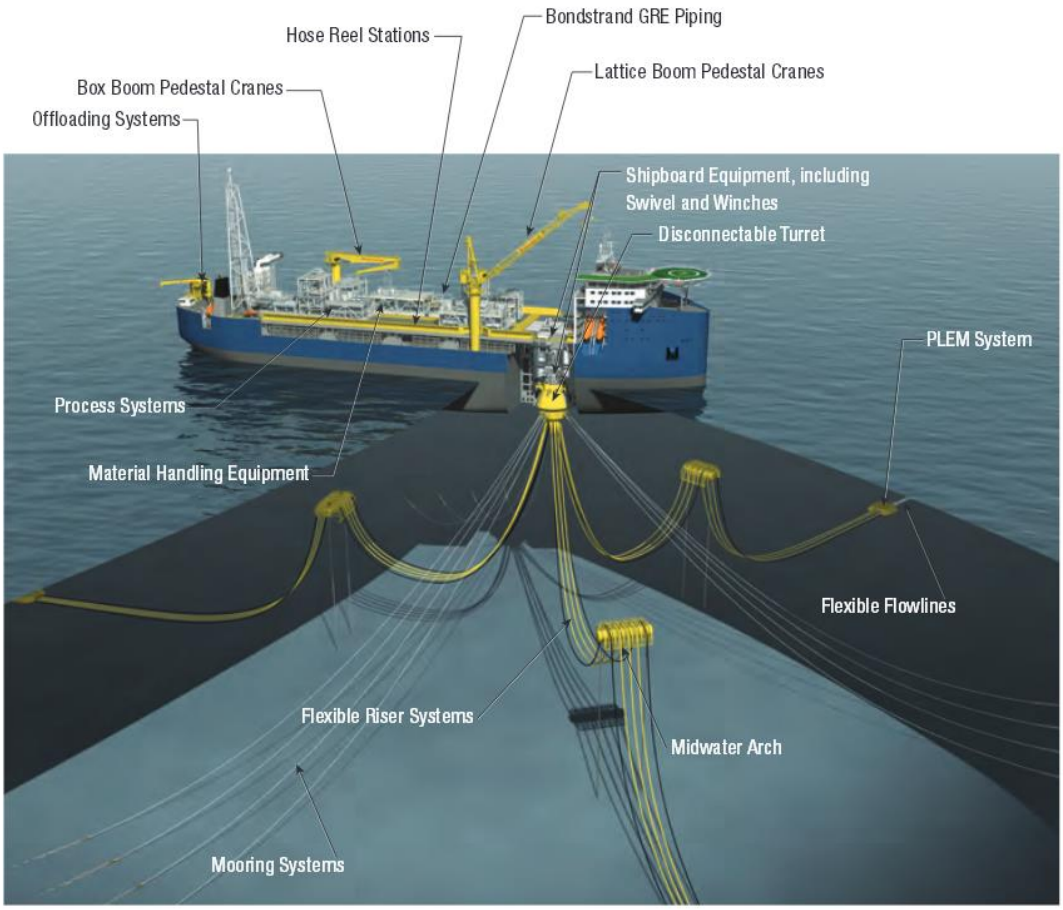

Figure 1.2 – Schematic representation of a FPSO unit for oil extraction and storage[22].

The global flexible pipe market for oil and gas offshore applications is significant, estimated at around 1,200 km per year (measured in theoretical length of standard pipe)[23]. Converting that into market value, it equates to approximately US $1.5 billion per year. It was estimated that the flexible pipe industry will spend around US $3 billion per year on deep water flexible pipe by 2016, a fourfold increase compared with 2012[24].

Flexible pipeline consists of different layers of material, most of them metallic (Figure 1.3), but there are two types of polymeric materials of crucial importance. The first polymeric layer (outer sheath) is located at the outer-shell of the pipe, which has the main function of protecting the inner metallic surfaces from seawater corrosion and the second (inner liner) is in permanent contact with the transported fluid and therefore reinforces from the inner side the isolation of the metal layers. Moreover, this polymeric

inner layer needs to have special mechanical and chemical properties compatible with the transported fluid to avoid leakages and guarantee high safety levels. In order to preserve the flexibility of the pipe construction, the metallic layers are not bound together.

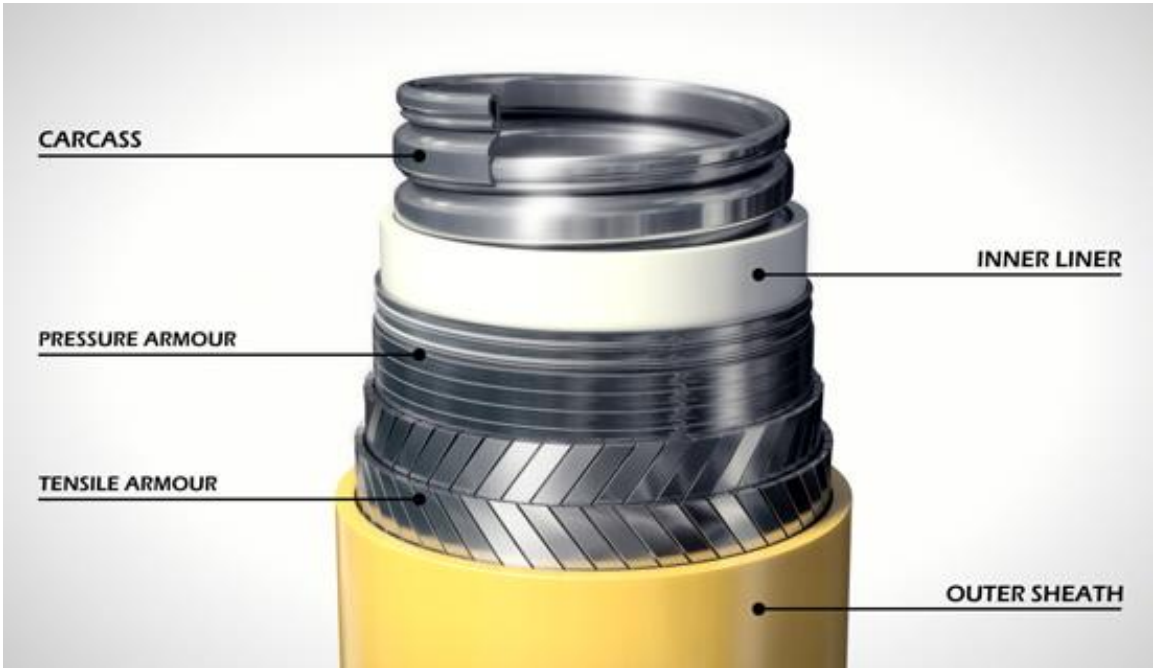

Figure 1.3 – Representation of the flexible pipelines commercialized by NOV.

Due to its critical importance for effective transport, the inner polymer is the main object of this study. Inside the pipeline, the gases may be transported at high temperature and pressure, in the supercritical region of CO_2. There are two main issues regarding the contact of supercritical fluids with polymers: a swelling phenomenon of the polymer of variable extension depending on the type of polymer used, which could lead to rupture of the pipeline; and the gradual degradation of the polymer that can lead to a loss of some key barrier properties of the polymer. In any case, there will always be a degree of permeation of fluid through the polymer, which should be quantified.

1.2. Supercritical Fluids – CO_2 and CH_4

A supercritical fluid is a fluid that has temperature and pressure above its critical values, e.g. in the critical region, shown in Figure 1.4. In this stage, the fluid has properties of both liquid and gas; it can permeate through solids like a gas and dissolve in materials like a liquid.

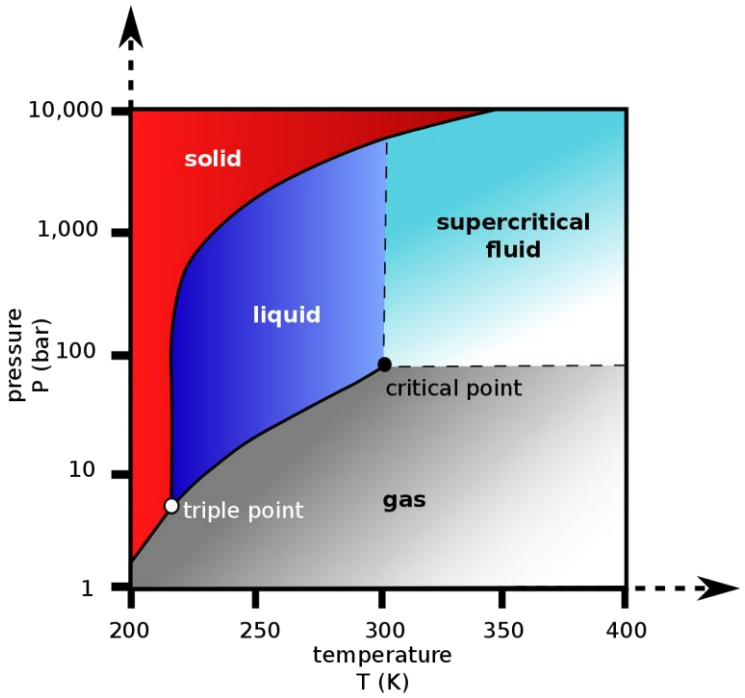

Figure 1.4 – P-T phase diagram of CO_2[25].

Table 1.1 shows the critical properties of CO_2 and CH_4.

Table 1.1 – CO_2 and CH_4 molecular weight and critical properties.

Component	Molecular Weight (g/mol)	Critical Temperature (K)	Critical Pressure (bar)
CO_2	44.01	304.13	73.77
CH_4	16.04	190.56	45.99

Supercritical CO_2 is widely used as a clean and versatile solvent and is a promising alternative to organic solvents such as chlorofluorocarbons. It is non-toxic, non-flammable, chemically stable and inexpensive. Another advantage of CO_2 is that it easily attains the supercritical state and can be removed from the system by simple depressurization[26].

A side effect of supercritical CO_2 contacting polymers is that the polymers may swell and plasticize at high pressure; this is a consequence of the substantial solubility of CO_2 in these polymers. Absorbed CO_2 causes several changes in the polymer properties such as volume and a considerable reduction in the viscosity of molten polymer due to an increase of free volume.

At the studied condition of temperature, the density is very sensitive near the critical point. Small changes of pressure represent big density variation. Figure 1.5 presents the density of CO_2 as a function of pressure at 304.13 (critical temperature), 318, 363 and 403 K.

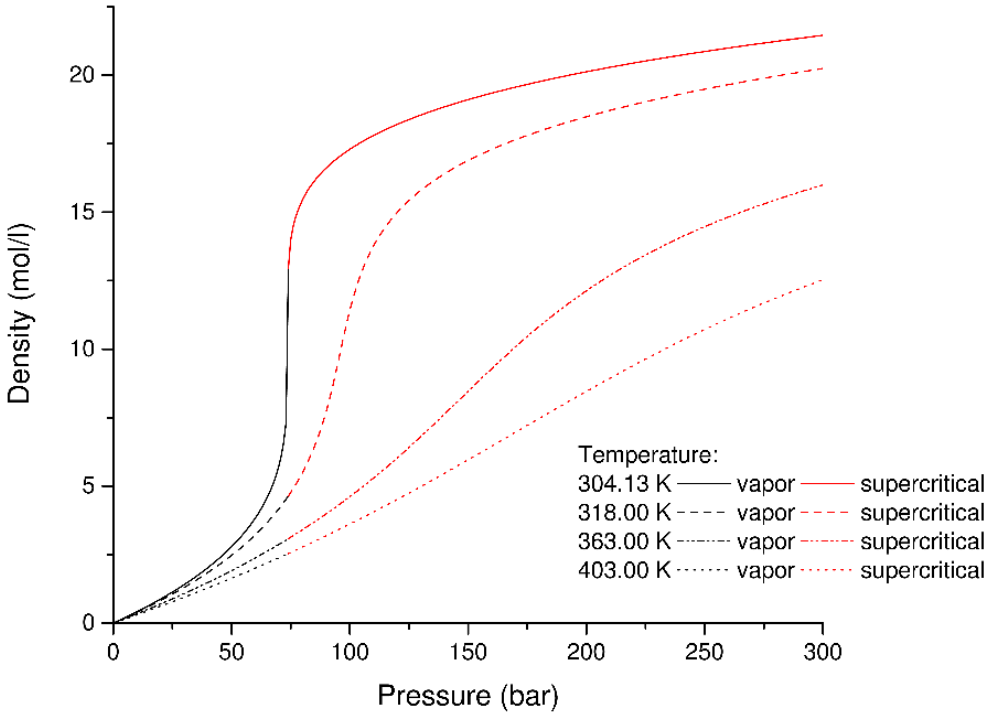

Figure 1.5 – CO_2 density as a function of pressure (data from REFPROP[27]).

As it can be seen the lower temperature shows more density sensitivity with increasing pressure; meaning small changes of pressure result in high changes of density. The presented temperatures were chosen to match the studied temperatures in this work and the critical temperature of CO_2.

Another effect of being in the supercritical state is the significant deviation from ideal gas behaviour, as is visible in Figure 1.6, which plots the fugacity as a function of pressure.

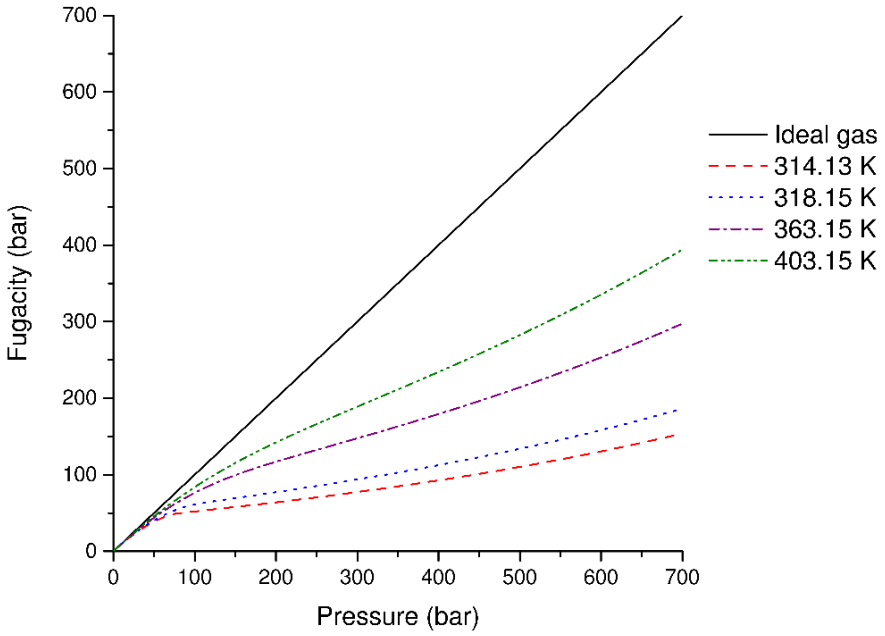

Figure 1.6 – CO_2 fugacity as a function of pressure at the critical temperature (314.13, 318 363 and 403 K for pure CO_2.

The dark full line represents the ideal gas behaviour, where the fugacity matches the pressure, as bigger as the deviation from this line the less ideal is the fluid. It can be seen in the figure above that lower temperature present bigger deviation to the ideality.

1.3. Polymers

Polymers are long chain-like materials consisting of repeating units called monomers. The number of these repeating units in a polymer is typically several thousands, sometimes as high as millions[28]. Polymers may be conveniently divided into four categories: amorphous polymers in the glassy or rubbery state, and semi-crystalline polymers in which the amorphous region is in the glassy or rubbery state. The factor that determines whether a polymer is in the glassy or rubbery state is the glass transition temperature, T_g (see Figure 1.7).

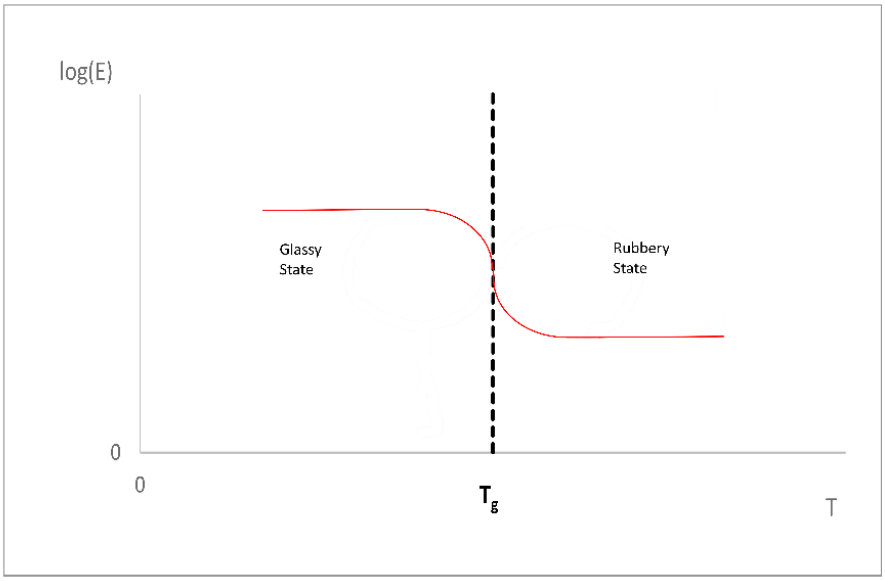

Figure 1.7 – Tensile modulus, E, as a function of temperature for an amorphous polymer (adapted from Mulder[29])

When a polymer is heated, there is a temperature (T_g) at which the polymer changes from glassy to rubbery state. Near this temperature, the tensile modulus (E) also decreases significantly, which is defined by the force F applied across an area A necessary to obtain a given deformation and is a characteristic parameter for a given polymer. The units of E is $N \cdot m^{-2}$ or Pa [29].

However this temperature, which is specific for each polymer, can be altered by adding plasticizer[30] or introducing crosslinks between polymer chains, restricting the mobility of the segments[31]. The

addition of plasticizer weakens the intermolecular interactions, increasing the free-volume of the system, and consequently T_g decreases[30]. Cross-linking restricts the segments mobility, hence T_g increases[31]

1.3.1. Semi-Crystalline Polymers

Semi-crystalline polymers are composed of an amorphous and a crystalline region, see Figure 1.8[32].

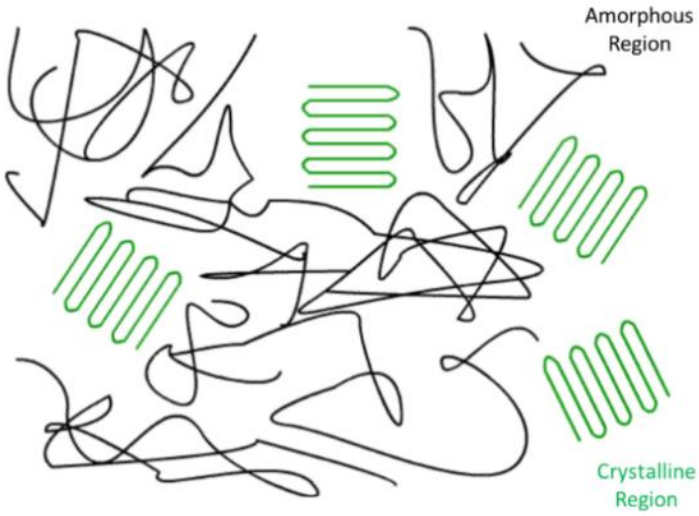

Figure 1.8 – Structure of a semi-crystalline polymer (adapted from Mulder[29])

Molecules arranged in a regular order compose the crystalline region, while in the amorphous region the molecules are randomly organized. The sorption and diffusion essentially only take place in the amorphous region, meaning the crystalline region acts as an excluded volume in the sorption process and a barrier to diffusion[29].

A simple assumption to treat the solubility of gases in semi-crystalline polymers is assuming that the existence of crystalline regions does not influence the sorption in the amorphous region[33–35]. This simples assumption can describe the solubility has linearly dependent on the fraction of amorphous polymer phase[35–40]:

$$S = \alpha \cdot S^* \qquad \text{Equation 1.1}$$

where α is the amorphous volume fraction and S^* is the solubility in completely amorphous polymer[35,37]. This approach can describe the solubility of light gases or CO_2 in a limited range of pressure[34]. However the sorption of gases in semi-crystalline polymers can be rather complex[41], especially in the cases where the swelling is induced by the sorbed molecules. In this cases the crystalline domain can lower the gases solubility of the amorphous phase[34,42]. The polymer chains in the amorphous polymer phase are perturbed by the crystallites of the semi-crystallite polymer, as elastic or local density effect[41,43].

Crystalline regions have two effects on the gas diffusion: increase of effective path length and the apparent reduction of the polymer chain mobility in the amorphous phase, resulting in a reduction of the gas permeability[44]. The crystallinity has an "anchoring" effect, which tends to immobilize the amorphous chain. The diffusivity can be expressed as:

$$D = \frac{D^*}{\tau \cdot \beta} \qquad \text{Equation 1.2}$$

being D^* the diffusivity in completely amorphous polymer, τ the geometric impedance factor, which reflects the more circuitous diffusion path due to the presence of impermeable crystallites, and β the chain immobilization factor, attributed to the "crosslinking" action of the crystallites on sequential mobility[35,37].

1.3.2. Rubbery vs Glassy Polymers

Above T_g the polymer is in the rubbery stage, where the segments can rotate freely along the main chain bonds[29]; the polymer becomes soft and elastic[32]. The sorption of gases in rubbery polymers is similar to the sorption of gases in low molecular weight liquids, and the gas concentration in the polymer often obeys Henry's equation[45,46]. For highly sorbing penetrants, such as organic vapours, or gases at high pressure, the penetrant concentration in the polymer may deviate from Henry's law. In this cases, the penetrant concentration can be often satisfied by the Flory-Huggins equation[45,46] (the different sorption modes are presented later in this chapter).

Below T_g, the polymer is in the glassy stage, which is characterized by virtually frozen molecules[29,47]. The polymer molecules have low intrasegmental mobility and long relaxation times. Moreover, the morphology of glassy polymers is viewed as inhomogeneous with respect to the transport of small

penetrant molecules[48]. In this stage, the transport mechanisms are not completely understood, however the sorption is defined by the dual-mode model in some works[45,46]. The gas penetration is very low, but the size-based selectivity is high, making them the most used membrane for gas separation on industrial scale.

1.3.2.1. Free-Volume Theory

The diffusion of gases in polymers may be described by the Free-Volume Theory, the central idea being that a molecular mixture contains "holes"[32,49].

As stated before, in the glassy state, the mobility of the chain segments is extremely limited and too small to allow rotation around the main chain. However, in the rubbery state the mobility of the chain segments increases and "frozen" microvoids no longer exist[29,49]. The free volume V_f may be defined as the volume generated by thermal expansion of the initially closed-packed molecules at 0 K.

$$V_f = V_T - V_0 \qquad \text{Equation 1.3}$$

where V_T is the observed volume at temperature T and V_0 is the volume occupied by the molecules at 0 K. The observed or the specific volume, at a particular temperature, can be obtained by the polymer density, whereas the volume occupied at 0 K can be estimated from group contribution[29].

When a polymer in the rubbery state is cooled down, above T_g, a decrease in the thermal expansion coefficient is observed at T_g [29,45]. In Figure 1.9 we see that a glassy polymer exhibits a specific volume of an equivalent hypothetical rubbery polymer, obtained by extrapolation of the specific volume data above T_g.

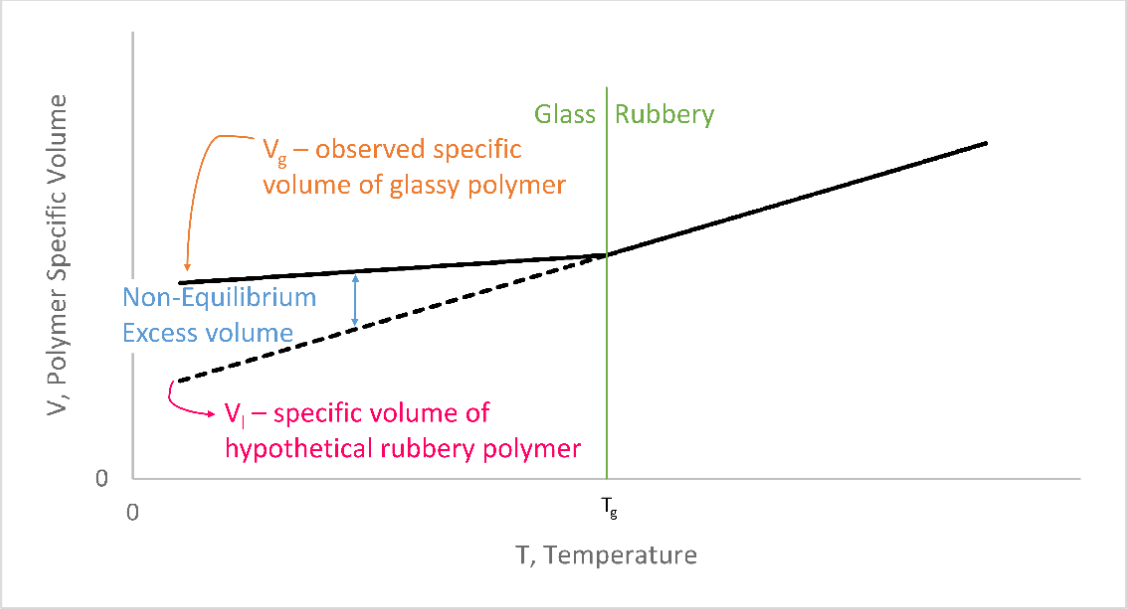

Figure 1.9 – Schematic representation of unrelaxed, non-equilibrium, excess volume, V_g-V_l in a glassy polymer (adapted from Ghosal and Freeman)[45].

Using the free-volume theory, based on viscosity, a fractional free volume ($v_f = V_f / V_T$) was found to be 0.025 for a number of glassy polymers and this value is now considered to be a constant.

Fox and Flory[50], in 1950, studied the glass transition and the free volume of polystyrene as a function of molecular weight and relaxation time. They found, above T_g (in the rubbery state), the free volume increases linearly with temperature according[29,49]:

$$v_f = v_{f,T_g} + \Delta\alpha \cdot \left(T - T_g\right) \qquad \text{Equation 1.4}$$

where v_{f,T_g} is related with the free-volume at 0 K and $\Delta\alpha$ is the difference between the value of thermal expansion coefficient above and below T_g. They also found that below T_g the same specific volume-temperature relationship held for all polystyrenes, independently of molecular weight. From this study, they concluded that: (a) below T_g the local conformation arrangement of the polymer segments was independent of both molecular weight and temperature, and (b) the glass transition temperature was an iso-free-volume state[49].

Simha and Boyer[51] found two relations between the thermal expansivities and T_g, assuming the free-volume at $T = T_G$ is constant. The first is:

$$(\alpha_R - \alpha_G)T_G = K_1 = 0.113 \qquad \text{Equation 1.5}$$

where α_R and α_G correspond to the slope of the line above T_g and below T_g in Figure 1.9, respectively. The second relation is:

$$\alpha_R T_G = K_2 = 0.164 \qquad \text{Equation 1.6}$$

The highlight of this finding is that, the free-volume at the glass transition temperature is indeed a constant and equal to 11.3%, for a wide variety of polymers. The quantities K_1 and K_2 provide a criterion for the glass temperature, especially for new polymers, or when the value is in doubt[49]. Sharma *et al.* later found $\alpha_R - \alpha_G = 3.2 \times 10^{-4}\ \text{deg}^{-1}$ [49].

The free-volume approach is very useful for describing and understanding transport of small molecules through polymers. The basic concept is that a molecule can only diffuse from one place to another if there is sufficient empty space, or free-volume. If the size of the penetrant increases the free-volume must also increase.

1.4. Polymer materials considered in this work

1.4.1. Poly(vinylidene fluoride) – PVDF

PVDF is a semi-crystalline polymer, where the amorphous fraction is rubbery at room temperature. It is one of the most studied polymers with a wide range of applications[52]. It is used in: filtration membranes for water treatment (e.g. micro and ultra-filtration, membrane bioreactors, etc.), membrane contactor processes (e.g. membrane distillation, acid gases absorptions and desorption, boron and pollutant removal from water, etc.), recovery of biofuels via pervaporation, support for preparing composite membranes and separator for lithium ion batteries[52].

The PVFD used in this work is a copolymer named SOLEF VF2-CTFE, which was obtained by polymerizing vinylidene fluoride and consists of 67% poly(vynilidene fluorideco-chloro trifluoro

ethylene), 33% polyvinylidene fluoride and small amounts of high-density polyethylene[53]. Some of its technical features are referred in Table 1.2.

Table 1.2 – PVDF technical features (data provided by NOV).

T_g (K)	Density (g/cm^3)	Crystallinity (%)	Max. Operational Temperature (K)
245	1.785	38	403

1.4.2. Cross-Linked Polyethylene – XLPE

This is a newly-developed polymer, which is made by cross-linking HDPE using peroxide in combination with infrared radiation. The cross-linking improves the mechanical properties of HDPE. The degree of cross-linking is substantially higher, around 90 mol%, compared with a typical value of 75% for the silane-based process. The result of this linkage is the restriction of movement of the PE chains relative to each other, so that when heated the network structure cannot deform and the excellent properties are kept even at higher temperature [54,55]. XLPE technical features are presented in Table 1.3.

Table 1.3 – XLPE technical features (data provided by NOV).

T_g (K)	Density (g/cm^3)	Crystallinity (%)	Max. Operational Temperature (K)
134	0.866	47.5	363

1.4.3. Polyamide 11 – PA11

Polyamides, often called Nylon, belong to a large family of polymers (eg. PA-66, PA6, PA11, PA12, PA46) that differ in the nature and unit length between amide groups[56]. The PA11 is a homopolymer of C11 amino acids. Polyamides have generally good mechanical resistance, reasonable heat and fatigue resistance, and chemical resistance to oil, greases or other hydrocarbons solvents[57]. PA11 is distinguished from the polymers of the same family, having greater flexibility and less sensitivity to water, which are clearly desirable properties in pipelines for offshore applications. In this study, the used PA11 contains

12% of N-n-Butylbenzenesulphonamide as plasticizer. Table 1.4, shows some of the relevant technical features of PA11.

Table 1.4 – PA11 technical features (data provided by NOV).

T_g (K)	Density (g/cm^3)	Crystallinity (%)	Max. Operational Temperature (K)
319	1.05	22.5	363

If water is present, the pH of the fluid contacting the polymer decreases and the maximum operational temperature for PA11 is lower due to hydrolysis effect, which can lead to changes in the polymer structure, decreasing the molecular weight and increasing the crystallinity.

1.5. Transport Phenomena

The first work on the transport of gases were apparently those of Thomas Graham in 1829. He observed that a wet pig bladder inflated to the bursting point when placed in a CO_2 atmosphere[58]. In 1855, by analogy to Fourier's equation of heat conduction, Fick proposed the equation of mass diffusion. In addition, Exner in 1875 and Stefan in 1878 showed, experimentally, that the permeation of gases though soap films was proportional to the product of solubility of the gas in water. This results were extended and applied to rubber by von Wroblewski in 1879[58].

In porous membranes mass transport proceeds through Knudsen flow[29], which is determined by the pore size, while in non-porous membranes the molecules need to first absorb in the dense matrix and only then diffuse through it. Polymers can be consider non-porous or dense membranes, so transport is divided into three stages[59]:

- Absorption of the gas (by chemical affinity or by solubility) by the polymer;
- Diffusion of the gas inside the polymer matrix;
- Desorption of the gas at the side of lower partial pressure.

Figure 1.10 represents schematically the transport phenomena through a polymer membrane.

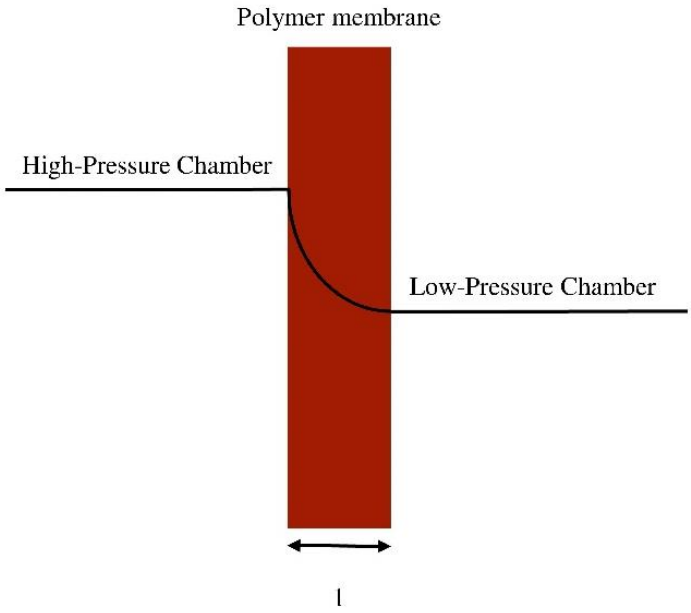

Figure 1.10 – Transport phenomena scheme.

In steady state, the transport phenomena is defined by three coefficients: permeability, solubility and diffusion coefficient[29,59,60]. The permeability, Pe, gives an idea about how easily it is for a molecule to penetrate a polymeric membrane, so it considers both the solubility and the diffusion, and is formulated as:

$$Pe = S \times D \qquad \text{Equation 1.7}$$

where D is the diffusion coefficient, which expresses the circulation of the gas molecules through the membrane due to random molecular motion and S is the solubility, which represents the equilibrium between the gas dissolved in the membrane and the gas surrounding it.

1.5.1. Diffusion Coefficient

Once the gas has been absorbed on the high-pressure side of the polymeric membrane, it diffuses towards the low-pressure side due to the difference in chemical potential. The gas flux, J, is then defined by:

$$J = \frac{Q}{A \cdot t}$$ Equation 1.8

where Q is the amount of gas crossing the membrane with area A during the time t [60,61].

Fick's first equation establishes a proportional relation between the flux of gas diffusing through a membrane and the concentration gradient between both sides of the membrane. The proportionally constant is called the diffusion (D).

$$J = -D\frac{dC}{dx}$$ Equation 1.9

A thin part of the membrane is represented below:

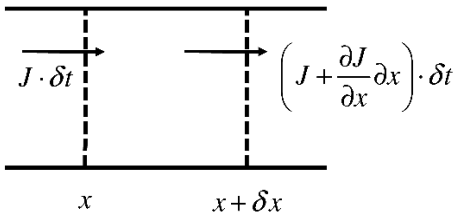

Figure 1.11 – Diffusion across two planes situated at the point x and $x + \delta x$ in a cross-section of a membrane[29].

The quantity of penetrant which enters the plane x at time δt is equal to $J \cdot \delta t$ and the quantity leaving the plane $x + \delta x$ is $\left[J + \left(\partial J/\partial x\right)\delta x\right]\delta t$. The change in concentration in the volume between x and $x + \delta x$ is then:

$$dC = -\left(\frac{\partial J}{\partial x}\right)\delta t$$ Equation 1.10

Combining Equation 1.9 with Equation 1.10, and assuming D is constant in the membrane leads to Fick's second equation:

$$\frac{\partial C}{\partial t} = -D\frac{\partial^2 C}{\partial x^2}$$ Equation 1.11

When the polymer, with thickness l, is exposed to a gas and the diffusion coefficient is constant, the integration of Equation 1.9 results in:

$$J\int_0^l dx = -D\int_{C_1}^{C_2} dC \qquad \text{Equation 1.12}$$

Finally:

$$J = \frac{D(C_1 - C_2)}{l} \qquad \text{Equation 1.13}$$

where C_1 and C_2 are the gas concentration in the membrane on the high pressure side and on the low pressure side, respectively, and l is the thickness of the membrane.

It is possible to obtain the value of D by the time-lag method, developed by Barrer[62]. This method consists in representing the amount of gas that crossed the membrane as a function of time. When t tends towards very long time, steady state is reached and a straight line is observed. Before the system reaches steady state, the flux and the concentration vary with time in every point inside the membrane and, from the interception of the time axis with the extrapolated linear steady state, it is possible to obtain the time-lag by the following equation:

$$D = \frac{l^2}{6\theta} \qquad \text{Equation 1.14}$$

where θ is the time-lag; this relation demonstrates that establishing the steady-state concentration profile within the membrane takes longer for small D [33,60,63].

The polymer structure is an important parameter to take into account when considering the transport of gases through a polymer, since the transport in a glassy polymer is quite different from transport in a rubbery polymer. It is possible to classify diffusion in terms of three categories, which depend on the relative mobilities of the gas and the polymer:

- Fickian – the rate of diffusion is smaller than the relaxation modes of the polymeric matrix. The sorption equilibrium is quickly reached with this type of diffusion, the boundary conditions are independent of the time and do not depend on swelling kinetics.
- Non-Fickian – the diffusion is faster than the relaxation processes of the polymer. This mechanism has a strong dependence on the swelling kinetics.

- Anomalous diffusion – this refers to a process where the diffusion and the polymer relaxation rates are comparable. The sorption and the transport of molecules are affected by the presence of pre-existing microvoids in the matrix; the penetration is mainly dependent on the structure of the polymer.

1.5.2. Solubility Coefficient

Sorption is a term used to describe the capacity of a gas to penetrate in the polymer matrix and can be described in more than one model (see Figure 1.12). The thermodynamics of the penetrant-polymer system, in particular the nature and the force of the interaction, determines the amount of penetrant in the polymer matrix at equilibrium.

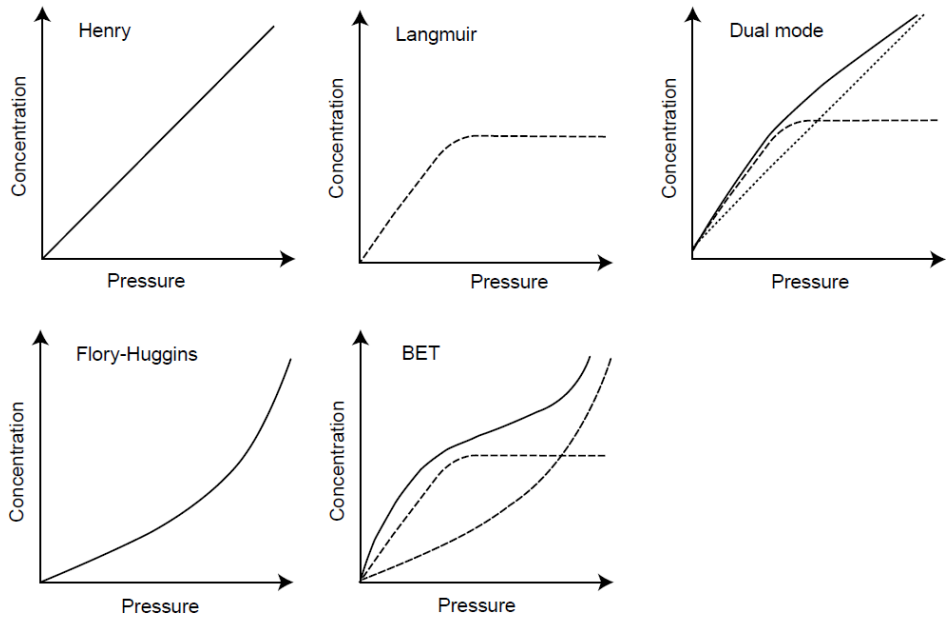

Figure 1.12 – Classical absorption models of the penetrant in the polymer matrix[33].

The classical models of sorption and they are:

- Henry's or Linear Sorption: this it is the simplest case as the gas is considered to be ideal and the relationship between the dissolved gas and there is a linear relation between the penetrant concentration and its partial pressure. This model is only observed at low pressure, when penetrant-polymer and

penetrant-penetrant interactions are weaker than polymer-polymer interactions, so the gas is dispersed in the matrix[29].

$$C_D = k_D P \qquad \text{Equation 1.15}$$

where C_D is the penetrant concentration by the Henry's sorption mode, k_D is the Henry's constant and P is the penetrant partial pressure.

- Langmuir Sorption: in this type of sorption, the predominant interactions are penetrant-polymer. The molecules of the penetrant occupy specific sites in the polymer, and when all sites are occupied, only a small amount of penetrant can solubilize subsequently[29]. The penetrant concentration is given by:

$$C_H = \frac{C_H^{'} \cdot b \cdot P}{1 + b \cdot P} \qquad \text{Equation 1.16}$$

where C_H is the penetrant concentration by the Langmuir's sorption mode $C_H^{'}$ is the Langmuir capacity factor or the saturation constant and b is the hole affinity constant.

- Dual-mode Sorption: this model combines the two models mentioned previously, the Henry and Langmuir Sorption[29,58]. At low pressures this model is closer to the Langmuir sorption model, while at higher pressures gets closer to the Henry's sorption model. Having this in mind is assumed it has two populations of diffusing molecules: by ordinary dissolution process (with concentration C_D) and trapped by absorption on microvoids or holes (with concentration C_H)[47]. So the total concentration can be written as:

$$C = C_D + C_H = k_D P + \frac{C_H^{'} \cdot b \cdot P}{1 + b \cdot P} \qquad \text{Equation 1.17}$$

This model is written with the assumption that gases do not interact with the polymer matrix, and so there is no swelling or plasticization.

- Flory-Huggins Sorption: this model assumes the penetrant-polymer interactions are weak compared with penetrant-penetrant interaction, so the concentration of penetrant continuously increases with pressure. It can be explained by the plasticization of the polymer by the gas absorbed or the association of clusters in the case of hydrophobic polymers. The model then takes the form of:

$$\ln a = \ln \frac{P}{P_0} = \ln \phi_1 + (1-\phi_1) + \chi (1-\phi_1)^2 \qquad \text{Equation 1.18}$$

where a is the activity of the component (quotient between vapour pressure, P, and the saturation vapour pressure, P^0), ϕ_1 is the volume fraction of the penetrant in the polymer and χ is the enthalpic interaction parameter between the penetrant and the polymer. When $\chi > 2$ the interactions are small, but some strong interactions exist for $0.5 < \chi < 2$ and high permeabilities may be expected, in the case of cross-linked polymers $\chi < 0.5$ [29].

- BET Sorption: The BET sorption mode combines the Langmuir and Flory-Huggins sorption mode and is representative of the absorption of water in highly hydrophobic polymers. Initially, the water molecules are strongly sorbed in specific sites, then, at higher pressure, a clustering process may occur. It represents a fundamental milestone in the interpretation of multilayer sorption isotherm. The concentration is represented by:

$$C = \frac{C_m \cdot k \cdot C_P / C_{sat}}{(1 - C_P / C_{sat}) \cdot \left[1 + (k-1)(C_P / C_{sat})\right]} \qquad \text{Equation 1.19}$$

where C_m is a parameter from BET isotherm, k is the equilibrium constant, C_P is the concentration of penetrant in the pore volume and C_{sat} is the saturation concentration of gas in the polymer at one temperature[64].

For lower pressure CO_2 behaves as ideal gas, so it is expect to observe Henry (or linear) sorption model; however the studied pressure in this work is too high to consider Henry sorption model in the full pressure range. The model, which better adapts to our system, will be discussed later in the solubility chapter.

1.5.3. Permeability Coefficient

Knowing that $Pe = D \times S$, from Equation 1.13 it is possible to derivate an equation that relates the permeability with pressure in the different chambers (upstream and downstream chamber), time and contact area. The equation is:

$$Pe = \frac{l}{A} \cdot \frac{\rho_{end} - \rho_{start}}{\rho_{STP}} \cdot \frac{V_{cell}}{\Delta P \cdot t} \qquad \text{Equation 1.20}$$

where l is the membrane thickness, A is the membrane contact area, ρ_{end} and ρ_{start} are the gas density at initial and final conditions of temperature and pressure, respectively, ρ_{STP} is the gas density at Standard Temperature and Pressure ($T = 273.15\,K$ and $P = 1\,bar$), V_{cell} is the volume of the downstream chamber, ΔP is the pressure gradient between the chambers and t is the total experimental time. Permeability depends on the polymer nature, the gas, pressure and temperature and it is expressed in $cm^3_{STP} \cdot cm^{-1} \cdot bar^{-1} \cdot s^{-1}$.

1.5.4. Parameters Affecting Transport Phenomena

1.5.4.1. Temperature Dependence

The temperature dependency of diffusion, solubility and permeability is described by the Arrhenius equation[29,60,65,66]:

$$D = D_0 \exp\left(-\frac{E_D}{RT}\right) \qquad \text{Equation 1.21}$$

$$S = S_0 \exp\left(-\frac{\Delta H_S}{RT}\right) \qquad \text{Equation 1.22}$$

$$Pe = Pe_0 \exp\left(-\frac{E_P}{RT}\right) \qquad \text{Equation 1.23}$$

where D_0, S_0 and Pe_0 are a temperature independent constant or pre-exponential factor for diffusion, solubility and permeability, respectively, E_D and E_P are the activation energies of diffusion and permeability, respectively, ΔH_S is the enthalpy of solution of the penetrant in the polymer, R is the universal gas constant and T the absolute temperature[67,68]. The three energy are related as follows:

$$E_P = E_D + \Delta H_S \qquad \text{Equation 1.24}$$

For gases the temperature dependence of the permeability coefficient is primarily governed by its kinetic component, E_D, since the thermodynamic component, ΔH_S, is relatively small[67,69]. Typically, gas diffusion increases significantly with temperature, if the polymer maintains its morphology and

crystalline structure. Moreover, the lower the permeability of gases, the higher activation energy is required, which is frequently a result of largest kinetic diameter.

The dissolution of a penetrant molecule into a polymer matrix, can be divided in two steps, condensation of the gas, and creation of a molecular scale gap in the polymer that accommodates the penetrant molecule. As result, the enthalpy of sorption ΔH_s can be computed, as follows:

$$\Delta H_s = \Delta H_{cond} + \Delta H_1 \qquad \text{Equation 1.25}$$

where ΔH_{cond} is the molar heat of condensation, and ΔH_1 is the partial molar heat of mixing. The partial molar heat mixing is a small and positive term, which can be estimated from the cohesive energy densities of the penetrant and the polymer by using Hildebrand´s theory:

$$\Delta H_1 = V_1 \left(\delta_1 - \delta_2\right)^2 \phi_2^2 \qquad \text{Equation 1.26}$$

In the case of CO_2, ΔH_s is negative due to the large negative contribution of ΔH_{cond} and a decrease of solubility will be observed with increasing temperature. The same does not occur for permanent gases, such as He or H_2, where ΔH_{cond} is small and ΔH_S is governed by ΔH_1.

1.5.4.2. Pressure Dependence

The effect of the permeability coefficient on pressure depends on the diffusing molecule type. Some literature[59,70] concludes that the pressure influence can be explained as the result of two opposite phenomena: one related to the hydrostatic pressure and the other due to the diffusing molecule concentration within the matrix, each of these effects leading to a different dependence of permeability:

- A hydrostatic pressure increase leading to an increase of the polymer density, thus reducing the free volume inside the polymer;
- The pressure increase corresponds to an increase of the penetrant concentration in the membrane. These diffusing molecules can plasticize the macromolecular chains, which mean an increase in free volume.

The first effect tends to retard the diffusion process by reducing the segmental motions whereas the second enhances it.

For high pressures strong anomalies can be observed with deviations from Henry's law. In this case, it is necessary to express the solubility terms of fugacity, f, rather than pressure, to take in to account the gas molecules compressibility:

$$C = S(T)\, f \qquad \text{Equation 1.27}$$

However, when the concentration of gas inside the polymer reaches higher values, this relation is no longer valid and it is necessary to use a thermodynamic model which better describes the influence of the gas concentration on the solubility, such as an equation of state model (e.g. SS, SL, SAFT or PC-SAFT).

1.6. Thesis outline

The main goal of this project was to clarify how transport properties, such as solubility and permeability, of gases in polymers were influenced by temperature, pressure and gas composition. Therefore, experimental measurements of those transport properties were conducted, using two different setups prepared to handle conditions of high pressure and temperature.

A magnetic suspension balance was used to measure the solubility of pure CO_2 in PVDF at 403 K and XLPE at 363 K up to 300 bar (Chapter 2), where the solubility temperature dependency and pressure dependency could be studied deeply.

The permeability of pure CO_2 and mixtures of CO_2 and CH_4 were measured in PVDF, XLPE and PA11 (the gas permeability in PA11 was just conducted for pure CO_2) at temperatures up to 403 or 363 K and pressures in the range of 150 to 650 bar, depending on the polymer. Since the studied gas is not under ideal conditions (high pressure), the permeability was calculated based in pressure and fugacity difference between the chambers and compared both methods (Chapter 3).

The permeability is related to the overall mass transport: it accounts for both solubility and diffusion, being proportional to the product of these two quantities. After measured the solubility and the permeability, the diffusion was calculated, and was observed the diffusion has a more pronounced effect in the permeability (Chapter 4).

In addition to the experimental lab work, a modelling study of the gas solubility in polymers was implemented. The goal was to describe the solubility as a function of pressure for each temperature and polymer. This model could be the basis for predicting the overall mass transport through polymers (Chapter 5).

Chapter 2

Chapter 2. Solubility Experiments

In order to measure the solubility four methods are commonly used: gravimetric[71–75], oscillatory[76–78], pressure decay or PVT (pressure-volume-temperature)[44,79] and flow[80]. The gravimetric method is based in the quantification of the weight variation caused by the penetrant molecules in the polymer matrix. However, the maximum operation pressure, which is low, is a drawback that can be overcome by the introduction of a magnetic coupling to transmit the weight to an external microbalance. The oscillation method, is an indirect method to measure the solubility, because the variation of polymer weight is related to a piezoelectric crystal (usually quartz) or metal reed. The pressure decay is the oldest method and it consists of placing the polymer sample in a chamber with known volume, and measure the decrease of pressure inside the container and relate it with the volume of gas absorbed by the polymer. The flow method is the least used method, relying on inverse gas chromatography, where the polymer is the stationary phase in a chromatographic column and retention times for the gas is obtained[71,81,82].

2.1. Materials and Setup

National Oilwell Varco (NOV) supplied the polymers used to measure the solubility. The samples came directly from an extruded pipe intended to be used in offshore applications, where the polymer is machined down to a thickness of 1 mm, approximately, and then cut into circular discs. Enough disks were used to make up a polymer mass of about 0.5 g (usually 5 disks). In this chapter the studied polymers are PVDF and XLPE. The solubility of CO_2 in PA11 was not studied because it changes weight in the presence of CO_2, as it will be discussed in Chapter 3. AGA A/S supplied CO_2 with a purity of 99.995 %.

The solubility measurements were obtained using a magnetic suspension balance (MSB) from Rubotherm GmbH, which is represented in Figure 2.1.

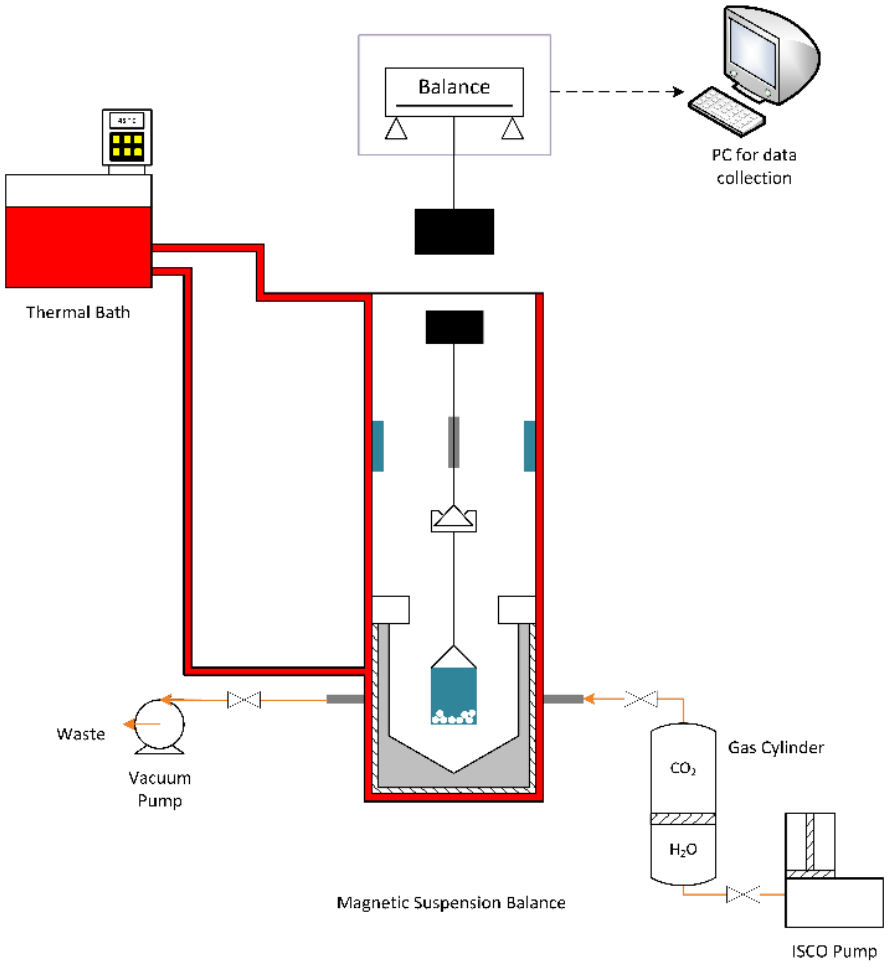

Figure 2.1 - Schematic diagram of the MSB.

It consists of a scale, which enables the weighing of samples in almost all environments at controlled temperature and pressure, while the scale itself remains at room conditions. The sample is placed in a sample container that is connected to a permanent magnet. Under the scale there is an electromagnet that attracts the magnet whenever there is an electric current passing through it[73]. This makes it possible to find the mass of the Sample Container/Sample system. The density of the gas at the current temperature and pressure conditions is determined by measuring the weight of the Sample Container/Sample/Sinker system, where the weight and the volume of the sinker are previously known. To correct the buoyancy an initial measurement with argon (Ar) is performed.

The MSB is connected to a thermostat to keep the system temperature constant. The temperature is measured by a Pt-100 thermocouple, which is installed near the Sample Container. To keep the pressure

constant an ISCO pump is used; the ISCO pump maintains the pressure in the system using water as a hydraulic fluid. The equipment is connected to a computer through the MessPro software, which records temperature, pressure, weight of the Sample Container/Sample system and the density as a function of the time. Resolution and accuracy of the MSB are 0.01 mg and 0.002%, respectively. The operating limits of balance are temperatures up to 473 K and pressures up to 350 bar, however since CO_2 is a corrosive gas the maximum temperature limit is 373 K.

All the experiments started with evacuation to remove any gases that may have been absorbed in the polymer.

2.2. Data Analysis

To obtain the solubility two experiments need to be performed. Firstly a run with an inert gas that is insoluble in the polymer (Ar), and then with the desired gas (CO_2) can be analysed.

From the experiment with Ar, a linear trendline of the measured weight as a function of the gas density is plotted and from the slope and the y-intercept the volume and the weight of the Sample Container/Sample system is obtained, respectively. Knowing the weight and volume of the Sample Container is possible to obtain the exact weight and volume of the sample. The mass of dissolved gas in the polymer matrix is then obtained from the experiment with CO_2 from Equation 2.1:

$$m_{CO_2} = m - m_{SC} - m_S + (V_{SC} + V_S) \times \rho_{CO_2} \qquad \text{Equation 2.1}$$

where m_{CO_2} is the mass of CO_2 dissolved in the polymer matrix, m is the weight given by the set-up, m_{SC} is the mass of the sample container, m_S is the mass of the sample, V_{SC} is the volume of the sample container, V_S is the volume of the sample and ρ_{CO_2} is the density of CO_2.

However, plotting m_{CO_2} as a function of ρ_{CO_2} it was noticed, after a certain ρ_{CO_2}, the CO_2 absorbed mass in the polymer decreased with increasing gas density (and so with gas pressure), for both polymers. This behaviour is due to the swelling of the polymer that cannot be neglected and it is necessary to consider it in the buoyancy correction.

The total volume variation (from the polymer itself and the absorbed gas) is obtained from plotting m_{CO_2} as a function of ρ_{CO_2}. The slope of the trendline between the experimental data points where the absorbed CO_2 mass decreases corresponds to the total volume change, ΔV.

$$m_{CO_2,corrected} = m - m_c - ms + (Vsc + Vs + \Delta V) \times \rho CO_2 \quad \text{Equation 2.2}$$

The corrected mass of CO_2 absorbed in the polymer ($m_{CO_2,corrected}$) is obtained with Equation 2.2, where ΔV, the change in the volume is defined by:

$$\Delta V = V_{CO_2} + V_{swelling} \quad \text{Equation 2.3}$$

where V_{CO_2} is the volume of the molecules dissolved in the polymer and $V_{Swelling}$ is the volume caused by the polymer swelling. Knowing the V_{CO_2} (calculated by the gas density and the corrected mass of CO_2), $V_{swelling}$ is obtained. The percentage of swelling is then calculated through:

$$\%swelling = \frac{V_{swelling}}{V_s} \cdot 100 \quad \text{Equation 2.4}$$

The solubility is the ratio between the absorbed gas mass in the polymer and the initial mass of the polymer and this value is expressed in $g_{gas} \cdot g_{polymer}^{-1}$

$$S = \frac{m_{CO_2,corrected}}{m_S} \quad \text{Equation 2.5}$$

For more details See Appendix 1, where a calculation example (XLPE at 363 K and pressure up to 300 bar) is presented.

2.3. Experimental Results and Discussion

The experimental solubility of pure CO_2 was studied as a function of temperature and pressure for two polymers: PVDF and XLPE, and the performed tests overview is listed in Table 2.1.

Table 2.1 – Matrix of the solubility tests, where ■ represent PVDF series 1, (■) PVDF series 2 and ● XLPE.

P (bar) / T (K)	318	333	348	363	383	403
15					(■)	(■)
25	■	■	■	■		
30					(■)	(■)
40	(■), ●	●	(■), ●	●		
45					(■)	(■)
50	■	■	■	■		
60					(■)	(■)
75	■	■	■	■	(■)	(■)
80	(■), ●	●	(■), ●	●		
100	■, (■), ●	■, ●	■, (■), ●	■, ●	(■)	
125	■	■	■	■		
140	(■), ●	●	(■), ●	●	(■)	
150	■	■	■	■		
180	(■), ●	●	(■), ●	●	(■)	
200	(■), ●	●	(■), ●	●	(■)	
240	(■), ●	●	(■), ●	●	(■)	
280	(■), ●	●	(■), ●	●		
300	(■), ●	●	(■), ●	●		

The test conditions regarding pressure and temperature were chosen according to NOV requirements, initially the goal for PVDF was 150 bar at 318, 333, 348 and 363 K, but along the project it was decided to study higher conditions of pressure(up to 300 bar) and temperature(up to 403 K). For clear presentation it was separated in series 1 for the first set of experiments (up to 150 bar at 318, 333, 348 and 363 K for PVFD) and in series 2 for the extended conditions of pressure and temperature (up to 300 bar at 383 and 403 K).

The solubility measurements are summarized in Table 2.2, Table 2.3 and Table 2.4 as a function of pressure and temperature. At each condition, the measurement was repeated three times, nevertheless in the presented tables only the average values are shown. The deviations of the repetitions are shown in the form of error bars in the plots of the experimental results. All the presented experimental results are corrected by the swelling (see section 2.4 for more detail).

Table 2.2 – Solubility of CO_2 in PVDF, series 1 at 318, 333, 348 and 360 K, for pressures up to 150 bar.

Pressure (bar)	**Temperature (K)**	**Solubility ($g_{gas}/g_{polymer}$)**	**Pressure (bar)**	**Temperature (K)**	**Solubility ($g_{gas}/g_{polymer}$)**
25	318	0.01634	25	348	0.01260
50	318	0.03679	50	348	0.02456
75	318	0.05558	75	352	0.03380
100	318	0.05530	100	348	0.04238
125	318	0.06614	125	348	0.04404
150	318	0.07624	150	348	0.04162
25	333	0.01466	25	360	0.01032
50	333	0.02905	50	360	0.02018
75	333	0.03965	75	360	0.02897
100	333	0.04453	100	360	0.03586
125	333	0.03846	125	360	0.03953
150	333	0.03684	152	360	0.03953

The solubility of CO_2 in PVDF was intended to be measured at 318, 333, 348 and 363 K, unfortunately the highest temperature was not reached and we were just able to measure it at 360 K.

Table 2.3 – Solubility of CO_2 in PVDF, series 2 at 317, 347, 384 and 405 K, for pressures up to 300 bar.

Pressure (bar)	**Temperature (K)**	**Solubility ($g_{gas}/g_{polymer}$)**	**Pressure (bar)**	**Temperature (K)**	**Solubility ($g_{gas}/g_{polymer}$)**
40	316	0.01696	15	384	0.01036
80	317	0.06502	30	384	0.00913
100	317	0.06502	45	384	0.01429
140	317	0.10912	60	384	0.01877
180	317	0.11763	75	384	0.02293
200	317	0.12053	100	384	0.02968
240	317	0.12477	140	384	0.03422
280	317	0.12816	180	384	0.03287
300	317	0.12979	200	384	0.03172
40	347	0.01946	240	384	0.03037
80	347	0.03695	15	405	0.00393
100	347	0.04319	30	405	0.00781
140	347	0.04284	45	405	0.01154
180	347	0.04209	60	405	0.01507
200	347	0.04319	75	405	0.01817
240	348	0.04523			
280	348	0.04671			
300	348	0.04792			

As seen previously the temperature goal was not reached. It was 318, 348, 384 and 403 K, but actually the measured temperatures were 317, 347, 384 and 405 K, which is close enough by the study point of view.

Table 2.4 – Solubility of CO2 in XLPE at different pressures and temperatures.

Pressure (bar)	**Temperature (K)**	**Solubility ($g_{gas}/g_{polymer}$)**	**Pressure (bar)**	**Temperature (K)**	**Solubility ($g_{gas}/g_{polymer}$)**
40	318	0.02207	40	348	0.01593
80	318	0.04361	80	348	0.02646
100	318	0.04361	100	348	0.02929
140	318	0.08354	140	348	0.02596
180	318	0.09480	180	348	0.02843
200	318	0.09854	200	348	0.03181
240	318	0.10427	240	348	0.04080
280	318	0.10771	280	348	0.04627
300	318	0.11101	300	348	0.04783
40	333	0.01679	40	362	0.01500
80	333	0.03069	80	362	0.02696
100	333	0.03281	100	362	0.03048
140	333	0.03127	140	362	0.03155
180	333	0.04840	180	363	0.03089
200	333	0.05445	200	363	0.03184
240	333	0.06266	240	362	0.03614
280	333	0.06830	280	362	0.03873
300	333	0.07115	300	362	0.04022

The experimental results are plotted in Figure 2.2 and Figure 2.3, with the error bars. To better compare the obtained results for solubility, both series 1 and 2, are presented in the same graph. The figures show the solubility of pure CO_2 in PVDF, at 318, 333, 348, 363, 383 and 403 K to pressures up to 300 bar, and XLPE, at 318, 333, 348 and 363 K to pressures up to 300 bar. It is possible to observe the solubility increases with increasing pressure; however, between 75 and 100 bar, an unusual solubility behaviour is observed, independent of the polymer, where the solubility does not increase with increasing pressure. This behaviour is more visible at lower temperature. Observing the CO_2 phase diagram (Figure 1.4), while considering constant temperature, the CO_2 changes state from gas to supercritical at 73.8 bar. Therefore, we believe this unusual behaviour is related with the change in the state of CO_2, from gas to supercritical and the inevitable swelling of the polymer in contact with supercritical CO_2.

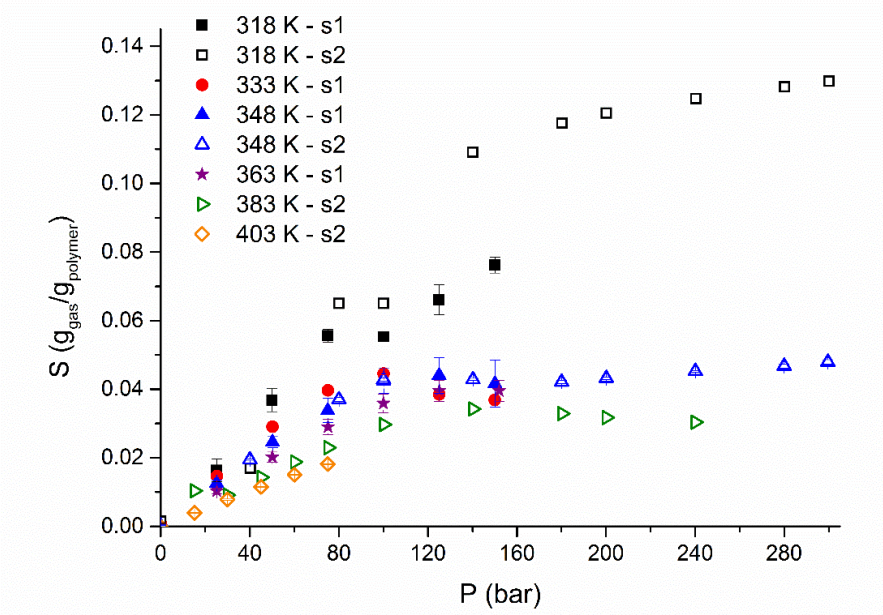

Figure 2.2 – Solubility of pure CO_2 in PVDF at 318, 33, 348, 363, 382 and 403 K up to 300 bar. The bars represent the error of the measurements.

Despite the same conditions, for most of the experimental points, s1 and s2 differ at 318 K. The explanation could not be found and s2 was just performed once, so it would be relevant to repeat the experimental data.

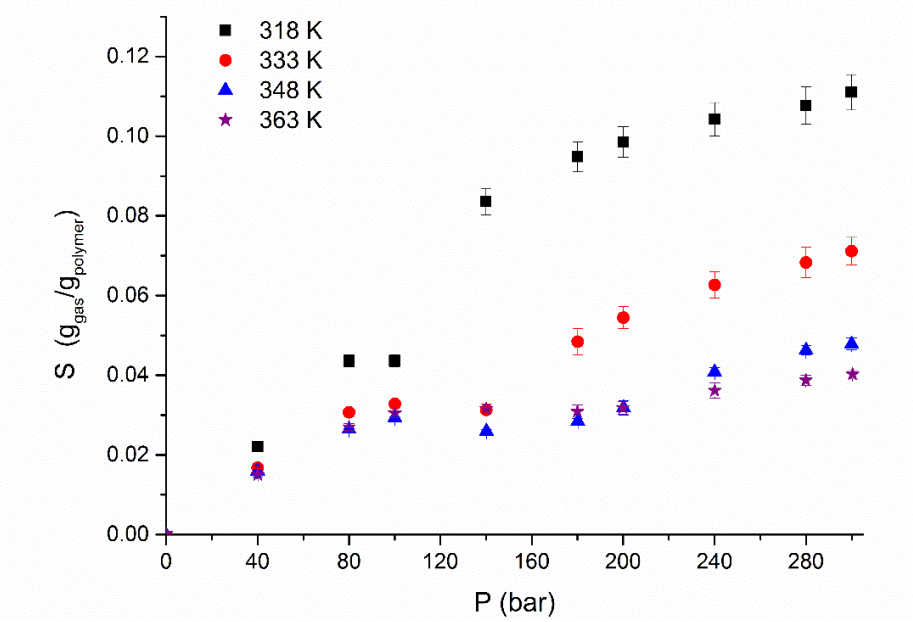

Figure 2.3 – Solubility of pure CO_2 in XLPE at 318, 333, 348 and 363 K up to 300 bar. The bars represent the error of the measurements.

As it is seen, from the Figure 2.2 and Figure 2.3, CO_2 has a higher solubility in PVDF than in XLPE for most of the tested conditions, this difference is higher at 348 K, however in the other three studied temperatures there is not a significant difference.

The influence of the temperature in the solubility coefficient was also studied and, for both polymers, it was observed that the solubility decreases with increasing temperature. The solubility of pure CO_2 in PVDF nearly doubles when the temperature decreases from 360 to 318 K, at 150 bar, while in XLPE the influence is more significant, decreasing by almost a factor of three when the temperature also decreases from 362 to 318 K, at 300 bar. Comparing both polymers it is possible to confirm, at 100 bar, the decrease of solubility with increase of temperature has approximately the same coefficient (1.5).

Through the plotting of linearized Arrhenius equation (Equation 1.22) is possible to determine the unknown variables from Equation 1.22, using the slope and the y-intercept of the trendline from the experimental data. Figure 2.4 and Figure 2.6 show the natural logarithm of CO_2 solubility, in the two studied polymers as a function of the inverse temperature for the different pressures, in order to obtain the ΔH_S.

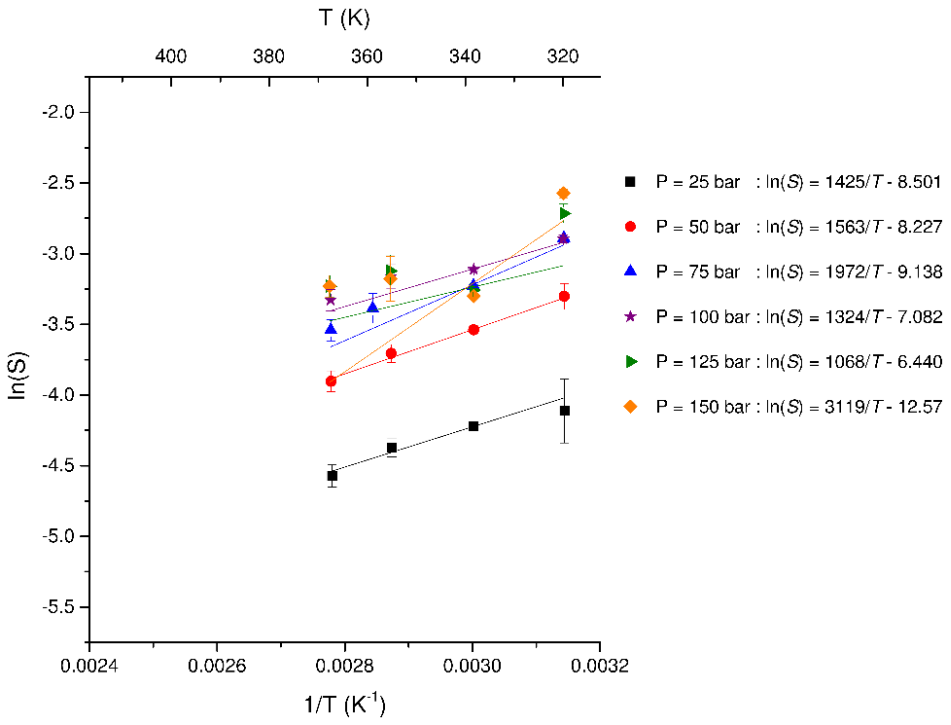

Figure 2.4 – Logarithm function of solubility as a function of inverse temperature for PVDF, series 1. Points are the experimental data and the lines are the linear fitting of those experimental points.

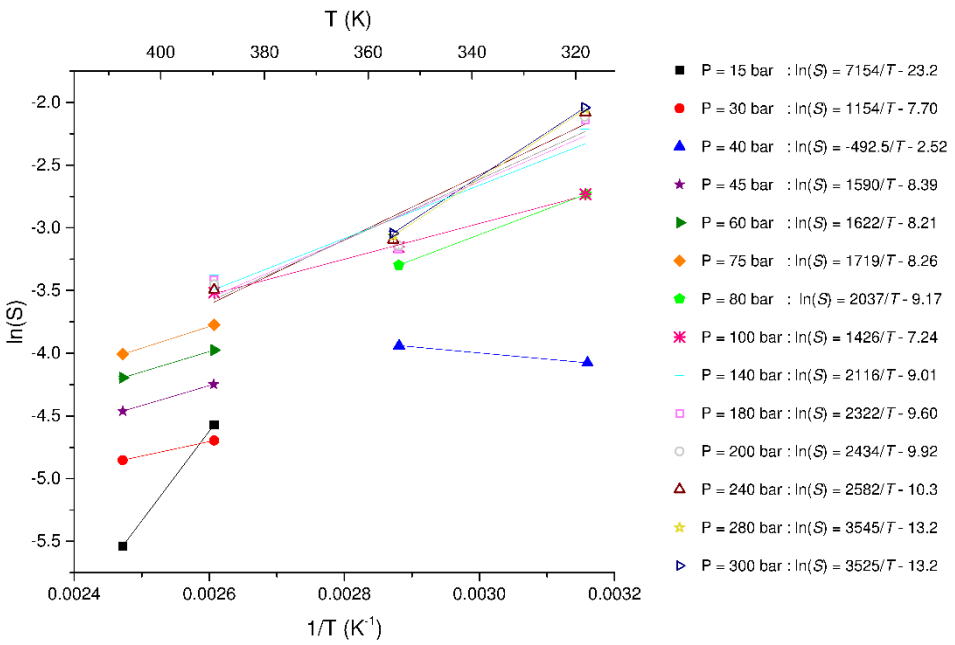

Figure 2.5 – Logarithm function of solubility as a function of inverse temperature for PVDF, series 2. Points are the experimental data and the lines are the linear fitting of those experimental points.

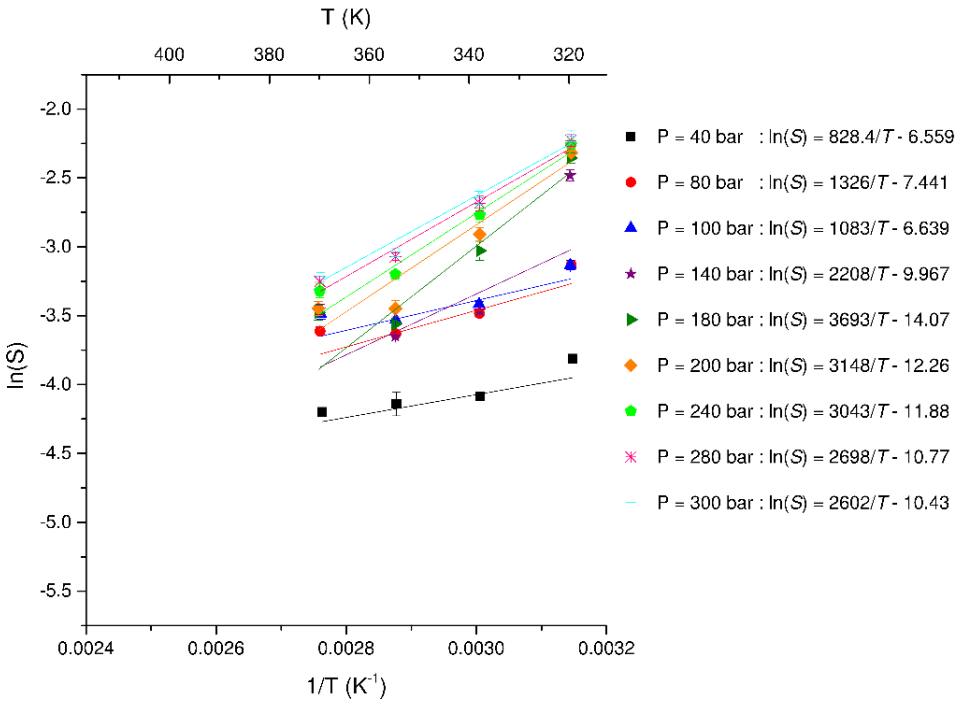

Figure 2.6 – Logarithm function of solubility as a function of inverse temperature for XLPE. Points are the experimental data and the lines are the linear fitting of those experimental points.

Using the linear regressions from Figure 2.4, Figure 2.5 and Figure 2.6, it is possible to obtain the heat of dissolution of one mole of penetrant in the polymer; ΔH_S values are shown in Table 2.5 and Table 2.6. A ΔH_S negative expresses the fact that CO_2 is less soluble in the polymer when the temperature is higher[33]. Comparing the PVDF values of ΔH_S with the literature[38] it is possible to verify that they are in the expected range (between -20 and -10 kJ/mol), although the reported values in literature are for 40 bar and we are presenting much higher conditions of pressure. The same comparison with the literature for XLPE was not possible since it is a new-developed polymer and there are no previous studies with this polymer.

Table 2.5 – Heat of solution (ΔH_S) of CO_2 in PVDF, for series 1 and 2, for different pressure conditions.

Series 1			**Series 2**		
Pressure (bar)	ΔH_S (kJ/mol)	r^2	**Pressure (bar)**	ΔH_S (kJ/mol)	r^2
25	-12	0.961	15	-59	-
50	-13	0.986	30	-10	-
75	-16	0.910	40	4	-
100	-11	0.908	45	-13	-
125	-9	0.571	60	-13	-
150	-26	0.450	75	-14	-
			80	-17	-
			100	-12	0.999
			140	-18	0.892
			180	-19	0.892
			200	-20	0.313
			240	-21	0.950
			280	-29	-
			300	-29	-

The only common pressure point between series 1 and 2 is 100 bar. Comparing the ΔH_S between both series the calculated error is 14%, therefore is concluded the difference in within the experimental error.

Table 2.6 – Heat of solution (ΔH_S) of CO_2 in XLPE for different pressure conditions.

Pressure (bar)	ΔH_S **(kJ/mol)**	**r²**
40	-7	0.511
80	-11	0.724
100	-9	0.694
140	-18	0.284
180	-31	0.821
200	-26	0.897
240	-25	0.939
280	-22	0.957
300	-22	0.966

Most previous experimental work in the area does not report the exact conditions of pressure presented in this work, apart from Bonavoglia *et al.*[83], our conditions are more extreme regarding pressure. In Figure 2.7 however it is possible to compare the experimental results obtained in this work with the literature for PVDF.

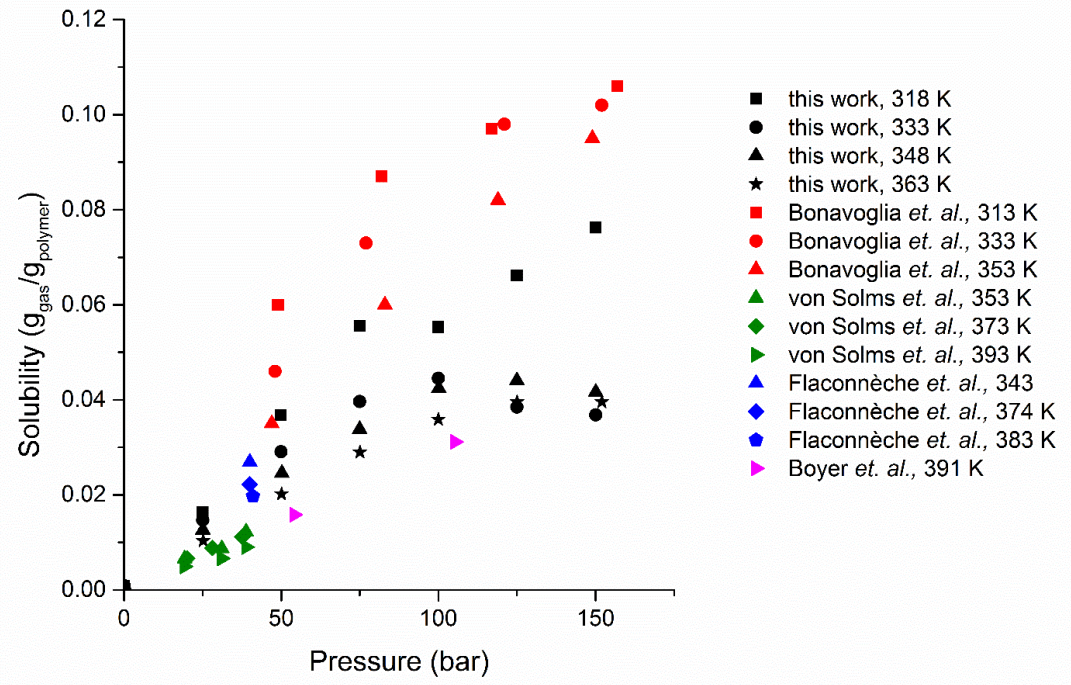

Figure 2.7 – Points measured in this work compared with literature data.

It is possible to conclude our results are in agreement with the literature, nevertheless is necessary to refer that PVDF used in the work by Bonavoglia *et al.*[83] is an amorphous polymer, so the higher solubility is expected since our polymer is semi-crystalline. The same comparison for XLPE is not possible, since is a new-developed polymer, where no other solubility data exists.

2.4. Swelling of polymers

The polymers contacting supercritical CO_2 tend to swell[74,84,85]. This swelling might not be significant for lower pressures, yet with increasing pressure it needs to be considered. There are two ways to obtain the swelling of the polymer, the first is experimental and the second through an EOS. The experimental measurements of the swelling are difficult to obtain, since it needs a special setup with a window to allow the direct visualisation of the sample. There are some equations of state reported which can predict swelling, however experimental validation is difficult since there is a paucity of data. In the present work, the swelling of both polymers was estimated based on an experimental data analysis method (referred in the Data Analyses section). The experimental estimation was also fitted with the sPC-SAFT EOS (See Chapter 5).

Table 2.7 shows the swelling of both polymers calculated based in this experimental method.

Table 2.7 – Swelling of PVDF and XLPE using an experimental estimation. The data refer to the highest conditions of pressure, 150 and 300 bar for PVDF and XLPE, respectively.

PVDF		**XLPE**	
Temperature (K)	**Swelling (%)**	**Temperature (K)**	**Swelling (%)**
318	24	318	1.9
333	18	333	2.5
348	20	348	2.9
363	17	363	3.6

It is possible to conclude the swelling increases with increasing temperature for XLPE, this is due to the increase in the chain mobility. The PVDF dependence is not obvious since it varies according the

temperature. As expected, the swelling of XLPE is quite low even for high temperatures since it is a cross-linked polymer having a low chain mobility.

The swelling affects the buoyancy of the polymer, since buoyancy is strongly related with the volume of the system polymer/dissolved gas. Since our experimental method needs to be corrected for the buoyancy effect, if the swelling is ignored the experimental results will be incorrect (see Appendix 1 for the detailed buoyancy correction).

Chapter 3

Chapter 3. Permeability Experiments

3.1. Materials and Setup

National Oil Varco (NOV) supplied the polymer samples used in this study. They came from extruded pipe intended for offshore use and were machined down to the required thickness (1 mm) and then cut into circular discs of 10 cm, approximately. AGA A/S supplied CO_2, with a purity of 99.995 %, CH_4, with a purity of 99.5% and the mixtures between CO_2 and CH_4, with a purity of 99.2%.

Figure 3.1 shows the 2-D permeation cell, which allows the measurement of the permeability.

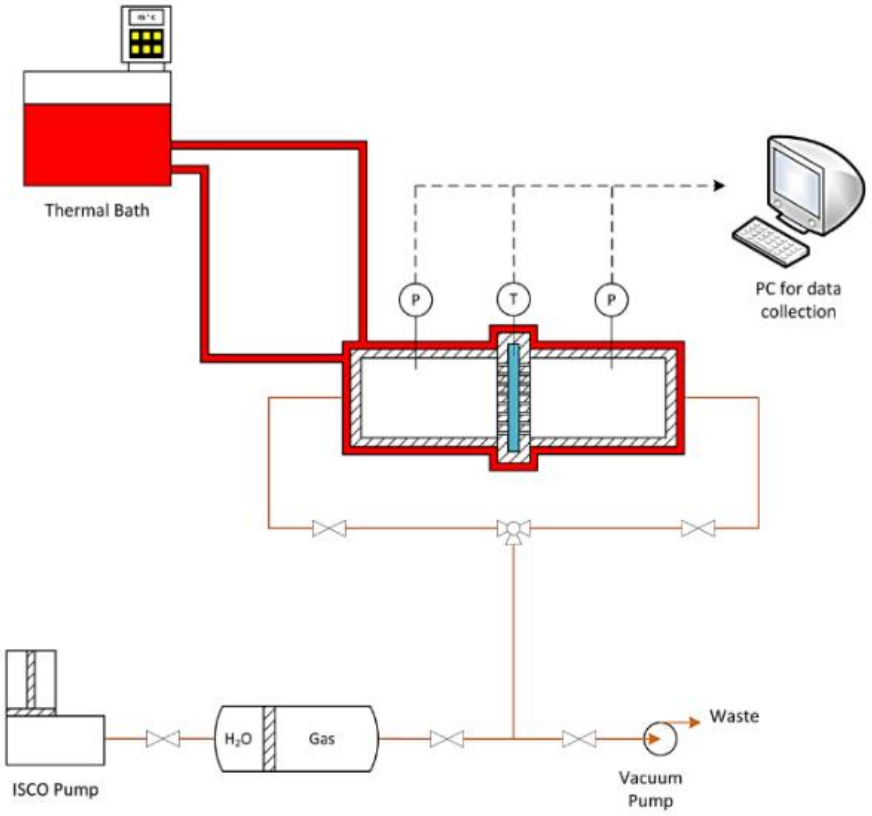

Figure 3.1 – Schematic diagram of the a) 2-D permeation cell set-up and b) Magnetic Suspension Balance (MSB).

The 2-D permeation cell was designed in house and the maximal operating temperature and pressure are limited to 420 K and 700 bar. The cell consists of two stainless steel chambers: an upstream (or high-pressure) chamber and a downstream (or low-pressure) chamber, and the polymer sample is placed between. During the measurement two porous plates support the polymer on both sides to prevent sagging. The plates allow the gas to freely contact the sample, where the exposed polymer area is 38.48 cm^2. The downstream chamber has a free internal volume of 22.057 cm^3, in the upstream chamber, a high pressure ISCO syringe pump is used, to ensure the pressure is constant during the entire experiment using water as a compressor fluid. The two chambers are held together by two stainless steel flanges, which are securely fastened by eight heavy-duty bolts. The entire cell (after assembly) is mounted on a hook on a frame in the fume hood, where the stainless steel tubing is connected to the chambers. Depending on the specified test temperature, hot water or glycerine is used to maintain the temperature of the system. The temperature is measured by a PT-100 thermocouple placed between two chambers, where the membrane is located, and Fisher-Rosemount pressure transducers are used to measure the pressure inside the chambers. The membrane is initially evacuated at the experimental temperature, in order to remove any atmospheric absorbed gas, by applying vacuum for several hours.

3.2. Data analysis

The upstream and downstream chamber are exposed to the gas at the desired pressures and temperature for 30 minutes and then the downstream chamber is depressurized 50 bar, so there is a pressure gradient of 50 bar between the chambers. The experiment is finished when a 25 bar difference, between chambers, is observed, which takes at least 170 hours, approximately. The thickness of the disc is measured, *prior* the test, using a calliper at several different locations and the values are averaged. The setup is connected to a computer and an in-house developed software records the pressure and the temperature, as function of time. The permeability is then calculated using Equation 1.20[82,86–88]. The initial and final gas densities are calculated using REFPROP[27] according to the conditions of pressure and temperature.

3.3. Experimental Results and Discussion

The experimental permeability of pure CO_2, pure CH_4 and mixtures between CO_2 and CH_4 were studied as function of temperature and pressure for three polymers: PVDF, XLPE and PA11. The performed tests are listed in Table 3.1.

Table 3.1 – Matrix of the permeability tests, where ■ represent PVDF, ● XLPE and ▲ PA11. The gas is represented by x/y, where x and y are CO_2 and CH_4 percentages.

P (bar) / T (K)	318	333	348	363	383	403
75	100/0 (■) 90/10 (■)			100/0 (■) 90/10 (■)	90/10 (■)	90/10 (■)
100	100/0 (■,●,▲) 90/10 (■,●) 75/25 (●) 50/50 (●) 25/75 (●) 0/100 (●)	100/0 (■,●,▲) 90/10 (■,●)	100/0 (■,●,▲) 90/10 (■,●)	100/0 (■,●,▲) 90/10 (■,●)		
150	100/0 (■) 90/10 (■)			100/0 (■) 90/10 (■)		
200	100/0 (●,▲) 90/10 (●) 75/25 (●) 50/50 (●) 25/75 (●) 0/100 (●)	100/0 (●,▲) 90/10 (●)	100/0 (●,▲) 90/10 (●)	100/0 (●,▲) 90/10 (●)		
345					90/10(■)	
350	100/0 (●,▲) 90/10 (●)	100/0 (●,▲) 90/10 (●)	100/0 (●,▲) 90/10(●)	100/0 (●,▲) 90/10 (●)		
650	100/0 (●,▲) 90/10 (●)	100/0 (●,▲) 90/10 (●)	100/0 (●,▲) 90/10 (●)	100/0 (●,▲) 90/10 (●)		

The test conditions were chosen in accordance with NOV requirements; however, a wide range of tests were performed in order to cover several conditions of temperature, pressure and gas compositions, to study the influence of this factors in the permeability. Most of the tests were performed only once, because of the duration of each test. Nevertheless, in order to evaluate the reproducibility of the tests, the experiments with XLPE at 200 bar and 318 K, with gas composition 90 mol% CO_2 and 10 mol% CH_4 and pure CO_2, were repeated. From these tests was found an error of 13% for the gas mixture and 5% for the pure CO_2 measurement, which are inside the acceptable range for these experimental conditions.

3.3.1. Pure CO_2

The results are presented in Table 3.2, Table 3.3 and Table 3.4, as well as the available literature comparison [86], for PA11 and PVDF. Literature results are reported for lower pressure conditions (*ca.* 40 bar)[86], than studied in this work. However, if the permeability trend from this work is extrapolated to these pressures, it is possible to verify for PVDF (Table 3.2) and PA11 (Table 3.4) that the obtained results are fair agreement with the reported literature values.

Table 3.2 – Permeability of pure CO_2 in PVDF at different temperatures and pressures, where USC is the upstream chamber. Literature values from Flaconnèche *et al*.[86] are indicated for comparison.

Pressure in the USC (bar)	**Temperature (K)**	**Pe x 10^7 ($cm^3_{STP}·cm^{-1}·bar^{-1}·s^{-1}$)**
40	343	0.485[86]
41	374	1.67[86]
78	318	0.569
77	360	1.50
101	318	0.79
106	333	1.29
104	348	1.78
107	363	2.49
149	319	1.14
150	364	5.91

Table 3.3 – Permeability of pure CO_2 in XLPE at different temperatures and pressures, where USC is the upstream chamber.

Pressure in the USC (bar)	**Temperature (K)**	**Pe x 10^7 ($cm^3_{STP}·cm^{-1}·bar^{-1}·s^{-1}$)**
101	319	0.999
103	333	1.78
103	348	2.79
103	362	4.59
207	318	0.531
201	334	1.26
201	348	2.40
199	363	4.35
351	319	0.516
351	334	1.32
350	349	2.39
351	363	4.43
656	318	0.163
648	334	0.467
645	347	0.887
646	363	2.07

Table 3.4 – Permeability of pure CO_2 in PA11 at different temperatures and pressures, where USC is the upstream chamber. Literature values from Flaconnèche *et al.*[86] are indicated for comparison.

Pressure in the USC (bar)	**Temperature (K)**	**Pe x 10^7 ($cm^3_{STP}·cm^{-1}·bar^{-1}·s^{-1}$)**
42	344	0.231 [86]
43	374	0.545 [86]
108	320	0.329
110	362	1.21
205	319	0.164
218	363	1.48
354	318	0.184
354	362	0.904
646	319	0.118
659	333	0.446
648	348	0.913
661	363	1.18

A significant variation of the permeability is observed with temperature. Table 3.2 shows when the temperature increases from 318 to 363 K the CO_2 permeability in PVDF increases by a factor of three, at 75 bar, and a factor of five at 150 bar. Similarly, Table 3.3 shows that increasing temperature, also from 318 to 363 K, increases the permeability by a factor of five in XLPE at 100 bar, while at a pressure of 650 bar the permeability increases by a factor of 13 for the same range of temperatures. Table 3.4 shows the permeability in PA11 also increases with increasing temperature by a factor of four at 100 bar and a factor of 11 at 650 bar. These results can be explained by the increase of the polymer chain mobility with temperature, resulting in an increase of the diffusivity [87], as it will be discussed later.

In order to verify the Arrhenius temperature dependency, the natural logarithm of permeability was plotted as function of the inverse temperature. The resulting graphs are presented in Figure 3.2, Figure 3.3 and Figure 3.4, for PVDF, XLPE and PA11, respectively.

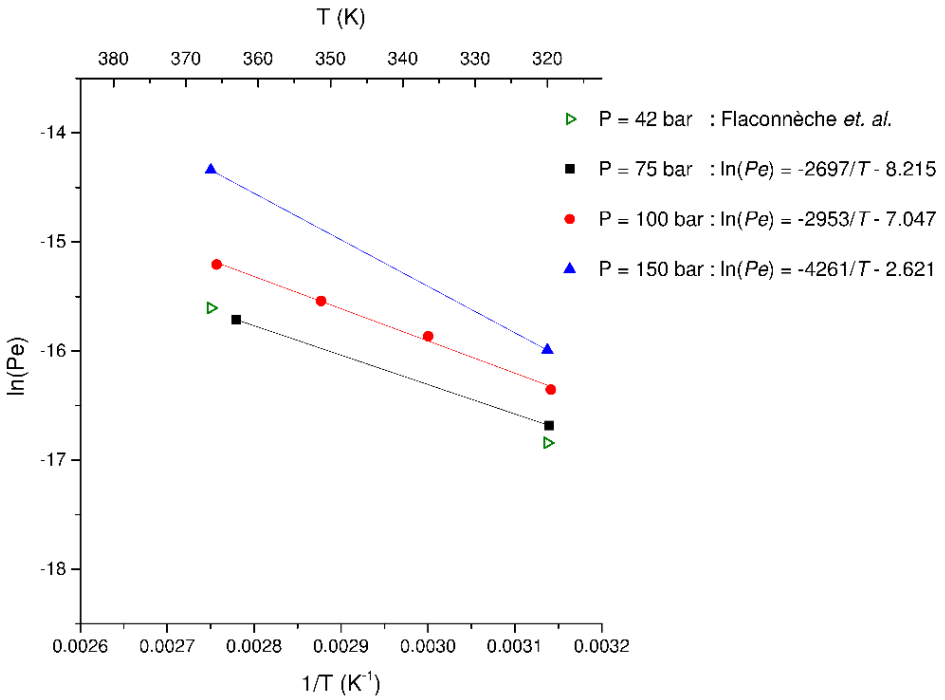

Figure 3.2 – CO_2 permeability in PVDF at different temperatures. Points are the experimental data and the lines are the corresponding linear data fits. The open triangles represent values reported in the literature[86].

It is possible to observe the Arrhenius temperature dependency is followed for the three polymers at the studied conditions of temperature.

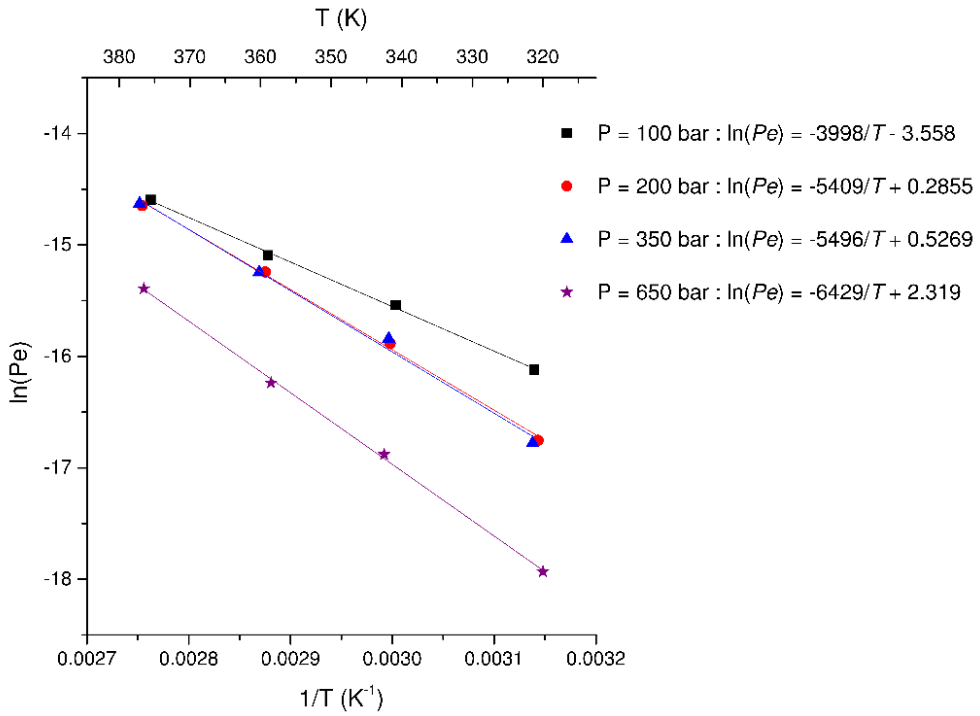

Figure 3.3 – CO_2 permeability in XLPE at different temperatures. Points are the experimental data and the lines are the corresponding linear data fits.

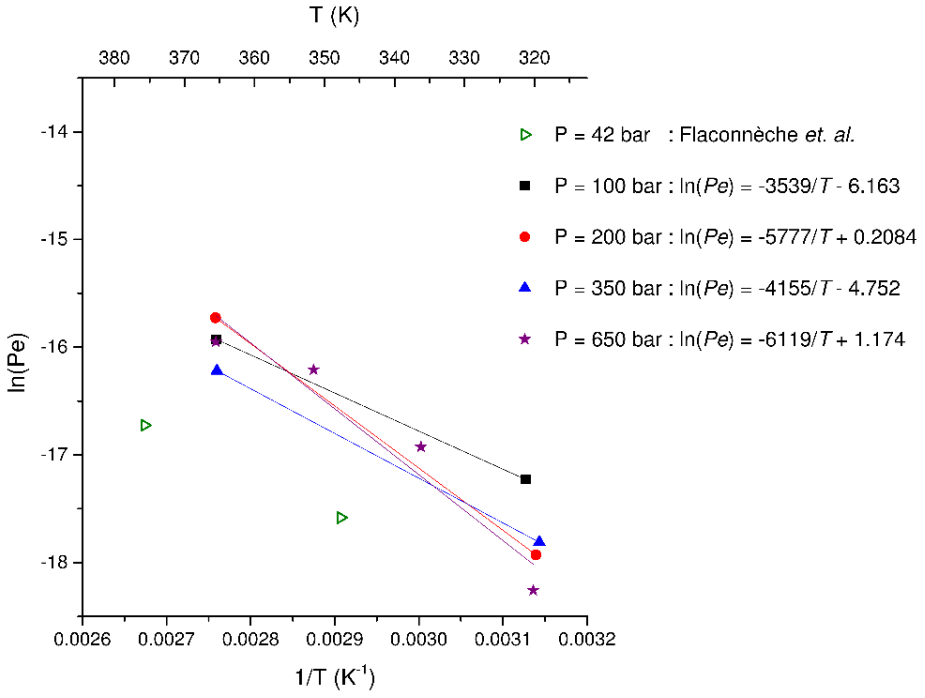

Figure 3.4 – CO_2 permeability in PA11 at different temperatures. Points are the experimental data and the lines are the corresponding linear data fits. The open triangles represent values reported in the literature[86].

Through Figure 3.2, Figure 3.3 and Figure 3.4, it is also possible to obtain the activation energy of permeability, using Equation 1.23, where the slope of the linear trendline represent the activation energy of permeability, E_P, for each polymer at a specific pressure, being the results showed in Table 3.5.

Table 3.5 – Apparent activation energy for permeability from Equation 1.23.

Polymer	**Pressure**	**E_P (kJ·mol^{-1})**	**r^2**
PVDF	75	22	-
	100	25	0.993
	150	35	-
XLPE	100	33	0.998
	200	45	0.997
	350	46	0.991
	650	53	0.999
PA11	100	29	-
	200	48	-
	350	35	-
	650	51	0.890

Comparing the obtained results of E_P with the literature, we could conclude it is in good agreement; however, this comparison can only be made for PVDF and PA11. In 1970 Ash *et al.*[89] obtained E_P equal to 34 kJ/mol for PA11, years later in 2001 Flaconnèche *et al.*[86] reported that E_P was between 30 and 36 kJ/mol for PVDF and 35 kJ/mol for PA11.

Observing Figure 3.2, Figure 3.3 and Figure 3.4 it is possible conclude the permeability may either increase or decrease with increasing pressure, depending on the polymer. For instance, PVDF shows an increase of permeability with increasing pressure by a factor of two at 318 K and by a factor of three at 363 K, between 75 and 150 bar. Yet, XLPE shows a decrease of permeability with increasing pressure by a factor of six at 318 K and by a factor of two at 363 K, between 100 bar and 650 bar. For PA11, we have not been able to identify a clear trend regarding pressure, since, depending on the temperature it may either increase or decrease. This effect may be explained by the loss of its plasticizer and will be discussed later.

The effect of pressure on the permeability depends on the penetrant and the polymer. The literature[90–92] suggests the pressure influence can be explained as the result of two opposite phenomena:

- Increasing pressure can lead to an increase of the polymer density, by reducing the free volume inside the polymer;
- Increasing pressure corresponds to an increase of penetrant concentration in the membrane and these molecules can plasticize the macromolecular chain, which mean an increase in free volume.

Each of these effects leads to a difference in permeability[29,91,92]: the first effect leads to a decrease of the permeability since the free volume inside the polymer matrix is lower reducing the diffusivity. The second effect leads to an increase in the permeability because the free volume in the polymer matrix is higher and makes it easier for the gas molecule to cross the membrane.

Comparing the influence of temperature and pressure in permeability, we conclude that temperature variations have a much more significant impact on permeability than variations in the pressure.

To the PA11 used in this work was added a plasticizer (12% of N-n-Butylbenzenesulphonamide) in order to decrease the glass transition temperature. The contact between supercritical CO_2 and the plasticized polymer resulted in partial removal of the plasticizer, this effect was previously observed by von Solms *et al*.[93], where the weight loss corresponded to the weight of plasticizer added to the virgin polymer. In the non-plasticized polymers, there are no change in the weight between the before and after measurement, although small weight losses could have been expected due to removal of additive. The loss of weight, in this study, for PA11 is reported in Table 3.6.

Table 3.6 – Percentage of PA11 loss of weight.

Pressure (bar)	Temperature (K)	Weight Loss (%)
100	320	3.1
100	363	0.0
200	319	1.9
200	363	3.1
350	318	2.0
350	362	4.5
650	319	4.4
650	333	1.5
650	348	2.1
650	363	3.3

Permeability in PA11 is slightly lower when compared with PVDF and XLPE for the same temperature and pressure. Usually, the incorporation of plasticizer increases the free-volume in polymers. Increasing permeation with increasing plasticization is an effect reported by Minelli *et al.*[92]. Thus, the loss of weigh showed in Table 3.6 can be related with the decrease of the free-volume on PA11 polymeric matrix, due to the consequent loss of plasticizer.

3.3.2. Mixtures

3.3.2.1. 90 mol% CO_2 + 10 mol% CH_4

The most studied mixture was 90 mol% CO_2 + 10 mol%CH_4, so it will be discussed in a section apart of the rest of mixtures. The experimental results are presented in Table 3.7 and

Table 3.8. The permeability was studied for the same conditions of temperature and pressure than pure CO_2, with the exception that permeability of 90 mol% CO_2 + 10 mol% CH_4 was not studied for PA11. Moreover, two new temperatures and an extra point of pressure were added for PVDF. In this case, no comparison with the literature could be made, since to the best of our knowledge there are no available reports for this specific composition and polymers.

Table 3.7 – Permeability of 90 mol% CO_2 + 10 mol% CH_4 in PVDF at different temperatures and pressures, where USC is the upstream chamber.

Pressure in the USC (bar)	**Temperature (K)**	**Pe x 10^7 ($cm^3_{STP}·cm^{-1}·bar^{-1}·s^{-1}$)**
76	319	0.388
75	364	1.44
75	383	3.46
75	404	5.41
99	319	0.349
101	329	0.838
101	348	1.46
101	363	1.57
148	316	0.481
150	362	2.97
345	384	26.5

Table 3.8 – Permeability of 90 mol% CO_2 + 10 mol% CH_4 in XLPE at different temperatures and pressures, where USC is the upstream chamber.

Pressure in the USC (bar)	**Temperature (K)**	**Pe x 10^7 ($cm^3_{STP}·cm^{-1}·bar^{-1}·s^{-1}$)**
104	320	0.904
104	333	1.50
104	348	2.41
103	363	3.82
202	320	0.745
208	334	1.56
202	350	3.95
202	364	7.50
354	319	0.506
353	334	1.41
352	350	2.93
351	364	5.01
648	318	0.290
648	334	0.752
648	348	1.26
650	362	2.11

The first conclusion for this gas mixture compared with pure CO_2 is the fact that the presence of CH_4 decreases the gas permeability. Apart from this effect it is possible to observe the trends regarding temperature and pressure are the same; the permeability increases with increasing temperature and two opposite effects, depending on the polymer, are observed with increasing pressure.

Table 3.7 shows the permeability of the gas mixture in PVDF increases by a factor of three, at 75 and 100 bar, for temperature increase from 319 to 404 K and from 319 to 363 K, respectively. However, the first mentioned pressure has a higher temperature increase (85 K) than the second (44 K), so we can conclude the temperature has not a significant impact in terms of permeability increase for PVDF. For XLPE (see

Table 3.8) for temperature increases from 318 to 363 K the permeability increases by a factor of four at 200 bar and by a factor of two at 650 bar; noticing that, at lower pressure the impact of the increasing temperature seems to be more substantial than at higher pressure.

Regarding increasing pressure, it is possible to observe PVDF shows also an increase of permeability; however, XLPE shows a decrease of permeability. For PVDF, at 363 K, the permeability increases by a factor of three with pressure increase from 75 to 150 bar, this increase is more relevant at 383 K, when the permeability increases six times when the pressure increases from 75 to 345 bar. The permeability of gas mixture in XLPE, with pressure increase from 100 to 650 bar, decreases two times, at 318 K, and by a factor of three at 363 K. As explained before in the pure CO_2 permeability, this opposite effect, regarding increase of pressure, is related with the two consequences in the free-volume.

To verify the Arrhenius equation, as was done for pure CO_2, the natural logarithm of the permeability was plotted as function of inverse temperature; the resulting graphs are presented below.

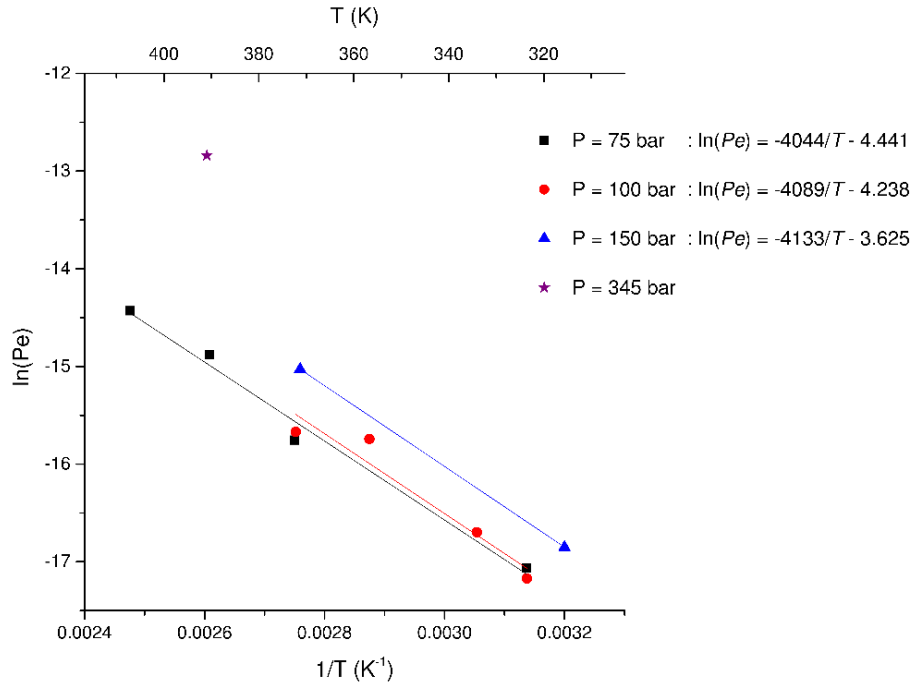

Figure 3.5 – Permeability of 90 mol% CO_2 + 10 mol% CH_4 in PVDF. Points are experimental data and the lines are the corresponding linear data fits.

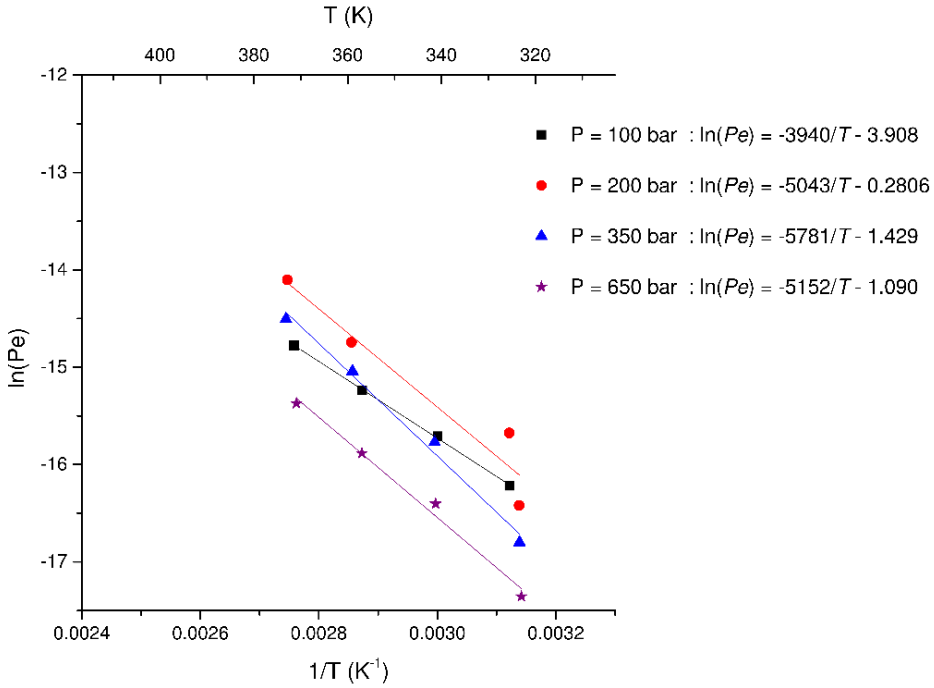

Figure 3.6 – Permeability of 90 mol% CO_2 + 10 mol% CH_4 in XLPE. Points are experimental data and the lines are the corresponding linear data fits.

From Figure 3.5 and Figure 3.6, it is possible to obtain the E_P for each polymer and pressure using the slope of the trendline. The resulting E_P's are presented in Table 3.9.

Table 3.9 – Apparent activation energy for permeability from Equation 1.23.

Polymer	Pressure	E_P (kJ·mol^{-1})	r^2
PVDF	75	34	0.9807
	100	34	0.9016
	150	34	-
XLPE	100	33	0.9991
	200	49	0.9809
	350	48	0.9863
	650	43	0.9823

It is noticed that, comparing E_P from pure CO_2 permeability and 90 mol% CO_2 + 10 mol% CH_4, does not change significantly, as it was expected being the permeability is lower. This might be due to the fact the mixture in study has a high concentration of CO_2, which will maintain the E_P. Literature[86] report E_P between 60 and 62 kJ/mol for pure CH_4 in PVDF, so it was expected the obtained values of E_P in this report were higher for 90 mol% CO_2 + 10 mol% CH_4 than compared with pure CO_2.

3.3.2.2. Others

In order to study the influence of gas concentration in the polymer a set of experiments were performed at 100 and 200 bar and 318 K, with different molar faction of CO_2. The obtained results are present in Table 3.10. The values for pure CO_2 and CH_4 are also presented in order to better identify the gas concentration dependence.

Table 3.10 – Permeability of different gas mixtures between CO_2 and CH_4 in XLPE for 100 bar and 200 bar, at 318 K.

100 bar		**200 bar**	
% CO_2	**Pe x 10^7 (cm^3_{STP}·cm^{-1}·bar^{-1}·s^{-1})**	**% CO_2**	**Pe x 10^7 (cm^3_{STP}·cm^{-1}·bar^{-1}·s^{-1})**
0	0.427	0	0.325
25	0.613	25	0.583
50	0.718	50	0.766
75	1.12	75	0.703
90	0.904	90	0.745
100	0.999	100	0.531

Two effects are observed, depending on the pressure. At 100 bar the permeability dependence is more linear, if the 75 mol% CO_2 is considered to be an outlier, nevertheless, at 200 bar, a maximum permeability is obtained at 50 mol% CO_2 and then, the permeability decreases with increasing CO_2 concentration. This tendency is more clearly identified in Figure 3.7.

Donohue[94] studied the permeation of mixtures between CO_2 and CH_4 at 20 bar in cellulose acetate membranes, and reported that the permeability increase with increasing CO_2 concentration, although no linearly. Andersen *et al.*[95] also studied the influence of CO_2 concentration in PVDF at 393 K and 25 bar for mixtures containing CO_2, CH_4 and water, but for lower concentration (3% and 25%), it was reported the permeability was independent of the partial pressure of the gases, but this might be due to the presence of water, which represented half of the volume.

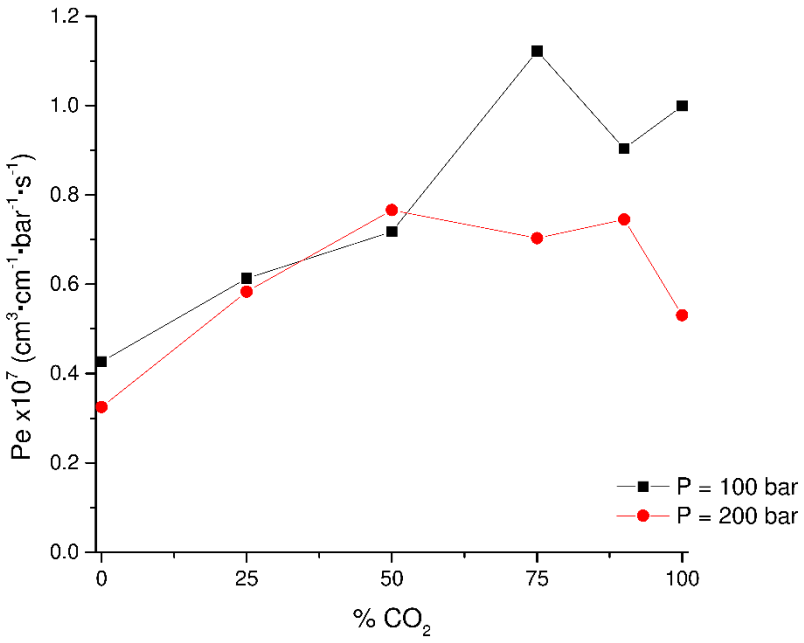

Figure 3.7 – Permeability of different gas mixtures between CO_2 and CH_4 in XLPE for 100 bar and 200 bar, at 318 K. Note that the lines are only to guide the eyes.

Our result, for CO_2 dependence in the permeability, was not conclusive and more results needed to be performed in order to understand better the dependency, maybe at intermediate pressure (e. g. 150 bar). Despite this fact the membrane selectivity was determined.

The selectivity, α_{CO_2/CH_4} is defined by[67]:

$$\alpha_{CO_2/CH_4} = \frac{Pe_{CO_2}}{Pe_{CH_4}} \qquad \text{Equation 3.1}$$

It was determined the selectivity for CO_2 (gas more permeable) to be 2.3 at 100 bar, and 1.7 at 200 bar, in XLPE. Thus, the selectivity is decreasing with increase pressure. As a reminder, the former results of permeability showed for XLPE; also denote a decreasing trend with pressure increase. This effect, where a decrease of permeability is linked with a lower selectivity, was also reported by Ghosal and Freeman[45] and Matteucci *et al.*[63].

3.3.2.3. Gas Chromatography Analysis

Some of the mixtures from the permeability measurements were analysed in order to understand differences in gas component permeability. The measured tests are presented in Table 3.11.

Table 3.11 – Matrix of the GC analysis, where ■ represent PVDF and ● XLPE. The gas is represented by x/y, where x and y are CO_2 and CH_4 percentages.

P (bar) / T (K)	**318**	**333**	**348**	**383**	**403**
75					90/10 (■)
100	75/25 (●) 50/50 (●) 25/75 (●)	90/10 (■)	90/10 (■)		
200	90/10 (●) 75/25 (●) 50/50 (●) 25/75 (●)				
345				90/10(■)	

The initial gas composition, in the chambers, which were fed directly from scientific grade bottles, was assumed to correspond to the supplied composition. After the experiment, a GC (Agilent Technologies 7890A) was used to determine the final gas composition. The comparison between the initial and final composition for PVDF showed in Table 3.12 and for XLPE in Table 3.13.

Table 3.12 – Final gas composition for the permeability of 90 mol% CO_2 and 10 mol% CH_4 in PVDF at different temperatures and pressures.

P = 75 bar		**P = 100 bar**				**P = 345 bar**	
T = 403 K		**T = 333 K**		**T = 348 K**		**T = 383 K**	
%CO2	**%CH4**	**%CO2**	**%CH4**	**%CO2**	**%CH4**	**%CO2**	**%CH4**
95.1	4.9	95.0	6.1	89.9	4.4	92.4	7.6

Table 3.13 – Initial and final gas composition for the permeability of gas mixture in XLPE at 318 K.

P = 100 bar				**P = 200 bar**			
Initial		**Final**		**Initial**		**Final**	
%CO_2	**%CH_4**	**%CO_2**	**%CH_4**	**%CO_2**	**%CH_4**	**%CO_2**	**%CH_4**
75	25	73.9	23.6	90	10	92.6	11.1
50	50	52.9	47.6	75	25	72.1	25.8
25	75	26.5	70.1	50	50	49.1	49.9
				25	75	25.3	73.4

The initial gas composition was not measured since a scientific grade gas was used. The sum of final gas composition does not equal 100% in most of the experiments; this is because during the collection of the gas some fraction of atmospheric gases may have interfered with the collected gas, resulting in their presence during the analysis. In order to properly analyse the possible change in gas composition the composition factor was calculated and it is presented in Table 3.14 and Table 3.15.

Table 3.14 – CO_2 to CH_4 ratio after permeation for PVDF at initial ratio of 9.

P = 75 bar	**P = 100 bar**		**P = 345 bar**
T = 403 K	**T = 333 K**	**T = 348 K**	**T = 383 K**
19.4	15.6	20.4	12.2

PVDF showed a high CO_2 to CH_4 and a significantly high selectivity to CO_2 was determined (meaning the CH_4 was retained in the upstream chamber). However, more experiments are required to take stronger conclusions about PVDF gas selectivity.

Table 3.15 – CO_2 to CH_4 composition ratio before and after the experiments in XLPE.

P = 100 bar		**P = 200 bar**	
Initial	**Final**	**Initial**	**Final**
3	3.13	9	8.3
1	1.1	3	2.8
0.33	0.38	1	0.98
		0.33	0.34

Comparing the CO_2 to CH_4 ratio for XLPE it is possible to conclude that the difference between the initial and final value are within the experimental analysis error. Therefore, XLPE is not significantly permeable to CO_2 compared with CH_4, this result is also confirmed by the low selectivity obtained in the previous section.

3.4. Pressure *vs.* Fugacity

The measured conditions of pressure and temperature are far away from the stage where it can be assumed an ideal gas behavior; despite this, the permeability was calculated using the pressure difference. In this section it will be compared the difference between permeability calculated by using the pressure (Equation 1.20) and fugacity (Equation 3.2) gradient.

$$Pe = \frac{l}{A} \cdot \frac{\rho_{end} - \rho_{start}}{\rho_{STP}} \cdot \frac{V_{cell}}{\Delta f \cdot t} \qquad \text{Equation 3.2}$$

where Δf is the fugacity difference between the chambers (upstream and downstream).

Figure 3.8, Figure 3.9 and Figure 3.10 show both the permeability of pure CO_2 calculated using pressure and fugacity difference in PVDF, XLPE and PA11, respectively.

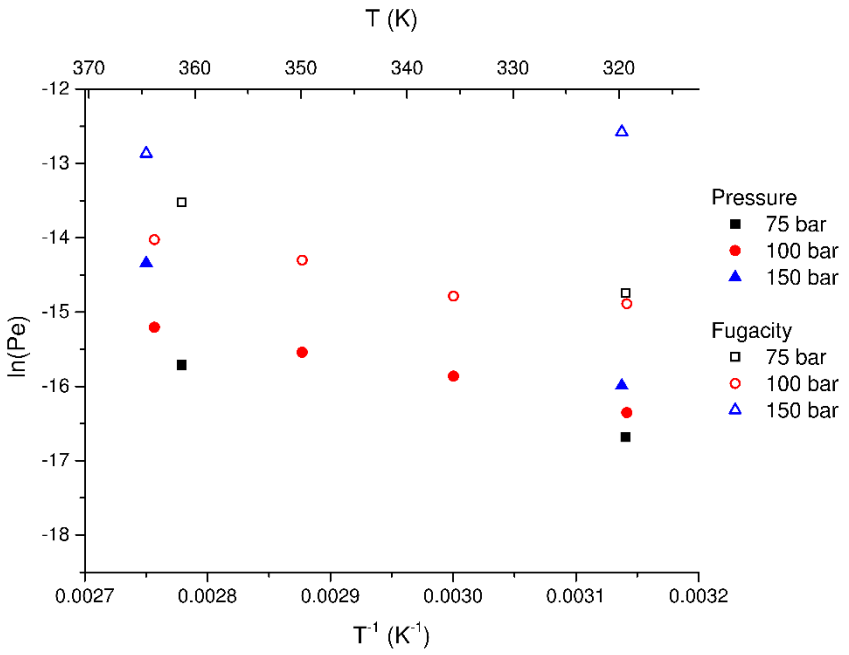

Figure 3.8 – Comparison between the permeability of pure CO_2 calculated by the pressure (full symbols) and fugacity (open symbols) difference for PVDF.

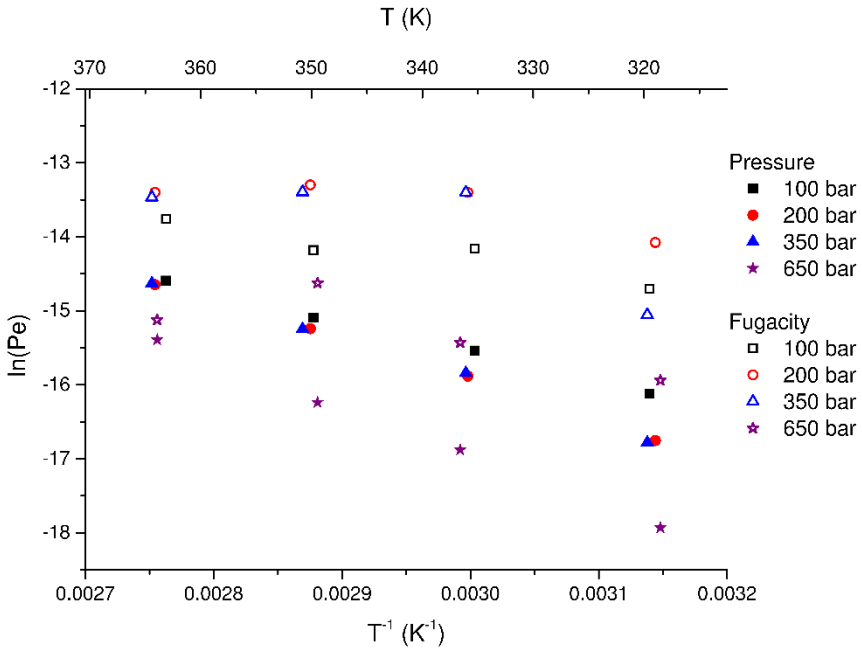

Figure 3.9 – Comparison between the permeability of pure CO_2 calculated by the pressure (full symbols) and fugacity (open symbols) difference for XLPE.

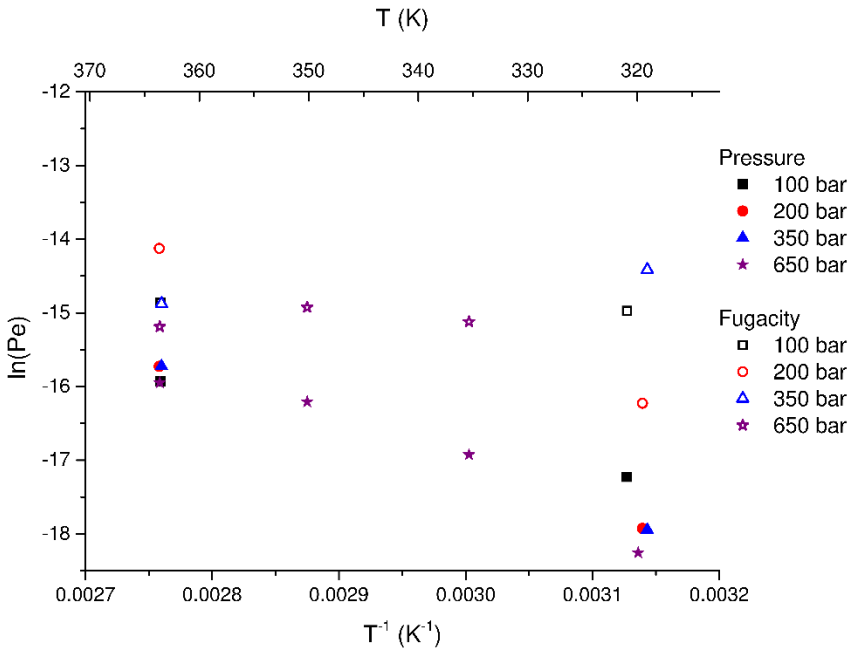

Figure 3.10 – Comparison between the permeability of pure CO_2 calculated by the pressure (full symbols) and fugacity (open symbols) difference for PA11.

It is possible to observe the permeability is slightly higher if the permeability is calculated by the fugacity difference, as it was expected since the fugacity gradient will be lower (Figure 1.6) and it is in the dominator position in the permeability fraction. Pointing out the pressure and temperature dependency is maintain regardless the calculation method.

The same analysis was made for the gas mixture of 90 mol% CO_2 and 10 mol% CH_4 and the resulting graphs are presented in Figure 3.11 and Figure 3.12. It was concluded the permeability is higher when the calculation method based in a fugacity rather than a pressure gradient, nevertheless the pressure and temperature dependence is kept.

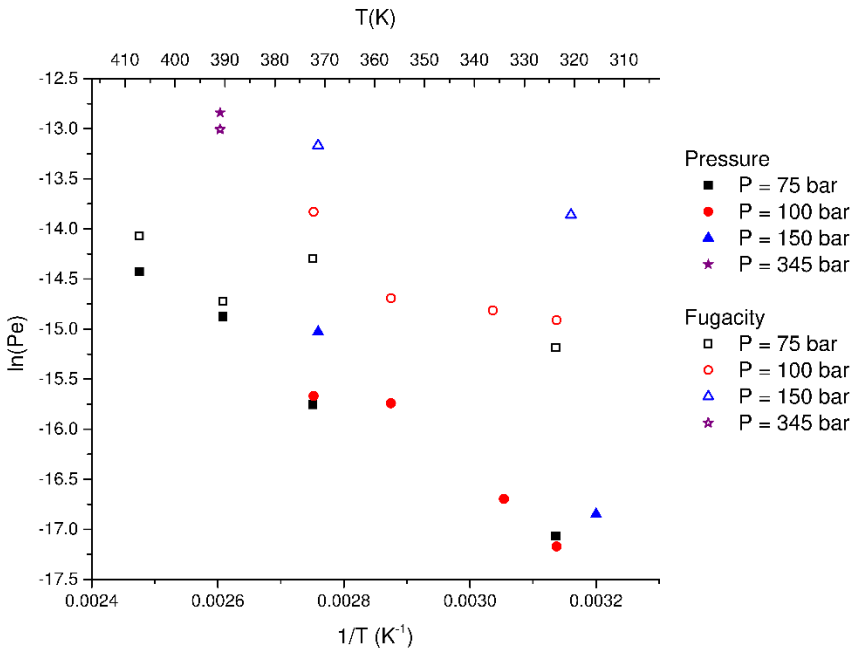

Figure 3.11 – Comparison between the permeability of 90 mol% CO_2 and 10 mol% CH_4 calculated by the pressure (full symbols) and fugacity (open symbols) difference for PVDF.

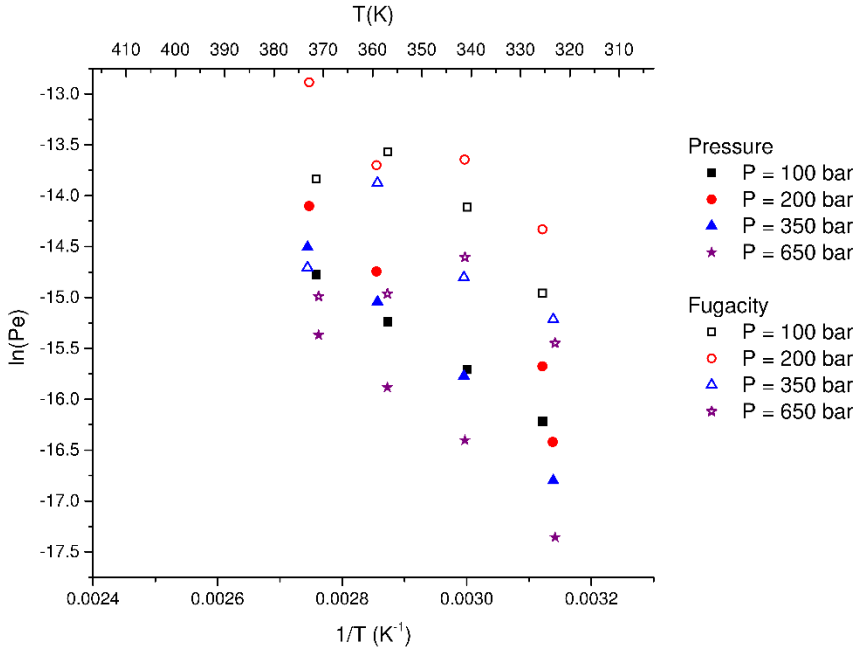

Figure 3.12 – Comparison between the permeability of 90 mol% CO_2 and 10 mol% CH_4 calculated by the pressure (full symbols) and fugacity (open symbols) difference for XLPE.

3.5. SEM analysis

During the permeability study, the tested polymers were exposed to extreme conditions of pressure and temperature that in some cases reaches 650 bar and 318 K. Visual inspection of the tested polymers, evidenced some differences when comparing with the virgin materials. Further characterization of the surface was conducted through scanning electron microscope (SEM), on a FEI Quanta 200 microscope. The purpose of the technique was to clearly identify if the polymers had any structural changes after contacting with supercritical CO_2 and its mixtures with CH_4. Figure 3.13 shows the obtained images for PVDF virgin foil, and after permeability test conducted at 650 bar and 318 K, both naked eye and 500X SEM analysis.

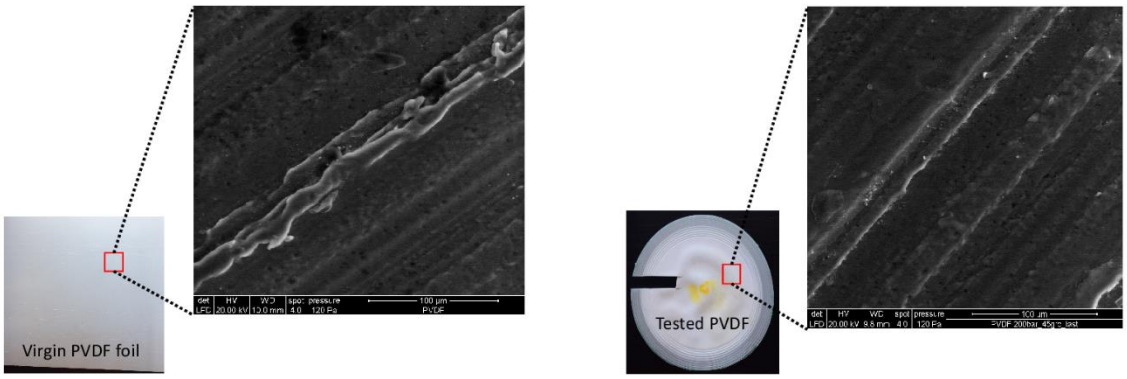

Figure 3.13 – SEM images of PVDF, before and after, permeability tests conducted at 650 bar and 318 K° with a mixture composed by 90 mol% CO_2 and 10 mol% CH_4.

Despite the optical difference observed of the polymer samples, before and after the permeability tests, no clear structural change is observed on SEM. One should take into consideration that SEM is a technique that provides better contrast of the samples images in the case of conductive materials, otherwise they charge deflecting the primary beam and deteriorating signal detection. Therefore, in the case of polymer samples, which are semi-crystalline, this could be a limitation, which hinders further conclusions about structural changes at the surface. To better understand the changes in the polymer structure some X-ray diffraction testes needed to be performed.

Similar SEM analysis were conducted with other polymers, which contacted CO_2 at different conditions of pressure and temperature, and the results are presented in the Appendix 3.

Chapter 4

Chapter 4. Diffusion Calculation

As discussed in the introduction, the permeability is the coefficient between solubility and diffusion. Therefore knowing only two of these coefficients, is possible to calculate the third one (Equation 1.17). In this chapter, the matching conditions of solubility and permeability are presented and the diffusion calculated. The measured solubility and permeability are presented in Table 4.1 and Table 4.2.

Table 4.1 – Measured solubility and permeability of CO_2 in PVDF at the matching conditions of pressure and temperatures (adapted from Table 2.2 and Table 3.2).

Pressure (bar)	**Temperature (K)**	**Solubility ($g_{gas}/g_{polymer}$)**	**Permeability x 10^7 ($cm^3_{STP} \cdot cm^{-1} \cdot bar^{-1} \cdot s^{-1}$)**
75	318	0.05558	0.569
75	360	0.02897	1.50
100	318	0.05530	0.790
100	333	0.04453	1.29
100	348	0.04238	1.78
100	360	0.03586	2.4883
150	318	0.07624	1.14
152	360	0.03953	5.91

Table 4.2 – Measured solubility and permeability of CO_2 in XLPE at the matching conditions of pressure and temperatures (adapted from Table 2.4 and Table 3.3).

Pressure (bar)	**Temperature (K)**	**Solubility ($g_{gas}/g_{polymer}$)**	**Permeability x 10^7 ($cm^3_{STP} \cdot cm^{-1} \cdot bar^{-1} \cdot s^{-1}$)**
100	318	0.04361	0.999
100	333	0.03281	1.78
100	348	0.02929	2.79
100	362	0.03048	4.59
200	318	0.09854	0.531
200	333	0.05445	1.26
200	348	0.03181	2.40
200	363	0.03184	4.35

The diffusion is then calculated and presented in Table 4.3. The solubility of CO_2 in PVDF and XLPE could not be measured for higher conditions of pressure, in order to match with more permeability measurements, due to the limit of the MSB.

Table 4.3 – Calculated diffusion of CO_2 in PVDF and XLPE at the conditions when solubility and permeability were matching.

PVDF			**XLPE**		
Pressure (bar)	**Temperature (K)**	**Diffusion x10^7 ($cm^2 \cdot s^{-1}$)**	**Pressure (bar)**	**Temperature (K)**	**Diffusion x10^7 ($cm^2 \cdot s^{-1}$)**
75	318	0.532	100	318	1.93
75	363	2.66	100	333	6.51
100	318	0.983	100	348	7.15
100	333	1.98	100	363	14.5
100	348	2.86	200	318	1.76
100	363	4.71	200	333	4.93
150	318	1.50	200	348	6.56
150	363	15.0	200	363	22.8

Analysing Table 4.3, it is concluded that the diffusion increases with increasing temperature; this is due to the increasing of chain mobility with the temperature. Both permeability and diffusion increase with increasing temperature, however solubility decreases with increasing temperature. Since the permeability is the product of solubility and diffusion coefficient, it is possible to conclude the diffusion has a much more significant temperature dependency than the solubility on the permeability, so the increase of chain mobility has more impact than the difficulty of CO_2 absorption at higher temperatures. From Table 4.3 is possible to observe diffusion of CO_2 in PVDF increases by a factor of five, when temperature increases from 318 to 363 K at 100 bar, and by a factor of 10 when temperature increases from 318 to 363 K, at 150 bar. The diffusion of CO_2 in XLPE is even more significant when the temperature increases from 318 to 363 K and the diffusion coefficient increase by a factor of eight at 100 bar and by a factor of 14 at 200 bar.

The diffusion pressure dependency is less significant for both polymers, when compared with temperature dependency, in the studied cases. Depending of the polymer, it is showed the diffusion may increase or decrease with increasing pressure, CO_2 diffusion in PVDF increase with increasing pressure,

however in XLPE it decreases with increasing pressure. This effect was also observed previously for the permeability coefficient and was explained before by the free volume theory. It is possible to conclude the permeability coefficient follows the pressure dependency of the diffusion coefficient, as well the temperature dependency, as stated before.

Plotting the calculated results in terms of natural logarithm of the diffusion as a function of inverse temperature it is possible to observe the experimental results follow the Arrhenius equation (Figure 4.1 and Figure 4.2).

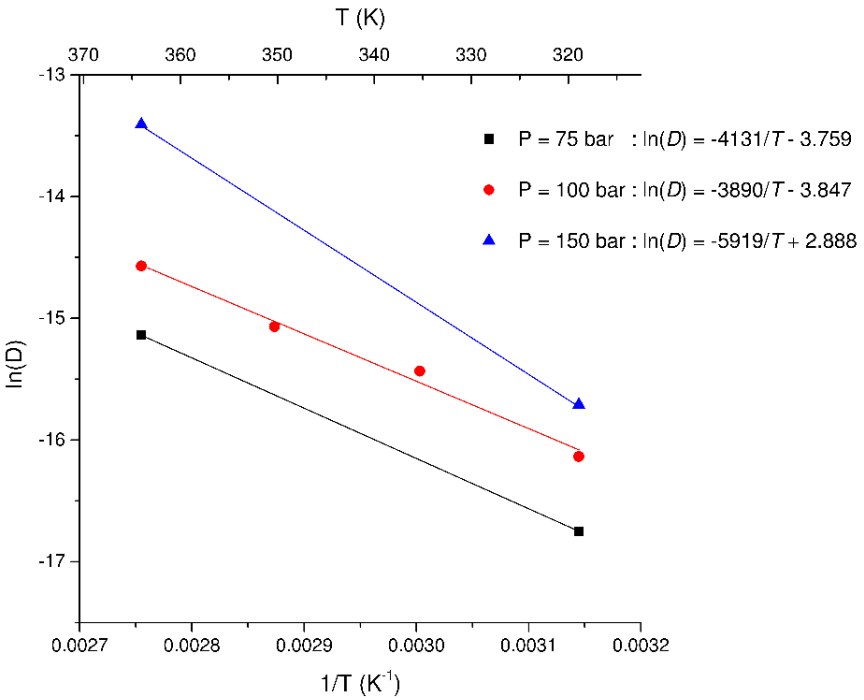

Figure 4.1 – Calculated CO_2 diffusion in PVDF at the studied conditions of pressure and temperature. The symbols correspond to the specific state points and the lines are the correspondent linear fitting.

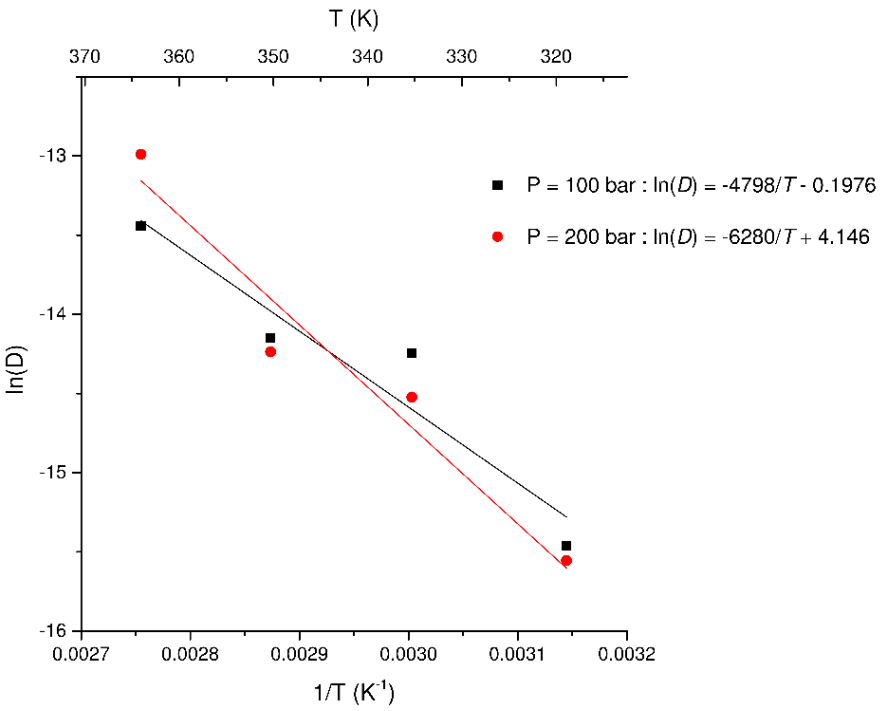

Figure 4.2 – Calculated CO_2 diffusion in XLPE at the studied conditions of pressure and temperature. The symbols correspond to the specific state points and the lines are the correspondent linear fitting.

With the slope of the linear fitting, the activation energy of diffusion (E_D) is obtained and presented in Table 4.4.

Table 4.4 – Apparent activation energy of diffusion from Equation 1.21.

Polymer	**Pressure (bar)**	E_D **(kJ/mol)**	$\mathbf{r^2}$
PVDF	75	34	-
	100	32	0.9813
	150	49	-
XLPE	100	40	0.91455
	200	52	0.94893

Flaconnèche *et al.* reported E_D to be between 44 and 49 kJ/mol, although the studied pressure was 40 bar, which is quite lower than the presented by this study.

Another predictive method to obtain E_D is by Equation 1.24, this method is based in the heat of dissolution of the penetrant in the polymer and the apparent activation energy of the permeability. The original ΔH_S can be found in Table 2.5 andTable 2.6 and E_{Pe} in Table 3.9. The predicted apparent activation energies of diffusion are presented in Table 4.5.

Table 4.5 – Predicted apparent activation energy of diffusion from Equation 1.24.

Polymer	**Pressure (bar)**	ΔH_S **(kJ/mol)**	E_{Pe} **(kJ/mol)**	E_D **(kJ/mol)**
PVDF	75	-16	34	50
	100	-11	34	45
	150	-26	34	60
XLPE	100	-9	33	42
	200	-26	49	75

The predictive method present values of apparent activation energy of diffusion higher, but not with a significant variation.

Chapter 5

Chapter 5. Modelling of Solubility and Swelling with sPC-SAFT

Modern equations of state are an useful tool to understand, predict and correlate the solubility of gases in polymers. At low pressures, Henry's law is a useful relation that can be applied in gas-polymers systems[53,76], but above a critical gas concentration, the gas sorption isotherm begins to deviate significantly. The most common approaches to modelling the solubility and the swelling are Simha-Somcynsky (SS-EOS)[96,97], Sanchez-Lacombe (SL EOS)[34,72,98,99], Statistical Associating Fluid theory (SAFT)[98,100] and Perturbed-Chain Statistical Associating Fluid Theory (PC-SAFT)[97,98,101,102]. Due to the simplicity of SL-EOS, most researchers prefer this EOS to determine not only the solubility of light gases in polymers, but also the swelling of the polymers. In this work it is used a simplified version of PC-SAFT was used to accurately predict the swelling and the solubility in different polymers with different gases[98,103].

PC-SAFT is an equation of state initially proposed by Gross and Sodowski[104], and sPC-SAFT is a simplified version[105] that reduces the computation times without sacrificing any of the accuracy of the original equation of state[102,105]. sPC-SAFT reduces to original PC-SAFT in the pure-component limit, thus there is no need of reparametrization with sPC-SAFT, and parameters from previous works with PC-SAFT may thus be used in sPC-SAFT[102].

PC-SAFT is a molecular-based EOS, which accounts for the effect of molecular size and shape, dispersion forces and association of molecules.

The starting point is the most general form of the Helmholtz energy for a mixture of associating molecules.

$$\tilde{a} \equiv \frac{A}{NkT} = \tilde{a}^{id} + \tilde{a}^{hc} + \tilde{a}^{disp} + \tilde{a}^{assoc} \qquad \text{Equation 5.1}$$

where $\tilde{a}^{id}$ is the ideal gas contribution, $\tilde{a}^{hc}$ is the contribution of the hard-sphere chain reference system, $\tilde{a}^{disp}$ is the dispersion contribution arising from the square-well attractive potential and $\tilde{a}^{assoc}$ is the contribution due to association.

The expressions for the contributions from the ideal gas ($\tilde{a}^{id}$) and dispersion ($\tilde{a}^{disp}$) are from Gross and Sadowski[104].

The contribution to the hard-chain term is made up the two contributions: the hard-sphere term and chain formation term,

$$\tilde{a}^{hc} = m\tilde{a}^{hc} - \sum_i x_i (m_i - 1) \ln g_{ii}^{hs}\left(d_{ii}^{+}\right) \qquad \text{Equation 5.2}$$

where $\bar{m}$ is a mean segment length defined simply as $\bar{m} = \sum_i x_i m_i$ and the hard-sphere term is given by:

$$\tilde{a}^{hs} = \frac{4\eta - 3\eta^2}{(1-\eta)^2} \qquad \text{Equation 5.3}$$

where x_i is the mole fraction of component i. The radial distribution function at contact is:

$$g^{hs}\left(d^{+}\right) = \frac{1 - \eta/2}{(1-\eta)^3} \qquad \text{Equation 5.4}$$

The Equation 5.3 and Equation 5.4 constitute modification 2 proposed by von Solms *et al.*[105]. The volume fraction $\eta = \pi\rho\bar{m}d^3/6$ is based on the diameter of an equivalent one-component mixture

$$d = \left(\frac{\sum_i x_i m_i d_i^3}{\sum_i x_i m_i} \right)^{1/3} \qquad \text{Equation 5.5}$$

where the individual d_i are temperature-dependent segment diameters

$$d_i = \sigma_i \left[1 - 0.12 \exp\left(-3\frac{\varepsilon_i}{kT} \right) \right] \qquad \text{Equation 5.6}$$

The mixing rules for the parameters are needed:

$$\sigma_{ij} = \frac{(\sigma_i + \sigma_i)}{2} \qquad \text{Equation 5.7}$$

$$\varepsilon_{ij} = \sqrt{\varepsilon_i \varepsilon_i}\left(1 - k_{ij}\right) \qquad \text{Equation 5.8}$$

So each component is described with 3 parameters, a length parameter, m, a segment size parameter, σ, and a segment energy parameter, ε. Each component can be thought of as consisting of m

spherical segments bonded together, with each segment having a diameter σ and energy of attraction ε[77]. In order to apply the sPC-SAFT EOS it is necessary to find these three parameters for each component. The common method to determine pure-component parameters is to fit vapour pressure and liquid density data, however this is not possible for polymers since experimental data does not exist most of the times[106–108].

The used pure component parameter for sPC-SAFT for CO_2 were reported by Lundsgaard et al.[109], the parameters regarding the polymers were obtained after a reparameterization to fit the experimental measurements of solubility presented in this work. Table 5.1 shows the used parameters.

Table 5.1 – sPC-SAFT parameters.

Component	m/M_w	σ **(Å)**	ε/k **(K)**	**Ref**
CO_2	0.0558	2.5987	156.49	Lundsgaard *et al.*[109]
PVDF	0.0192	3.5300	270.18	this work
XLPE	0.0263	3.8662	252.31	this work

Knowing these three pure-components and the binary interaction parameter, k_{ij}, it is possible to use sPC-SAFT to obtain the phase equilibria. In this work, a binary interaction parameter was fitted to the measured experimental solubility data.

The gas solubility of CO_2 in both polymers was calculated with sPC-SAFT by iterating the pressure for the gas and liquid phase until the fugacity of the gas component in the two phases are equal, noticing that there are no vapour pressure of the polymers, hence no mole fraction and component subscript on the right side of the equilibrium:

$$x_2^L \varphi_2^L \left(T, P, x_2^L\right) = \varphi^G \left(T, P\right) \qquad \text{Equation 5.9}$$

where x_2^L is the mole fraction of the gas component in the liquid and φ_2^L and φ^G are the fugacities of the gas component in the liquid and gas phase. As it is generally acceptable that the gas only absorbs in the amorphous regions of the polymer[29,43,44], the solubility of the gas in the polymer calculated also as a function of the crystallinity.

$$S(T,P,X_C)=\frac{w_2(1-X_C)}{w_1}$$ Equation 5.10

where, S is the solubility, w_1 and w_2 are the weight fractions of the polymer and the gas component respectively and X_C is the crystallinity of the polymer. The crystallinity for both polymers is stated under the materials section.

The swelling is calculated as ratio increase of the specific volume:

$$S_w(T,P)=\frac{v_{sw}(T,P)-v_{pp}(T,P)}{v_{pp}(T,P)}\times 100$$ Equation 5.11

where v_{pp} is the specific volume of the pure polymer and v_{sw} is the average specific volume of the swelled polymer calculated by:

$$v_{sw}(T,P)=\frac{V_{m,sw}(T,P)}{\sum_{i=1}^{2}x_i M_{w,i}}$$ Equation 5.12

where, $V_{m,sw}(T,P)$ is the molar volume of the swelled polymer and $M_{w,i}$ and x_i are the molecular weight and molar ratio of component i.

5.1. Solubility

The experimental CO_2 solubility measurements reported in Chapter 2 were fitted using sPC-SAFT and the results are presented in Figure 5.1, Figure 5.2 and Figure 5.3.

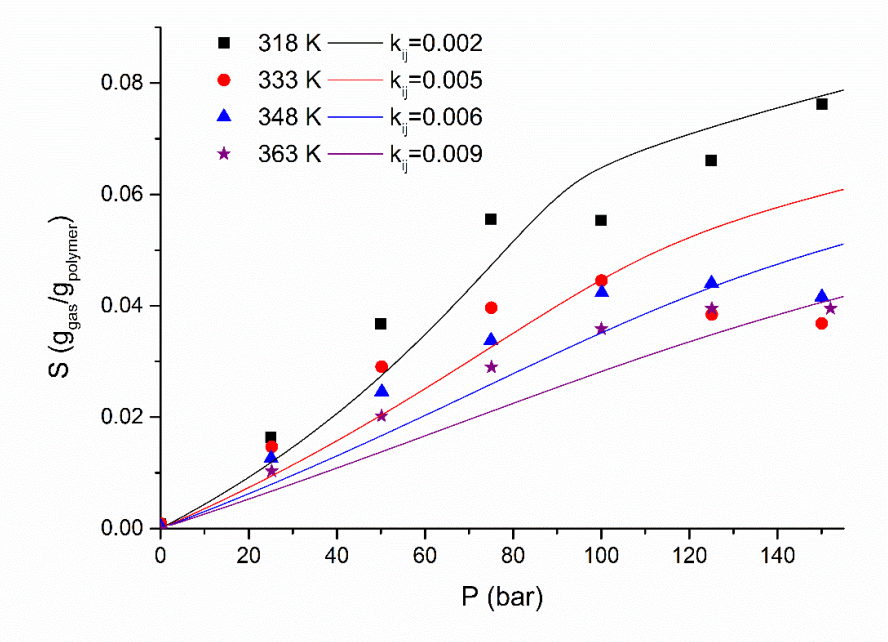

Figure 5.1 – Modelling results for solubility of pure CO_2 in PVDF, series 1, as a function of pressure, with respective binary parameter depending of temperature.

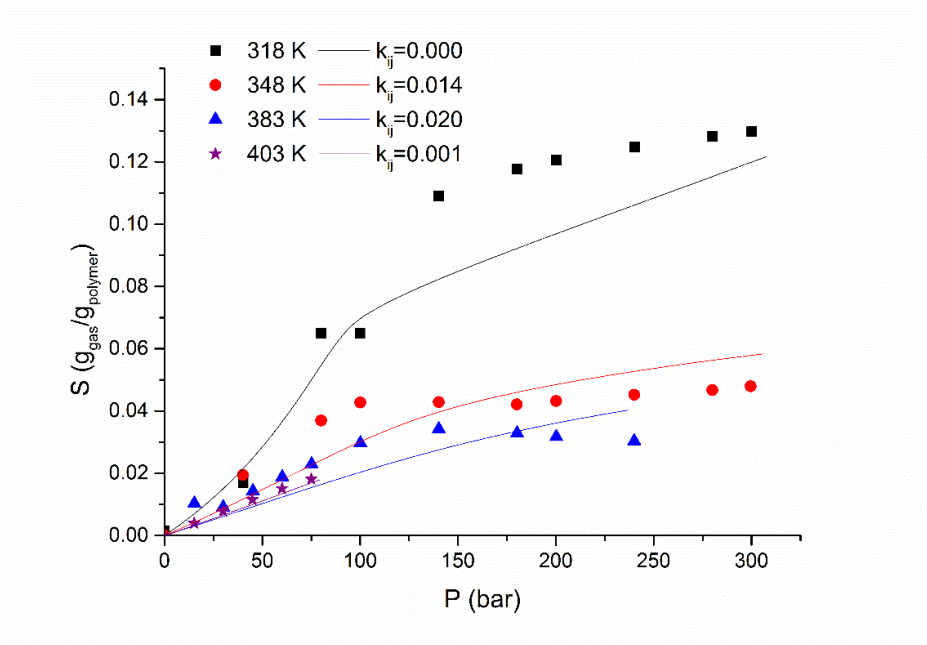

Figure 5.2 – Modelling results for solubility of pure CO_2 in PVDF, series 2, as a function of pressure, with respective binary parameter depending of temperature.

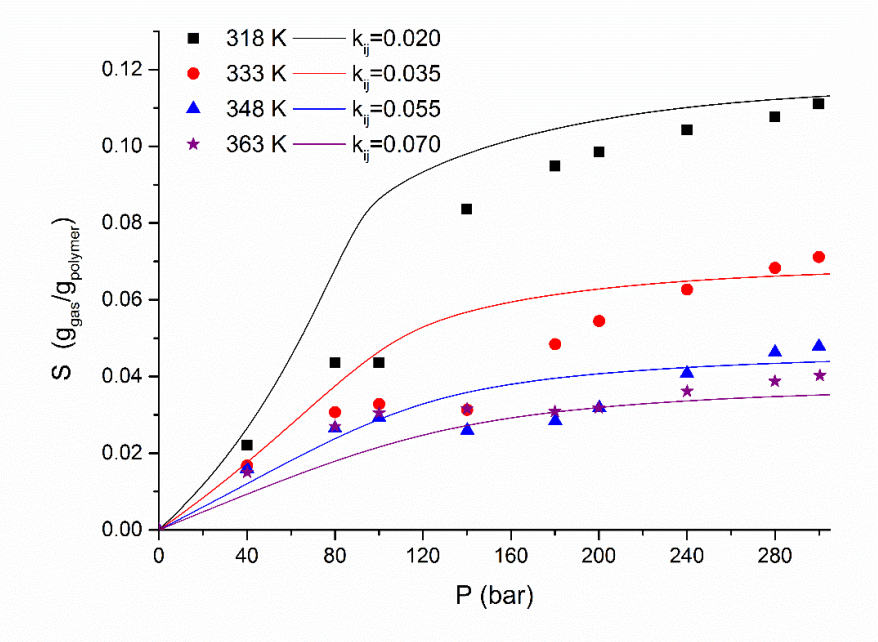

Figure 5.3 – Modelling results for solubility of pure CO_2 in XLPE as a function of pressure, with respective binary parameter depending of temperature.

As can be seen sPC-SAFT model can successfully correlate the data with a small binary interaction parameter, different for each polymer and temperature. It is observed that k_{ij} increases with increasing temperature for both polymers, and the k_{ij} for XLPE is higher than the binary parameter for PVDF for the same temperature range.

5.2. Swelling

In Chapter 2 the swelling was estimated experimentally. Apart this experimental estimation, the swelling can also be estimated using sPC-SAFT. Two different sets of k_{ij} 's were investigated, firstly it was used the k_{ij} obtained from the fitting with the experimental results of solubility and afterwards a new k_{ij} was found to match with our experimental estimation of swelling. In Figure 5.4 and Figure 5.5 these fits are presented for PVDF and XLPE, respectively. The squares represent the experimental

estimation, the dash lines represent the swelling estimated using the k_{ij} from the solubility experimental measurements and the solid line the sPC-SAFT fitting of the experimental swelling.

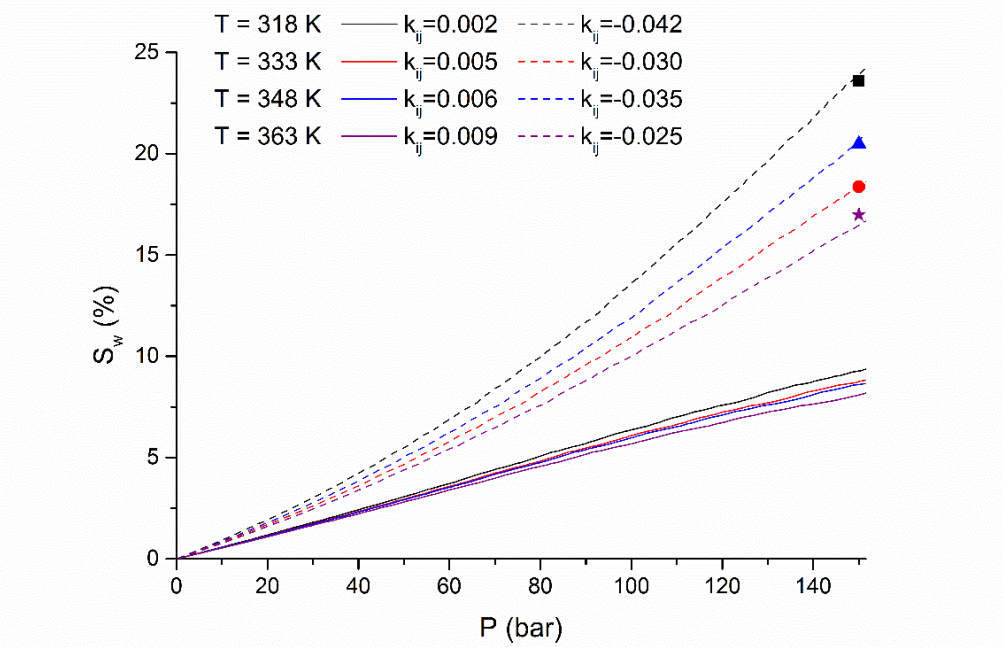

Figure 5.4 – Predicted swelling of PVDF. The dots represent the swelling estimated by the experimental measurements, the solid lines are the sPC-SAFT prediction using the obtained k_{ij} from the solubility and the dash lines the swelling prediction by sPC-SAFT to match the experimental swelling estimation.

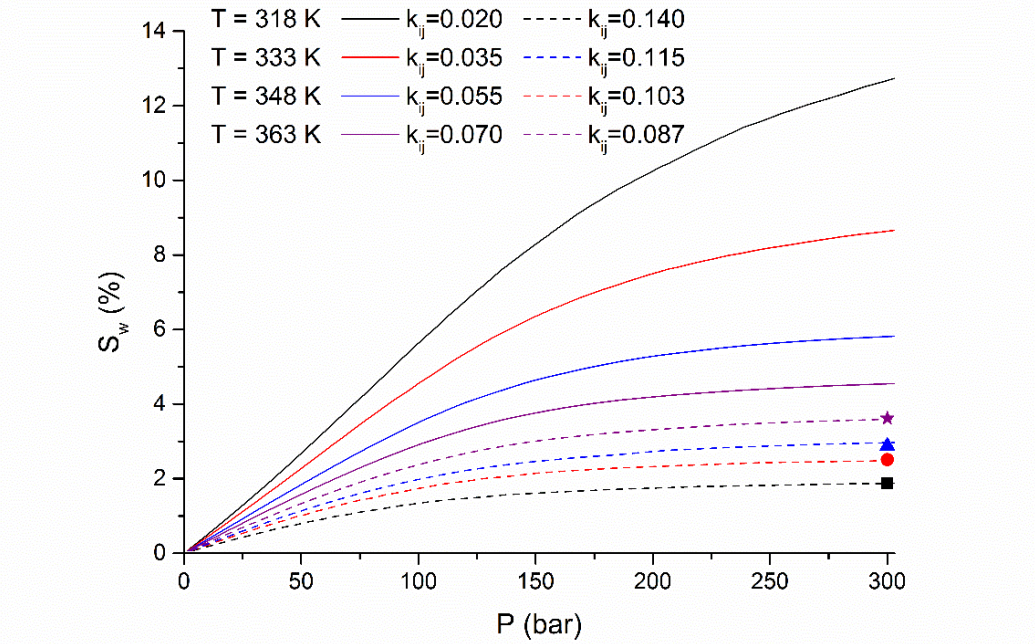

Figure 5.5 – Predicted swelling of XLPE. The dots represent the swelling estimated by the experimental measurements, the solid lines are the sPC-SAFT prediction using the obtained k_{ij} from the solubility and the dash lines the swelling prediction by sPC-SAFT to match the experimental swelling estimation.

As it can be seen the experimental swelling estimation is superior to the estimation using the k_{ij} from the solubility experimental measurements for PVDF, while for XLPE the effect is opposite: The experimental estimate is inferior to the estimation obtained using sPC-SAFT with the k_{ij} from the solubility. Observing Figure 5.4 and Figure 5.5 is concluded that, the k_{ij}, fitted to the experimental solubility is always lower than the one which fits the experimental estimation, for the studied temperatures and polymers. It was observed the k_{ij} from the fitting to our experimental solubility measurements, increased with increasing temperature, however when we fit the sPC-SAFT to our experimental estimation swelling the k_{ij} decreased, in absolute value, with increasing temperature.

From both estimations is possible to conclude XLPE has lower swelling, even at high temperatures, when compared with PVDF. This behaviour is justified because XLPE is a cross-linked polymer so the chain mobility is very low, which prevents the swelling of the polymer.

Bonavoglia *et al*.[83] reported values of swelling around 10% for PVDF contacting CO_2 at 333 K and 150 bar, so our estimation of swelling using sPC-SAFT, with k_{ij} fitted to the experimental solubility results, seems to be the more reliable of our two estimations.

Chapter 6

Chapter 6. Conclusions

The objective of this study was to measure transport properties in polymers used in flexible pipelines for offshore applications. Flexible pipelines are widely used, especially in the oil and gas industry, where the injection of CO_2 into reservoirs can be used as an Enhanced Oil Recovery method. Since oil reservoirs are increasing in depth, pressure and temperature (beyond 3000 m, where the pressure can exceed 1000 bar and the temperature can be as high as 423 K, CO_2 needs to be transported under these extreme conditions.

The solubility of pure CO_2 was measured in PVDF, up to 403 K, and XLPE, up to 363 K, up to 300 bar. A magnetic suspension balance was used to conduct the experiments. This setup records the exact sample weight, pressure, temperature and gas density under equilibrium conditions. It was observed, for both studied polymers, that the solubility followed an Arrhenius dependency, resulting in a decrease of solubility with temperature increase; increasing pressure resulted in an increase of gas solubility in the polymer. However, the solubility shows an unusual pressure dependency between 75 and 100 bar, for both polymers, where the solubility seems to be constant with increasing pressure. This unusual behaviour is justified by the change from gas to the supercritical state by CO_2. The ΔH_S was calculated from the linearization of the Arrhenius equation, and, as expected, its value is negative for both polymers at the studied pressures. CO_2 showed a higher solubility in PVDF than in XLPE, at similar conditions of pressure and temperature. A sPC-SAFT equation of state model was used to correlate the experimental data where a binary interaction parameter was required for each polymer and temperature.

A 2D-permeation cell, built in-house, was used to experimentally obtain the permeability of pure CO_2 and its mixtures with CH_4 for PVDF, XLPE and PA11 at different conditions of pressure and temperature. The permeability increased with increasing temperature following the Arrhenius equation, from which the activation energy can be determined. With increasing pressure, two effects were observed: For PVDF and PA11 the gas permeability increased and for XLPE, the gas permeability decreased. This is related to the two opposite effects that pressure increase has on the polymer free-volume. One is increasing the polymer density, which leads to a decrease of free-volume, and the other is the increase of penetrant concentration, which then plasticizes the polymer and increases the free-volume. The plasticized polymer (PA11), showed a decrease of weight from the pre to post-test, by an average of 2.58%, which was not observed for the other polymers.

The mixture 90 mol% CO_2 + 10 mol% CH_4 , was the mixture for which most experiments were performed, although other concentrations were considered in order to establish the effect of gas

concentration. It was observed that the presence of CH_4 in the mixture decreases the gas permeability in the membrane. The molecular radius of CH_4 is larger than CO_2, so when CH_4 is present in the mixture, it also blocks the passage of CO_2 molecules through the polymeric membrane. In order to understand better the gas composition effect on the permeability, different gas compositions were measured, in XLPE at 100 and 200 bar at 318 K. The obtained results were not entirely conclusive since different behaviour was observed at different pressures. At 100 bar the permeability increases linearly with increase of CO_2 concentration in the mixture, however, at 200 bar the permeability reached a maximum increase up to a concentration of 50 mol% CO_2 and then decreased with increasing CO_2 concentration. The selectivity of XLPE was calculated and found to be very low; this was also confirmed by the GC analyses of the gas present in the downstream chamber after the measurement, which proved not to be significantly different from the initial gas composition.

At the conditions of pressure and temperature for which the permeability measurements were performed, there is a significant deviation from ideal gas behaviour. For this reason, calculation of the permeability based in fugacity difference instead of pressure difference was also performed and both calculations were compared and presented (essentially an alternative definition of permeability). the permeability absolute values increased when defined this way, although no clear insights were obtained using this alternative definition. When contacting supercritical CO_2 the polymer sample changed from translucent to opaque, especially for PVDF at certain conditions of pressure and temperature (e.g. 345 bar, 383 K in the presence of 90 mol% CO_2 and 10 mol% CH_4). In order to analyse any possible structural modification SEM analysis were performed, however no clear trend was found regarding this phenomenon.

The permeability depends on both thermodynamic and transport coefficients: the solubility and the diffusion. Knowing two of these coefficients it is possible to obtain the third. Since the solubility and the permeability were determined experimentally, the diffusion of gas in the polymeric membranes was calculated. The diffusion has a more pronounced effect on the overall transport (permeability), chiefly because the diffusion increases strongly with temperature, even though solubility shows a decrease with temperature. While pressure dependencies were observed these were much weaker than the temperature dependencies.

Chapter 7

Chapter 7. Future Work

The experimental data present in this field is scarce, especially when high pressure is part of the equation. This study mainly reflects the measurement of solubility and permeability at high pressure, although clearly more work can be done.

The solubility tests were conducted with pressure increments of 15, 20, 25 or 40 bar; in the future smaller increments could be used, especially between 75 and 100 bar (where it is observed an unusual behaviour), to have a better understanding of the sorption isotherm. Another issue is that, when polymer contacts supercritical CO_2, it swells. Experimental data of the swelling is not available for these polymers under the studied conditions of pressure and temperature. Therefore, it would be advisable to conduct some experimental swelling measurements *in situ*, for instance with a Magnetic Suspension Balance containing a view cell. Alternatively, have a correlation in order to predict it in an accurate way.

It would be interesting to conduct more tests of permeability at different CO_2 concentrations, to fully understand the dependence of gas permeability with the composition at more pressures (100 and 200 bar were the only pressure considered). Visually the polymer is changing when contacting CO_2 at certain conditions of pressure and temperature (from translucent to white opaque), this observation was more pronounced for PVDF. In an attempt to understand what was changing structurally, SEM measurements were done, however it was not possible to obtain an understanding of what was happening based on the SEM images. So some X-ray diffraction tests could be considered in the future.

Chapter 8

Chapter 8. List of Symbols

a	Activity of the component
$\tilde{a}^{assoc}$	Contribution due to association
$\tilde{a}^{disp}$	Dispersion contribution
$\tilde{a}^{hc}$	Contribution of the hard-sphere
$\tilde{a}^{id}$	Ideal gas contribution
A	Membrane contact area
b	Hole affinity constant
C	Penetrant concentration
C_1	Gas concentration in the membrane in the high pressure side
C_2	Gas concentration in the membrane in the low pressure side
C_D	Diffusing molecules by ordinary dissolution
C_H	Diffusing molecules trapped on microvoids or holes
$C_H^{'}$	Langmuir capacity factor
C_m	Parameter from BET isotherm
C_P	Concentration of penetrant
C_{sat}	Saturation concentration of gas
D	Diffusion
D_0	Pre-exponential factor for diffusion
D^*	Diffusivity in completely amorphous layer
d_i	Temperature dependent segment diameters
E_D	Activation energy for diffusion
E_{Pe}	Activation energy for permeability
f	fugacity

J	Gas flux
k	Equilibrium constant
K_1 and K_2	Criterion for glass transition
k_D	Henry's constant
k_{ij}	Binary interaction parameter
l	Thickness of the membrane
m	Weight given by the MSB
$\bar{m}$	Mean segment lenght
m_{CO_2}	Mass of CO_2 dissolved
m_S	mass of the sample
m_{SC}	Mass of the sample container
$M_{w,i}$	Molecular weight of component i
P	Pressure
P^0	Saturation vapour pressure
Pe	Permeability
Pe_0	Pre-exponential factor for permeability
Q	Amount of gas crossing the membrane
R	Universal gas constant
S	Solubility
S_0	Pre-exponential factor for solubility
S^*	Solubility in completely amorphous layer
t	Time
T	Absolute temperature
T_g	Glass transition temperature
V_0	Volume occupied by the molecules at temperature 0 K

V_{cell}	Volume of the downstream chamber
V_f	Free volume
V_{f,T_g}	Free-volume at 0 K
V_{PP}	Specific volume of the pure polymer
V_S	Volume of the sample
V_{SC}	Volume of the sample container
v_{sw}	Average specific volume of the swelled polymer
$V_{swelling}$	Volume caused by polymer swelling
V_T	Observed volume at temperature T
x_2^L	Mole fraction of the gas component in liquid
X_C	Crystallinity of the polymer
x_i	molar fraction of component i

Greek Symbols

α	Amorphous volume fraction
α_{CO_2/CH_4}	Membrane selectivity
α_G	Slope line below T_g
α_R	Slope line above T_g
β	Chain immobilization factor
Δ_α	Difference between the volume of thermal expansion coefficient above and below T_g
ΔH_{cond}	Molar heat of condensation
ΔH_l	Partial molar heat of mixing
ΔH_S	Heat of solution of the penetrant in the polymer
ΔP	Pressure gradient between the chambers
ΔV	Total volume change

ρ_{CO_2}	Density of CO_2
ρ_{end}	Gas density at initial conditions of pressure and temperature
ρ_{start}	Gas density at final conditions of pressure and temperature
ρ_{STP}	Gas density at STP conditions
ϕ	Volume fraction of the penetrant
τ	Geometric impedance factor
φ_2^L	Fugacity coefficient of the gas component in the liquid phase
φ_2^G	Fugacity coefficient of the gas component in the gas phase
χ	Enthalpic interaction

Chapter 9

Chapter 9. References

(1) Lake, L. W.; Society of Petroleum Engineers (U.S.). *Enhanced Oil Recovery*; Printed by Society of Petroleum Engineers, 2010.

(2) National Oilwell Varco Denmark I/S. Flexibles. 2015, p 13.

(3) Administration, U. S. E. I. *International Energy Outlook 2016*; 2016.

(4) Sheng, J. *Modern Chemical Enhanced Oil Recovery*; Gulf Professional Publishing, 2011.

(5) Montaron, B. Carbonate Evolution. *Oil & Gas Middle East*. 2008.

(6) Exxon Mobil. *The Outlook for Energy: A View of 2040*; 2016.

(7) Perera, M.; Gamage, R.; Rathnaweera, T.; Ranathunga, A.; Koay, A.; Choi, X. A Review of CO2-Enhanced Oil Recovery with a Simulated Sensitivity Analysis. *Energies* **2016**, *9* (7), 481.

(8) Tunio, S. Q.; Tunio, A. H.; Ghirano, N. A.; Adawy, Z. M. El. Comparison of Different Enhanced Oil Recovery Techniques for Better Oil Productivity. *Int. J. Appl. Sci. Technol.* **2011**, *1* (5), 143.

(9) Raffa, P.; Broekhuis, A. A.; Picchioni, F. Polymeric Surfactants for Enhanced Oil Recovery: A Review. *J. Pet. Sci. Eng.* **2016**, *145*, 723.

(10) Negin, C.; Ali, S.; Xie, Q. Most Common Surfactants Employed in Chemical Enhanced Oil Recovery. *Petroleum* **2017**, *3* (2), 197.

(11) Rudyk, S.; Spirov, P.; Al-Hajri, R.; Vakili-Nezhaad, G. Supercritical Carbon Dioxide Extraction of Oil Sand Enhanced by Water and Alcohols as Co-Solvents. *J. CO2 Util.* **2017**, *17*, 90.

(12) Safdel, M.; Anbaz, M. A.; Daryasafar, A.; Jamialahmadi, M. Microbial Enhanced Oil Recovery, a Critical Review on Worldwide Implemented Field Trials in Different Countries. *Renew. Sustain. Energy Rev.* **2017**, *74*, 159.

(13) Brandt, A. R.; Unnasch, S. Energy Intensity and Greenhouse Gas Emissions from Thermal Enhanced Oil Recovery. *Energy & Fuels* **2010**, *24* (8), 4581.

(14) Nian, Y.-L.; Cheng, W.-L. Insights into Heat Transport for Thermal Oil Recovery. *J. Pet. Sci. Eng.* **2017**, *151*, 507.

(15) Green, D. W.; Willhite, G. P. *Enhanced Oil Recovery*; SPE Textbook Series Vol. 6, 1998.

(16) Schrag, D. P. Preparing to Capture Carbon. *Science (80-.).* **2007**, *315* (5813).

(17) Perera, M. S. A.; Ranjith, P. G.; Airey, D. W.; Choi, S. K. Sub- and Super-Critical Carbon Dioxide Flow Behavior in Naturally Fractured Black Coal: An Experimental Study. *Fuel* **2011**, *90* (11), 3390.

(18) Perera, M. S. A.; Ranjith, P. G. Carbon Dioxide Sequestration Effects on Coal's Hydro-Mechanical Properties: A Review. *Int. J. Energy Res.* **2012**, *36* (10), 1015.

(19) Perera, M. S. A.; Ranjith, P. G.; Choi, S. K.; Bouazza, A.; Kodikara, J.; Airey, D. A Review of Coal Properties Pertinent to Carbon Dioxide Sequestration in Coal Seams: With Special Reference to Victorian Brown Coals. *Environ. Earth Sci.* **2011**, *64* (1), 223.

(20) Ranathunga, A. S.; Perera, M. S. A.; Ranjith, P. G. Deep Coal Seams as a Greener Energy Source: A Review. *J. Geophys. Eng.* **2014**, *11* (6), 63001.

(21) Shekher, V. Flexible Pipelines. *Mech. Eng.* **1987**, *109* (2), 82.

(22) https://www.nov.com/ (accessed May 2017)

(23) http://www.epmag.com/rising-tide-685301 (accessed May 2017)

(24) Thomas, M. A rising tide https://www.epmag.com/rising-tide-685301 (accessed January 2017).

(25) Diagram Site http://www.printablediagram.com/co2-phase-diagram/ (accessed December 2017)

(26) Almeida, S. Measurement and Modeling of Supercritical CO2 Solubility and Permeability in Polymers for Offshore Applications, 2012.

(27) NIST. REFPROP. 2013 software.

(28) Doi, M. *Soft Matter Physics*, 1st ed.; Oxford University Press, 2013.

(29) Mulder, M. *Basic Principles of Membrane Technology*; Kluwer, 2003.

(30) Chee, K. K. Prediction of Glass Transition Temperatures of Plasticized Polymers. *Eur. Polym. J.* **1985**, *21* (1), 29.

(31) Stutz, H.; Illers, K.-H.; Mertes, J. A Generalized Theory for the Glass Transition Temperature of Crosslinked and Uncrosslinked Polymers. *J. Polym. Sci. Part B Polym. Phys.* **1990**, *28* (9), 1483.

(32) Wesselingh, J. A.; Krishna, R. *Mass Transfer in Multicomponent Mixtures*; Delft University Press, 2000.

(33) Klopffer, M. Transport Properties of Gases in Polymers: Bibliographic Review. *OIL GAS Sci. Technol. D IFP ENERGIES Nouv.* **2001**, *56* (3), 223.

(34) Minelli, M.; De Angelis, M. G. An Equation of State (EoS) Based Model for the Fluid Solubility in Semicrystalline Polymers. *Fluid Phase Equilib.* **2014**, *367*, 173.

(35) Michaels, A. S.; Parker, R. B. Sorption and Flow of Gases in Polyethylene. *J. Polym. Sci.* **1959**, *41* (138), 53.

(36) Bitter, J. G. A. Effect of Crystallinity and Swelling on the Permeability and Selectivity of Polymer Membranes. *Desalination* **1984**, *51* (1), 19.

(37) Vieth, W.; Wuerth, W. F. Transport Properties and Their Correlation with the Morphology of Thermally Conditioned Polypropylene. *J. Appl. Polym. Sci.* **1969**, *13* (4), 685.

(38) Flaconnèche, B.; Martin, J.; Klopffer, M. H. Permeability , Diffusion and Solubility of Gases in Polyethylene , Polyamide 11 and Poly (Vinylidene Fluoride). **2001**, *56* (3), 261.

(39) Michaels, A. S.; Bixler, H. J. Solubility of Gases in Polyethylene. *J. Polym. Sci.* **1961**, *50* (154), 393.

(40) Kiparissides, C.; Dimos, V.; Boultouka, T.; Anastasiadis, A.; Chasiotis, A. Experimental and Theoretical Investigation of Solubility and Diffusion of Ethylene in Semicrystalline PE at Elevated Pressures and Temperatures. *J. Appl. Polym. Sci.* **2003**, *87* (6), 953.

(41) Bashir, M. A.; Ali, M. A.; Kanellopoulos, V.; Seppälä, J. Combined EoS and Elastic Constraints Models to Predict Thermodynamic Properties for Systems Involving Semi-Crystalline Polyolefins. *Fluid Phase Equilib.* **2015**, *388*, 107.

(42) Novak, A.; Bobak, M.; Kosek, J.; Banaszak, B. J.; Lo, D.; Widya, T.; Harmon Ray, W.; de Pablo, J. J. Ethylene and 1-Hexene Sorption in LLDPE under Typical Gas-Phase Reactor Conditions: Experiments. *J. Appl. Polym. Sci.* **2006**, *100* (2), 1124.

(43) Serna, L. V.; Becker, J. L.; Galdámez, J. R.; Danner, R. P.; Duda, J. L. Elastic Effects on Solubility in Semicrystalline Polymers. *J. Appl. Polym. Sci.* **2008**, *107* (1), 138.

(44) Boyer, S. A. E.; Grolier, J.-P. E. Simultaneous Measurement of the Concentration of a

Supercritical Gas Absorbed in a Polymer and of the Concomitant Change in Volume of the Polymer. The Coupled VW-pVT Technique Revisited. *Polymer (Guildf).* **2005**, *46* (11), 3737.

(45) Ghosal, K.; Freeman, B. D. Gas Separation Using Polymer Membranes: An Overview. *Polym. Adv. Technol.* **1994**, *5* (11), 673.

(46) Fleming, G. K.; Koros, W. J. Dilation of Polymers by Sorption of Carbon Dioxide at Elevated Pressures. 1. Silicone Rubber and Unconditioned Polycarbonate. *Macromolecules* **1986**, *19* (8), 2285.

(47) KOROS, W. CO2 SORPTION IN POLY(ETHYLENE-TEREPHTHALATE) ABOVE AND BELOW GLASS-TRANSITION. *J. Polym. Sci. Part B-polymer Phys.* **1978**, *16* (11).

(48) Stern, S. Polymers for Gas Separation - The Next Decade. *J. Membr. Sci.* **1994**, *94*, 1.

(49) Sperling, L. H. *Introduction to Physical Polymer Science*; Wiley, 1992.

(50) Fox, T. G.; Flory, P. J. Second Order Transition Temperatures and Related Properties of Polystyrene. I. Influence of Molecular Weight. *J. Appl. Phys.* **1950**, *21* (6), 581.

(51) Simha, R.; Boyer, R. F. On a General Relation Involving the Glass Temperature and Coefficients of Expansion of Polymers. *J. Chem. Phys.* **1962**, *37* (5), 1003.

(52) Kang, G.; Cao, Y. Application and Modification of Poly(vinylidene Fluoride) (PVDF) Membranes: A Review. *J. Memb. Sci.* **2014**, *463*, 145.

(53) von Solms, N. Direct Measurement of Gas Solubility and Diffusivity in Poly(vinylidene Fluoride) with a High-Pressure Microbalance. *Eur. Polym. J.* **2005**, *41* (2), 341.

(54) Andreopoulos, A. G.; Kampouris, E. M. Mechanical Properties of Crosslinked Polyethylene. *J. Appl. Polym. Sci.* **1986**, *31* (4), 1061.

(55) Beveridge, C.; Sabiston, A. Methods and Benefits of Crosslinking Polyolefins for Industrial Applications. *Mater. Des.* **1987**, *8* (5), 263.

(56) Biron, M. Chapter 4 - Detailed Accounts of Thermoplastic Resins BT - Thermoplastics and Thermoplastic Composites; Elsevier: Oxford, 2007; pp 217–714.

(57) Knudsen, P. Technical data sheet www.pkkaps.dk.

(58) Stannett, V. The Transport of Gases in Synthetic Polymeric Membranes : An Historic

Perspective. *J. Memb. Sci.* **1978**, *3* (2), 97.

(59) Stern, S. A. Tests of a "Free-Volume" Model of Gas Permeation Throught Polymer Membranes. II. Pure Ar, SF6, CF4, and C2H2F2 in Polyethylene. *J. Polym. Sci. Part B Polym. Phys.* **1986**, *24* (10), 2149.

(60) Crank, J. *Diffusion in Polymers*; Academic press, 1968.

(61) Crank, J. *Mathematics of Diffusion*; Oxford University Press, 1975.

(62) Barrer, R. M.; Rideal, E. K. Permeation, Diffusion and Solution of Gases in Organic Polymers. *Trans. Faraday Soc.* **1939**, *35* (1), 628.

(63) Matteucci, S.; Yampolskii, Y.; Freeman, B. D.; Pinnau, I. Transport of Gases and Vapors in Glassy and Rubbery Polymers. In *Materials Science of Membranes for Gas and Vapor Separation*; John Wiley & Sons, Ltd: Chichester, UK, 2006; pp 1–47.

(64) Honarvar, H.; Sajadian, S. A.; Khorram, M.; Samimi, A. Mathematical Modeling of Supercritical Fluid Extrapolation of Oil from Canola and Sesame Seeds. *Brazilian J. Chem. Eng.* **2013**, *30* (1), 159.

(65) George, S. C.; Thomas, S. Transport Phenomena through Polymeric Systems. *Prog. Polym. Sci.* **2001**, *26* (6), 985.

(66) Costello, L. M.; Koros, W. J. Thermally Stable Polyimide Isomers for Membrane-Based Gas Separations at Elevated Temperatures. *J. Polym. Sci. Part B Polym. Phys.* **1995**, *33* (1), 135.

(67) Costello, L. M.; Koros, W. J. Temperature Dependence of Gas Sorption and Transport Properties in Polymers: Measurement and Applications. *Ind. Eng. Chem. Res.* **1992**, *31* (12), 2708.

(68) Ostwal, M.; Lau, J. M.; Orme, C. J.; Stewart, F. F.; Way, J. D. The Influence of Temperature on the Sorption and Permeability of CO2 in Poly(fluoroalkoxyphosphazene) Membranes. *J. Memb. Sci.* **2009**, *344* (1–2), 199.

(69) Koros, W. J.; Fleming, G. K. Membrane-Based Gas Separation. *J. Memb. Sci.* **1993**, *83* (1), 1.

(70) Stern, S. A. Effect of Pressure on Gas Permeability Coefficients. A New Application of `free Volume' Theory. *J. Polym. Sci. Part A-2 (Polymer Physics)* **1972**, *10* (2), 201.

(71) Lei, Z.; Ohyabu, H.; Sato, Y.; Inomata, H.; Smith, R. L. Solubility, Swelling Degree and

Crystallinity of Carbon Dioxide–polypropylene System. *J. Supercrit. Fluids* **2007**, *40* (3), 452.

(72) Li, G.; Gunkel, F.; Wang, J.; Park, C. B.; Altstädt, V. Solubility Measurements of N2 and CO2 in Polypropylene and Ethene/octene Copolymer. *J. Appl. Polym. Sci.* **2007**, *103* (5), 2945.

(73) Areerat, S.; Hayata, Y.; Katsumoto, R.; Kegasawa, T.; Egami, H.; Ohshima, M. Solubility of Carbon Dioxide in Polyethylene/titanium Dioxide Composite under High Pressure and Temperature. *J. Appl. Polym. Sci.* **2002**, *86* (2), 282.

(74) Chen, J.; Liu, T.; Zhao, L.; Yuan, W. K. Determination of CO2solubility in Isotactic Polypropylene Melts with Different Polydispersities Using Magnetic Suspension Balance Combined with Swelling Correction. *Thermochim. Acta* **2012**, *530*, 79.

(75) Li, G.; Wang, J.; Park, C. B.; Simha, R. Measurement of Gas Solubility in Linear/branched PP Melts. *J. Polym. Sci. Part B Polym. Phys.* **2007**, *45* (17), 2497.

(76) Von Solms, N.; Nielsen, J. K.; Hassager, O.; Rubin, A.; Dandekar, A. Y.; Andersen, S. I.; Stenby, E. H. Direct Measurement of Gas Solubilities in Polymers with a High-Pressure Microbalance. *J. Appl. Polym. Sci.* **2004**, *91* (3), 1476.

(77) von Solms, N.; Kristensen, J. Refrigeration Plants Using Carbon Dioxide as Refrigerant: Measuring and Modelling the Solubility and Diffusion of Carbon Dioxide in Polymers Used as Sealing Materials. *Int. J. Refrig.* **2010**, *33* (1), 19.

(78) Pantoula, M.; Panayiotou, C. Sorption and Swelling in Glassy Polymer/carbon Dioxide Systems. *J. Supercrit. Fluids* **2006**, *37* (2), 254.

(79) Sato, Y.; Yurugi, M.; Fujiwara, K.; Takishima, S.; Masuoka, H. Solubilities of Carbon Dioxide and Nitrogen in Polystyrene under High Temperature and Pressure. *Fluid Phase Equilib.* **1996**, *125* (1–2), 129.

(80) SANCHEZ, I. SOLUBILITY OF GASES IN POLYMERS. *Pure Appl. Chem.* **1990**, *62* (11).

(81) Hilic, S.; Pádua, A. A. H.; Grolier, J.-P. E. Simultaneous Measurement of the Solubility of Gases in Polymers and of the Associated Volume Change. *Rev. Sci. Instrum.* **2000**, *71* (11), 4236.

(82) Flaconnèche, B. Transport Properties of Gases in Polymers: Experimental Methods. *Oil Gas Sci. Technol. D Ifp Energies Nouv.* **2001**, *56* (3).

(83) Bonavoglia, B.; Storti, G.; Morbidelli, M.; Rajendran, A.; Mazzotti, M. Sorption and Swelling of

Semicrystalline Polymers in Supercritical CO2. *J. Polym. Sci. Part B Polym. Phys.* **2006**, *44* (11), 1531.

(84) Sarti, G. C.; Gostoli, C.; Riccioli, G.; Carbonell, R. G. Transport of Swelling Penetrants in Glassy Polymers: Influence of Convection. *J. Appl. Polym. Sci.* **1986**, *32* (2), 3627.

(85) Carla, V.; Wang, K.; Hussain, Y.; Efimenko, K.; Genzer, J.; Grant, C.; Sarti, G. C.; Carbonell, R. G.; Doghieri, F. Nonequilibrium Model for Sorption and Swelling of Bulk Glassy Polymer Films with Supercritical Carbon Dioxide. *Macromolecules* **2005**, *38* (24), 10299.

(86) Flaconnèche, B.; Martin, J.; Klopffer, M. H. Permeability, Diffusion and Solubility of Gases in Polyethylene, Polyamide 11 and Poly (Vinylidene Fluoride). *Oil Gas Sci. Technol.* **2001**, *56* (3), 261.

(87) Adewole, J. K.; Jensen, L.; Al-Mubaiyedh, U. A.; von Solms, N.; Hussein, I. A. Transport Properties of Natural Gas through Polyethylene Nanocomposites at High Temperature and Pressure. *J. Polym. Res.* **2012**, *19* (2), 9814.

(88) Neela, V.; von Solms, N. Permeability, Diffusivity and Solubility of Carbon Dioxide in Fluoropolymers: An Experimental and Modeling Study. *J. Polym. Res.* **2014**, *21* (4), 401.

(89) ASH, R.; BARRER, R.; PALMER, D. Solubility and Transport of Gases in Nylon and Polyethylene. *Polymer (Guildf).* **1970**, *11* (8), 421.

(90) Taravel-Condat, C. The Use of Flexible Pipe for CO2 Enhanced Oil Recovery Applications. *Proc. ASME 31st Int. Conf. Ocean. Offshore Artic Eng. Vol 3* **2012**, 251.

(91) Lin, H.; Freeman, B. D. Gas Solubility, Diffusivity and Permeability in Poly(ethylene Oxide). *J. Memb. Sci.* **2004**, *239* (1), 105.

(92) Minelli, M.; Sarti, G. C. Permeability and Solubility of Carbon Dioxide in Different Glassy Polymer Systems with and without Plasticization. *J. Memb. Sci.* **2013**, *444*, 429.

(93) Solms, N. von; Rubin, A.; Andersen, S. I.; Stenby, E. H. Directs Measurement of High Temperature/High Pressure Solubility of Methane and Carbon Dioxide in Polyamide (PA-11) Using a High-Pressure Microbalance. *Int. J. Thermophys.* **2005**, *26* (1), 115.

(94) Donohue, M. D. Permeation Behavior of Carbon Dioxide-Methane Mixtures in Cellulose Acetate Membranes. *J. Memb. Sci.* **1989**, *42* (3).

(95) Andersen, T.; Skar, J. I.; Hansteen, C. Permeability of Methane, Carbon Dioxide and Water in PA11 and PVDF Used for Flexible Pipes. NACE International.

(96) Hasan, M. M.; Li, Y. G.; Li, G.; Park, C. B.; Chen, P. Determination of Solubilities of CO_2 in Linear and Branched Polypropylene Using a Magnetic Suspension Balance and a *PVT* Apparatus. *J. Chem. Eng. Data* **2010**, *55* (11), 4885.

(97) Li, G. Investigating the Solubility of CO2 in Polypropylene Using Various EOS Models. *Cell. Polym.* **2006**, *25* (4).

(98) Enders, S.; Kahl, H.; Winkelmann, J. Interfacial Properties of Polystyrene in Contact with Carbon Dioxide. *Fluid Phase Equilib.* **2005**, *228–229*, 511.

(99) Sato, Y.; Takikawa, T.; Takishima, S.; Masuoka, H. Solubilities and Diffusion Coefficients of Carbon Dioxide in Poly(vinyl Acetate) and Polystyrene. *J. Supercrit. Fluids* **2001**, *19* (2), 187.

(100) Bonavoglia, B.; Storti, G.; Morbidelli, M. Modeling of the Sorption and Swelling Behavior of Semicrystalline Polymers in Supercritical CO 2. *Ind. Eng. Chem. Res.* **2006**, *45* (3), 1183.

(101) Chmelar, J.; Gregor, T.; Hajova, H.; Nistor, A.; Kosek, J. Experimental Study and PC-SAFT Simulations of Sorption Equilibria in Polystyrene. *Polymer (Guildf).* **2011**, *52* (14), 3082.

(102) von Solms, N.; Michelsen, M. L.; Kontogeorgis, G. M. Prediction and Correlation of High-Pressure Gas Solubility in Polymers with Simplified PC-SAFT. *Ind. Eng. Chem. Res.* **2005**, *44* (9), 3330.

(103) Aionicesei, E.; Škerget, M.; Knez, Ž. Mathematical Modelling of the Solubility of Supercritical CO2 in Poly(l-Lactide) and Poly(d,l-Lactide-Co-Glycolide). *J. Supercrit. Fluids* **2009**, *50* (3), 320.

(104) Gross, J.; Sadowski, G. Perturbed-Chain SAFT: An Equation of State Based on a Perturbation Theory for Chain Molecules. *Ind. Eng. Chem. Res.* **2001**, *40* (4), 1244.

(105) von Solms, N.; Michelsen, M. L.; Kontogeorgis, G. M. Computational and Physical Performance of a Modified PC-SAFT Equation of State for Highly Asymmetric and Associating Mixtures. *Ind. Eng. Chem. Res.* **2003**, *42* (5), 1098.

(106) von Solms, N. Refrigeration Plants Using Carbon Dioxide as Refrigerant: Measuring and Modelling the Solubility, Diffusivity and Permeability of Carbon Dioxide in Polymers Used as

Packing and Sealing Materials. *6. Int. Conf. Heat Transf. Fluid Mech. Thermodyn.* **2008**.

(107) Tumakaka, F.; Gross, J.; Sadowski, G. Modeling of Polymer Phase Equilibria Using Perturbed-Chain SAFT. *Fluid Phase Equilib.* **2002**, *194–197*, 541.

(108) Gross, J.; Sadowski, G. Modeling Polymer Systems Using the Perturbed-Chain Statistical Associating Fluid Theory Equation of State. *Ind. Eng. Chem. Res.* **2002**, *41* (5), 1084.

(109) Rasmus Lundsgaard, Christian Wang, Adam Rubin, N. von S. *Modeling Solubility and Swelling in Supercritical Carbon Dioxide – Polymer Systems*.

Appendixes

Appendix 1 – Solubility Calculation Example

Polymer: XLPE

Temperature: 363 K

Measurement with Reference Gas (Argon)

Table A1.1 – Data obtain with argon measurement at equilibrium.

Segment	Temperature (K)	Pressure (bar)	m (g)	ρ_{gas} (g/cm^3)	$\rho_{gas,corr}$ (g/cm^3)
1	359	0.044	5.746685	-0.000339	0.000000
2	361	20.000	5.719019	0.025951	0.026290
3	361	39.960	5.691213	0.052361	0.052700
4	361	59.961	5.663282	0.078859	0.079198
5	361	79.974	5.635324	0.105333	0.105672
6	361	100.023	5.607411	0.131734	0.132073
7	361	119.959	5.579845	0.157813	0.158152
8	361	139.983	5.552357	0.183731	0.184070
9	361	159.981	5.525271	0.209297	0.209636
10	361	179.967	5.498601	0.234472	0.234811
11	361	189.967	5.485398	0.246903	0.247242
12	361	201.235	5.471658	0.259896	0.260235

$$\rho_{gas,corr} = \rho_{gas} + \rho_{gas\_1} \qquad \text{Equation A1.1}$$

$$\rho_{gas,corr\_1} = -0.000339 + 0.000339 = 0\, g/cm^3$$

$$\rho_{gas,corr\_2} = 0.025951 + 0.000339 = 0.026290\, g/cm^3$$

(Same procedure for the other segments)

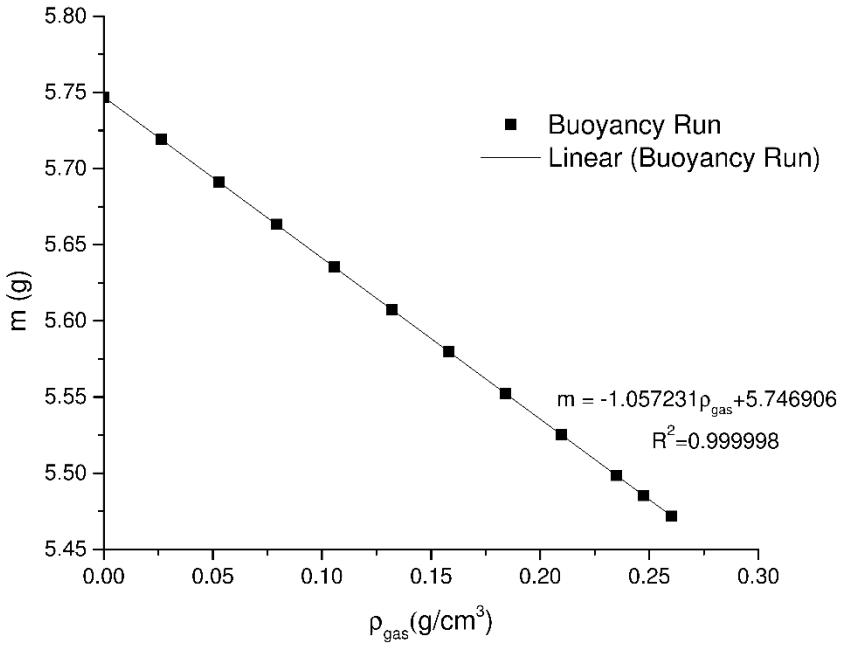

Figure A1.1 - Measurement with Argon to obtain the real weight and volume of the sample.

The trendline represented in the Figure A1.1 represents:

$$m = (V_{SC} + V_S) \times \rho_{CO_2} + (m_{SC} + m_S) = -1.057231 \times \rho_{CO_2} + 5.746906 \qquad \text{Equation A1.2}$$

where m is the total mass of the system, V_{SC} is the volume of the sample container, V_S is the volume of the sample, ρ_{gas} is the density of the measured gas (in this case, Argon), m_{SC} is the weight of the sample container and m_S is the weight of the sample. Knowing the V_{SC} and m_{SC} it is possible to obtain V_S and m_S.

$m_{SC} + m_S = 5.746906g$

$m_{SC} = 5.39517g$

$m_S = 0.351736g$

$V_{SC} + V_s = 1.057231cm^3$

$V_{SC} = 0.67899cm^3$

$V_s = 0.378241cm^3$

Measurement with Carbon Dioxide

Table A1.2 – Data obtained with CO_2 measurement at equilibrium.

Segment	Temperature (K)	Pressure (bar)	m (g)	ρ_{CO_2} (g/cm³)
1	357	0.048	5.746836	-0.000350
2	363	40.181	5.681713	0.064069
3	363	79.974	5.597307	0.145160
4	364	119.973	5.481954	0.252593
5	364	159.974	5.337215	0.384640
6	364	179.970	5.266175	0.449477
7	364	199.171	5.208395	0.502612

The method to correct the density of CO_2 is the same than the reference gas presented above.

Table A1.3 – Results of calculations to obtain the absolute solubility.

Segment	$\rho_{CO_2,corr}$ (g/cm³)	m_{abs} (g)	Solubility ($g_{gas}/g_{polymer}$)	Solubility abs ($g_{gas}/g_{polymer}$)
1	0.000000	-0.000070	-0.000199	-0.000199
2	0.064419	0.002913	0.008281	0.015129
3	0.145510	0.004239	0.012051	0.027518
4	0.252943	0.002467	0.007014	0.033902
5	0.384990	-0.002668	-0.007584	0.033340
6	0.449827	-0.005160	-0.014670	0.033147
7	0.502962	-0.006764	-0.019230	0.034235

The absorbed gas weight, m_{abs}, is calculated through:

$$m_{abs} = m - m_{SC} - m_S + (V_{SC} + V_S) \times \rho_{CO_2}$$ Equation A1.3

$$m_{abs\_1} = 5.746836 - 5.39517 - 0.351736 + (0.67899 + 0.378241) \times 0 = -0.00007\,g$$

$$m_{abs\_1} = 5.681713 - 5.39517 - 0.351736 + (0.67899 + 0.378241) \times 0.064419 = 0.002913g$$

(Same procedure for the other segments)

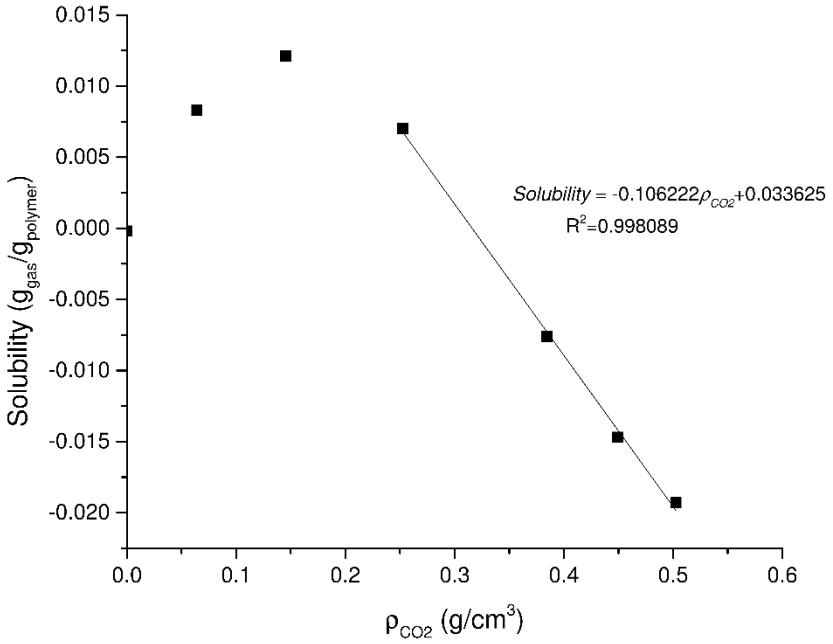

Figure A1.2 - Solubility of the penetrant as a function of Density to XLPE at 318 K up to 200 bar.

The volume of the absorbed gas cannot be neglected:

$V_{abs} = 0.106222 cm^3 / g$

where V_{abs} is the absorbed volume of gas per mass of polymer. The correction is then calculated by:

$$Solubility_{,abs} = Solubility + \rho_{CO_2} \times V_{abs}$$ Equation A1.4

$Solubility_{,abs_1} = -0.000199 + 0 \times 0.106222 = -0.000199 g_{gas} / g_{polymer}$

$Solubility_{,abs_2} = 0.008281 + 0.064419 \times 0.106222 = 0.015129 g_{gas} / g_{polymer}$

(Same procedure for the other segments)

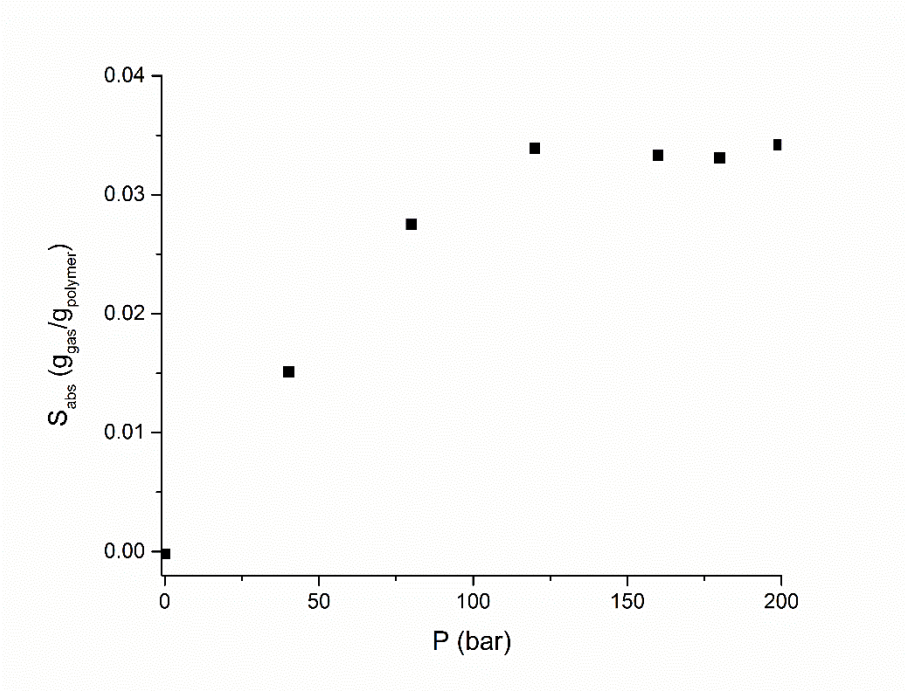

Figure A1.3 - Experimental results for Absolute solubility of Carbon Dioxide in XLPE at 363 K.

Appendix 2 – Permeability Calculation Example

Polymer: XLPE

Temperature: 363 K

Pressure upstream chamber (USC): 200 bar

Gas: 100% CO_2

Pressure-based Permeability

Equation 1.20 calculates the pressure-based Permeability coefficient:

$$Pe = \frac{l}{A} \cdot \frac{\rho_{end} - \rho_{start}}{\rho_{STP}} \cdot \frac{V_{cell}}{\Delta P \cdot t} \qquad \text{Equation A2.1}$$

where l is the membrane thickness, A is the membrane contact area, ρ_{end} and ρ_{start} are the gas density at initial and final conditions of temperature and pressure, respectively, ρ_{STP} is the gas density at Standard Temperature and Pressure ($T = 273.15\,K$ and $P = 1\,bar$), V_{cell} is the volume of the downstream chamber (DSC), ΔP is the pressure gradient between the chambers and t is the total experimental time. REFPROP[27] is used to obtain ρ_{STP}, ρ_{start} and ρ_{end}.

$\rho_{STP} = 4.4326 \times 10^{-5}$ mol/cm^3

Specifications from the set-up and the membrane:

$V_{cell} = 22.057$ cm^3 $A = 38.48$ cm^2 $l = 0.104$ cm

Specifications from the measurement:

Initial Conditions:	*Final Conditions:*	*General:*
$P_{DSC,start} = 147.42$ bar	$P_{DSC,end} = 173.97$ bar	$\Delta P = 35.41$ bar
$T_{start} = 362.36$ K	$T_{end} = 363.06$ K	$t = 178744$ s
$\rho_{start} = 8.3290 \times 10^{-3}$ mol/cm^3	$\rho_{end} = 1.0378 \times 10^{-2}$ mol/cm^3	

From the Equation above is then possible to obtain the Permeability coefficient:

$$Pe = 4.35 \times 10^{-7}\ cm^3_{STP} \cdot cm^{-1} \cdot bar^{-1} \cdot s^{-1}$$

Fugacity-based Permeability

Equation 3.2 calculates the fugacity-based Permeability coefficient:

$$Pe = \frac{l}{A} \cdot \frac{\rho_{end} - \rho_{start}}{\rho_{STP}} \cdot \frac{V_{cell}}{\Delta f \cdot t} \qquad \text{Equation A2.2}$$

where Δf is the fugacity difference between the chambers (upstream and downstream). REFPROP[27] is used to obtain ρ_{STP}, ρ_{start}, ρ_{end}, f_{start} and f_{end}.

$$\rho_{STP} = 4.4326 \times 10^{-5}\ \text{mol/cm}^3$$

Specifications from the set-up and the membrane:

$V_{cell} = 22.057$ cm^3	$A = 38.48$ cm^2	$l = 0.104$ cm

Specifications from the measurement:

Initial Conditions:	*Final Conditions:*	*General:*
$P_{DSC,start} = 147.42$ bar	$P_{DSC,end} = 173.97$ bar	$\Delta f = 10.053$ bar
$T_{start} = 362.36$ K	$T_{end} = 363.06$ K	$t = 178744$ s
$\rho_{start} = 8.3290 \times 10^{-3}$ mol/cm^3	$\rho_{end} = 1.0378 \times 10^{-2}$ mol/cm^3	
$f_{start} = 98.267$ bar	$\rho_{end} = 108.32$ bar	

From the Equation above is then possible to obtain the Permeability coefficient:

$$Pe = 1.53 \times 10^{-6}\ cm^3_{STP} \cdot cm^{-1} \cdot bar^{-1} \cdot s^{-1}$$

Appendix 3 – SEM analyses

In this appendix, the pictures obtained by SEM are shown. The gas composition is presented in x/y fraction, where x and y are CO_2 and CH_4 molar fraction, respectively. The virgin material represents the polymer before the measurements, prior to contact with supercritical CO_2. The samples chosen for analysis covered a wide range of criteria dependence (e.g. temperature, pressure and gas composition) with the goal of obtaining a better understanding of how the gas was changing the polymer structure at various temperature and pressure conditions. The used equipment was a FEI Quanta 200.

Table A2.1 – Real and SEM images of the analysed samples.

Measurement Conditions	Real Photo	SEM image
Polymer: PVDF virgin material		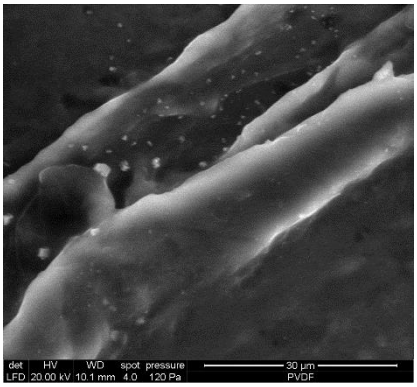
Polymer: PVDF Pressure: 75 bar Temperature: 383 K Gas: 90/10		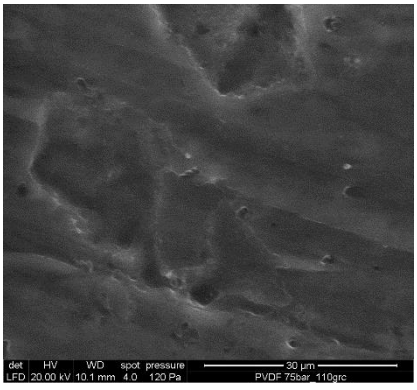

Measurement Conditions	Real Photo	SEM image
Polymer: PVDF Pressure: 75 bar Temperature: 403 K Gas: 90/10	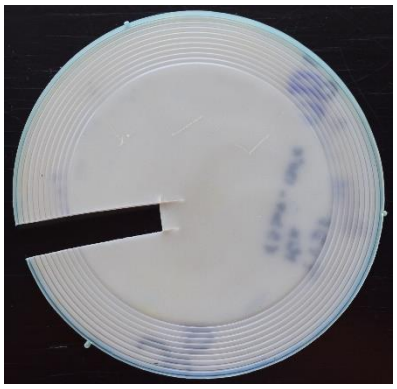	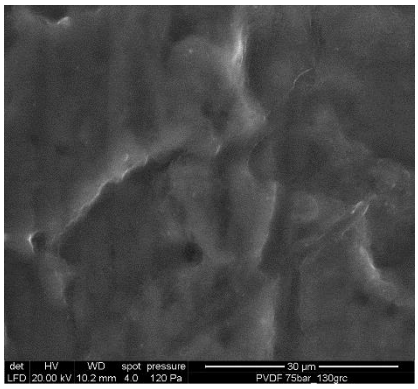
Polymer: PVDF Pressure: 200 bar Temperature: 318 K Gas: 90/10	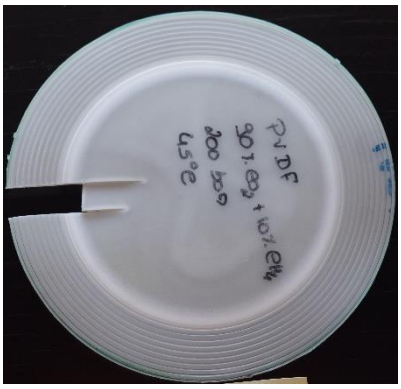	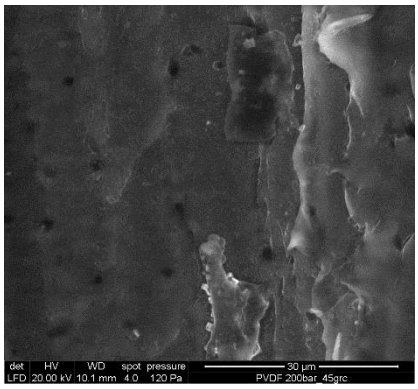
Polymer: PVDF Pressure: 620 bar (for 3 weeks) Temperature: 318 K Gas: 90/10	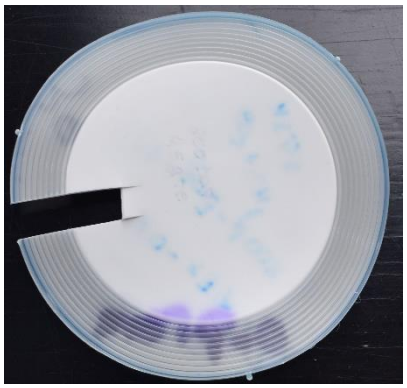	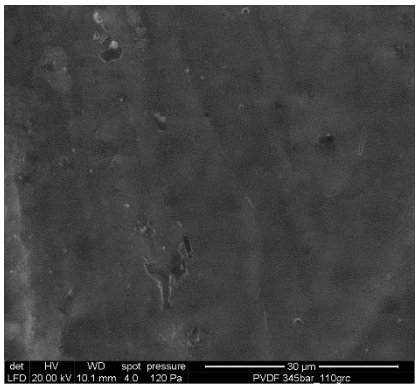
Polymer: PVDF Pressure: 345 bar Temperature: 383 K Gas: 90/10	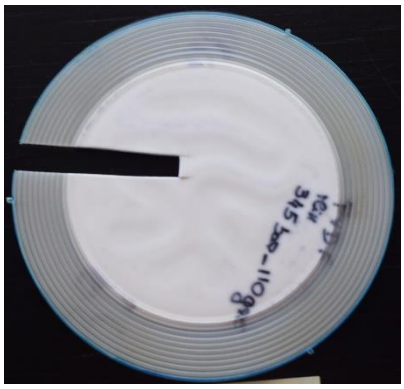	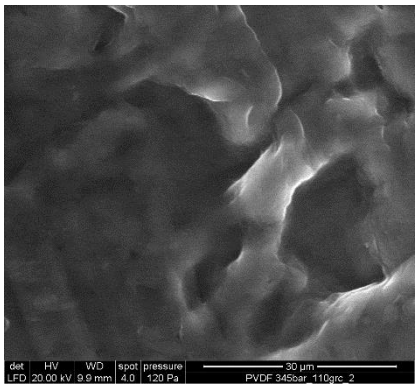

Measurement Conditions	Real Photo	SEM image
Polymer: XLPE virgin material		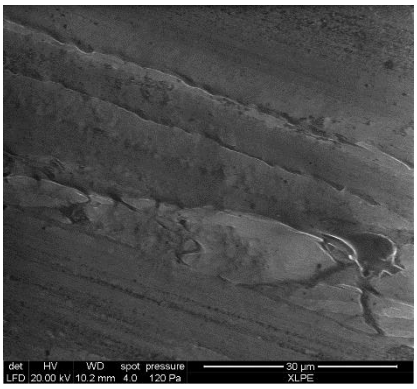
Polymer: XLPE Pressure: 200 bar Temperature: 318 K Gas: 0/100		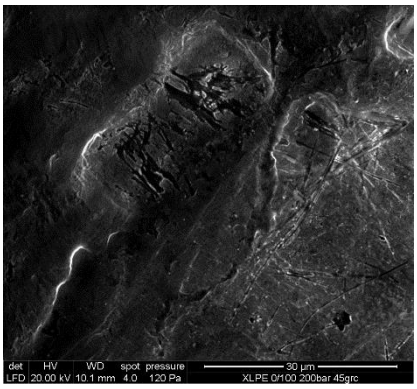
Polymer: XLPE Pressure: 200 bar Temperature: 318 K Gas: 25/75	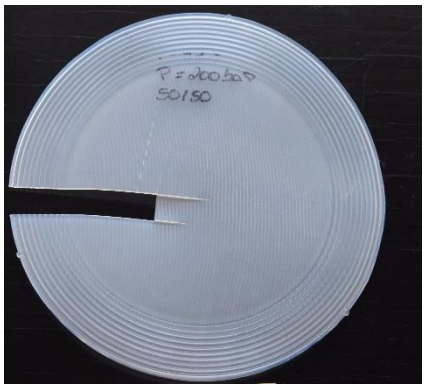	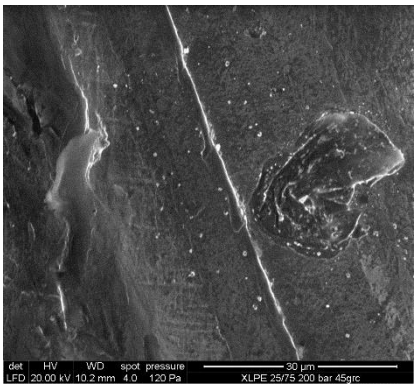
Polymer: XLPE Pressure: 200 bar Temperature: 318 K Gas: 50/50	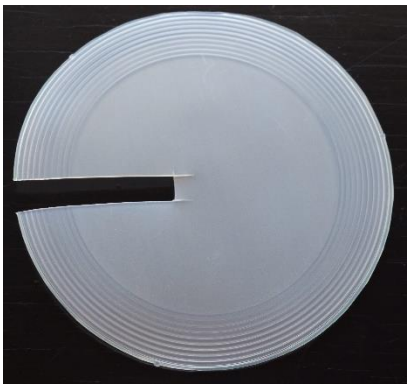	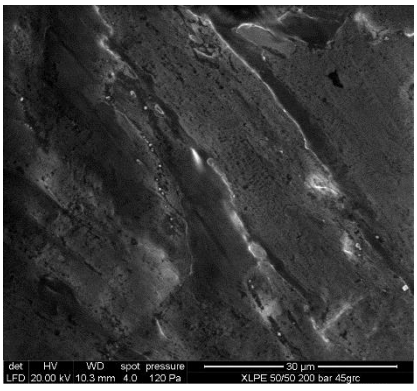

Measurement Conditions	Real Photo	SEM image
Polymer: XLPE Pressure: 200 bar Temperature: 318 K Gas: 75/25	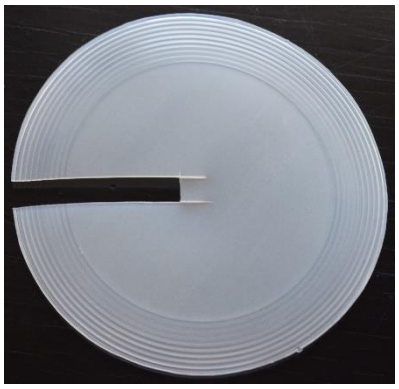	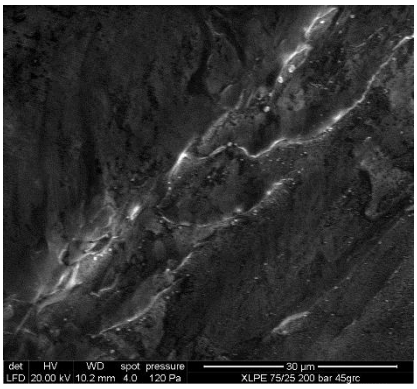
Polymer: XLPE Pressure: 200 bar Temperature: 318 K Gas: 90/10		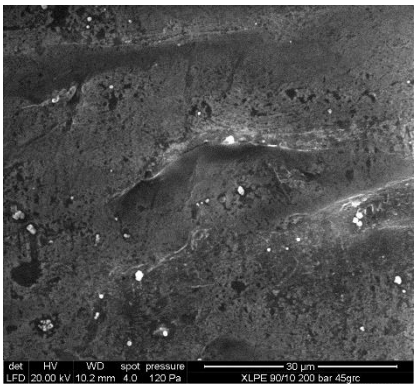
Polymer: XLPE Pressure: 200 bar Temperature: 318 K Gas: 100/0	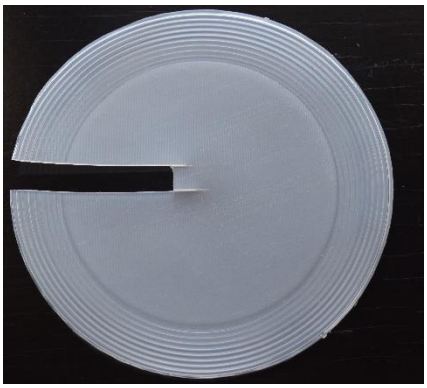	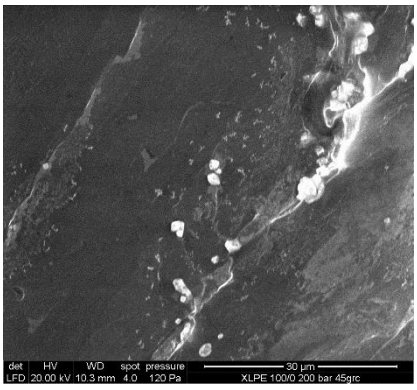
Polymer: XLPE Pressure: 200 bar Temperature: 363 K Gas: 90/10		

Measurement Conditions	Real Photo	SEM image
Polymer: XLPE Pressure: 650 bar Temperature: 318 K Gas: 90/10	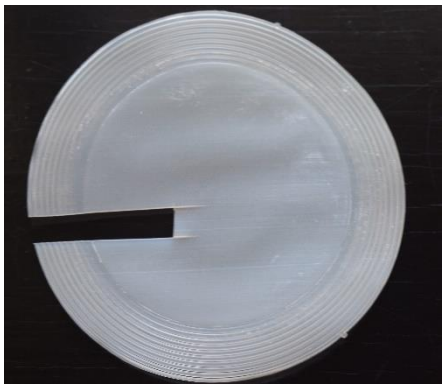	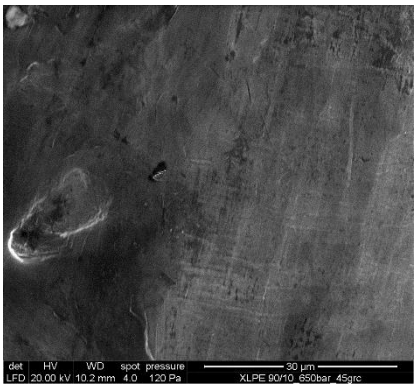
Polymer: PA11 virgin material		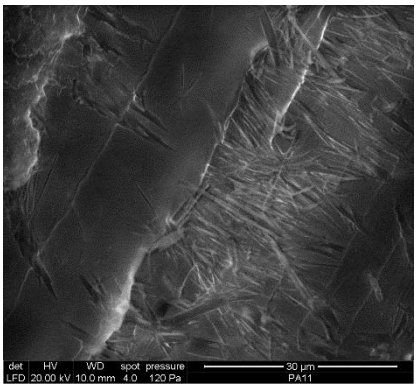
Polymer: PA11 Pressure: 100 bar Temperature: 318 K Gas: 90/10	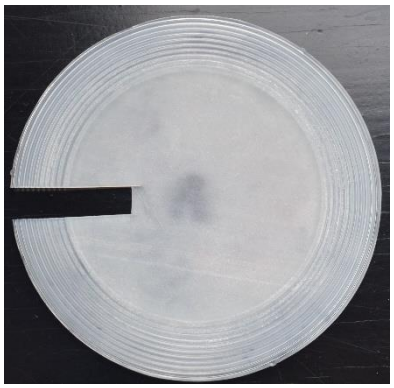	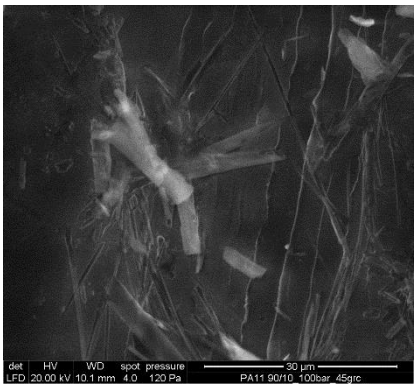
Polymer: PA11 Pressure: 100 bar Temperature: 318 K Gas: 100/0	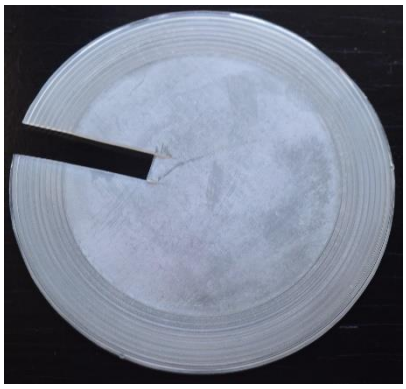	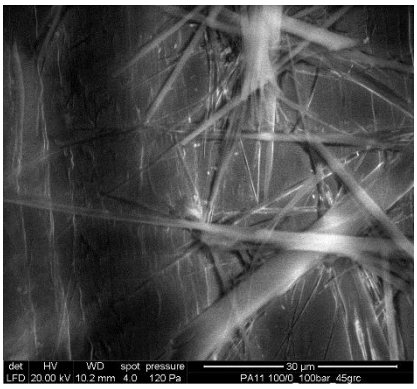

Measurement Conditions	Real Photo	SEM image
Polymer: PA11 Pressure: 350 bar Temperature: 363 K Gas: 100/0	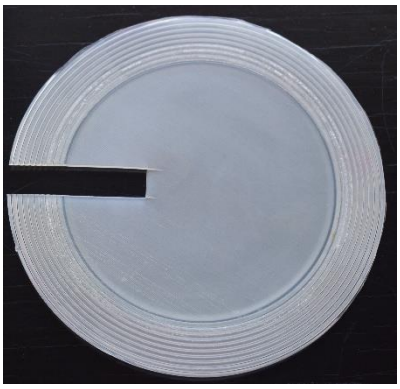	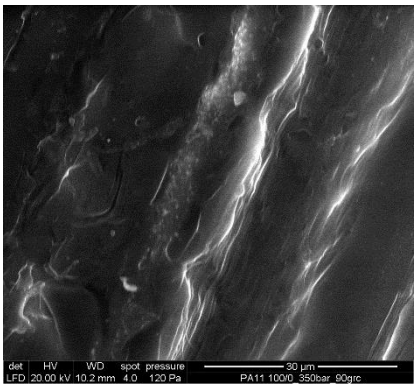
Polymer: PA11 Pressure: 650 bar Temperature: 318 K Gas: 100/0